

Polarisers based on anisotropic absorbance or scattering of light

Citation for published version (APA):

Dirix, Y. J. L. (1997). *Polarisers based on anisotropic absorbance or scattering of light*. [Phd Thesis 1 (Research TU/e / Graduation TU/e), Chemical Engineering and Chemistry]. Technische Universiteit Eindhoven.
<https://doi.org/10.6100/IR497329>

DOI:

[10.6100/IR497329](https://doi.org/10.6100/IR497329)

Document status and date:

Published: 01/01/1997

Document Version:

Publisher's PDF, also known as Version of Record (includes final page, issue and volume numbers)

Please check the document version of this publication:

- A submitted manuscript is the version of the article upon submission and before peer-review. There can be important differences between the submitted version and the official published version of record. People interested in the research are advised to contact the author for the final version of the publication, or visit the DOI to the publisher's website.
- The final author version and the galley proof are versions of the publication after peer review.
- The final published version features the final layout of the paper including the volume, issue and page numbers.

[Link to publication](#)

General rights

Copyright and moral rights for the publications made accessible in the public portal are retained by the authors and/or other copyright owners and it is a condition of accessing publications that users recognise and abide by the legal requirements associated with these rights.

- Users may download and print one copy of any publication from the public portal for the purpose of private study or research.
- You may not further distribute the material or use it for any profit-making activity or commercial gain
- You may freely distribute the URL identifying the publication in the public portal.

If the publication is distributed under the terms of Article 25fa of the Dutch Copyright Act, indicated by the "Taverne" license above, please follow below link for the End User Agreement:

www.tue.nl/taverne

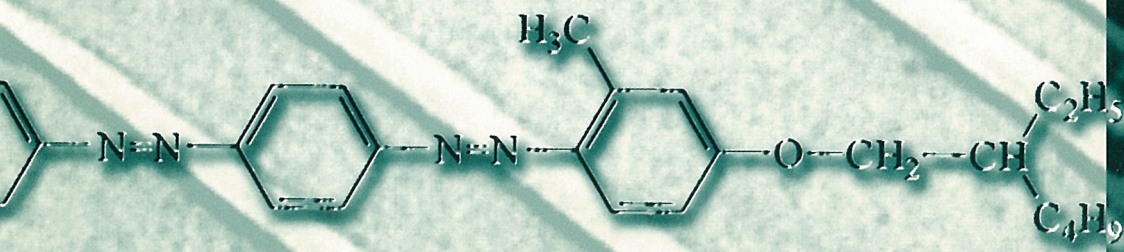
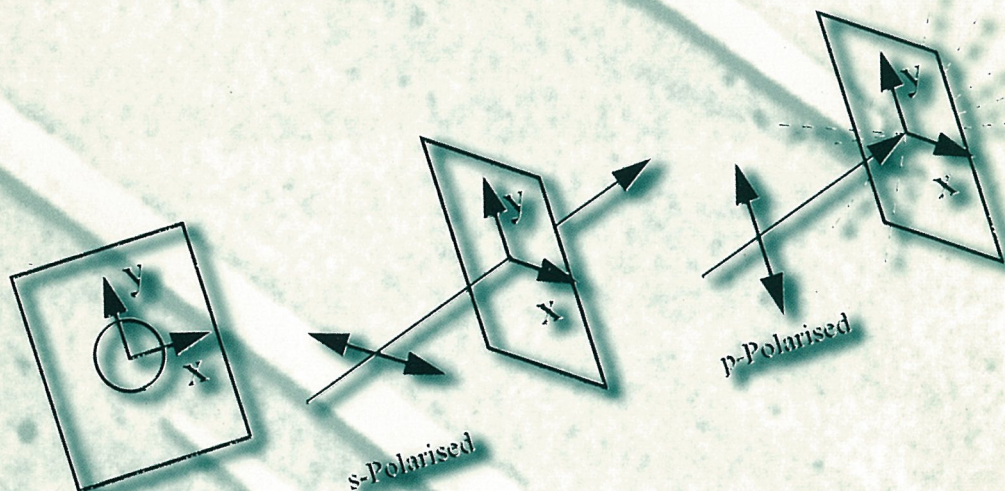
Take down policy

If you believe that this document breaches copyright please contact us at:

openaccess@tue.nl

providing details and we will investigate your claim.

POLARISERS BASED ON ANISOTROPIC ABSORBANCE OR SCATTERING OF LIGHT



**Polarisers Based on
Anisotropic Absorbance or Scattering of Light**

CIP-DATA LIBRARY TECHNISCHE UNIVERSITEIT EINDHOVEN

Dirix, Yvo J.L.

Polarisers Based on Anisotropic Absorbance or Scattering of Light / by Yvo J.L. Dirix.-
Eindhoven: Technische Universiteit Eindhoven, 1997.

Proefschrift. -

ISBN 90-386-0868-3

NUGI 813

Trefw.: polymeermengsels / optische polarisatie / lichtverstrooiing

Subject headings: polymer blends / polarizers / light scattering

Copyright © 1997 Y.J.L. Dirix

Omslagontwerp: Ben Mobach, TUE

Druk: Universiteitsdrukkerij, TUE

Polarisers Based on Anisotropic Absorbance or Scattering of Light

PROEFSCHRIFT

ter verkrijging van de graad van doctor aan de
Technische Universiteit Eindhoven, op gezag van
de Rector Magnificus, prof.dr. M. Rem,
voor een commissie aangewezen door het College
van Dekanen in het openbaar te verdedigen op
5 september 1997 om 16.00

door

Yvo Jean Louis Dirix

geboren te Stein

Dit proefschrift is goedgekeurd door de promotoren:

prof.dr. P.J. Lemstra

prof.dr. P. Smith

Copromotor:

dr.ing. C.W.M. Bastiaansen

Contents

Summary	iii
----------------------	-----

1 General Introduction

1.1	Polarisation of light	1
1.2	Objectives	6
1.3	Scope of the thesis	6
1.4	References	8

Part A: Absorbance Polarisers

2 Orientation Mechanism of Guest-Host Systems

2.1	Introduction	13
2.2	Experimental	16
2.3	Results	19
2.4	Discussion	27
	2.4.1 Orientation of the host-polymer	27
	2.4.2 Orientation of the guest-molecules	28
2.5	Conclusions	33
2.6	References	34

3 Modelling of the Optical Properties of Dichroic Polarisers

3.1	Introduction	37
3.2	Theoretical section	38
3.3	Model predictions	41
3.4	Experimental	43
3.5	Model verification	45
3.6	Ultimate optical properties	49
3.7	Discussion	52
3.8	Conclusions	54
3.9	References	55

Part B: Scattering Polarisers

4 Light-Scattering Polarisers

4.1	Introduction	59
4.2	Experimental	62
4.3	Results	65
4.4	Discussion	76
4.5	Conclusions	79
4.6	References	80

5 Angular Distribution of Light Scattering

5.1	Introduction	83
5.2	Experimental	84
5.3	Results and discussion	88
5.4	Conclusions	103
5.5	References	104

Technology Assessment	105
------------------------------------	-----

Appendices

A: Characterisation of polarisers	111
B: The Lambert-Beer's law approximation	115
C: Depolarisation in light-scattering polarisers	117

Samenvatting	119
---------------------------	-----

Dankwoord	122
------------------------	-----

Curriculum Vitae	123
-------------------------------	-----

Summary

Polymeric sheet polarisers are nowadays widely used in liquid-crystal display (LCD) applications. These polarisers are produced from oriented sheets of a host polymer containing dichroic guest molecules. The dichroic guest molecules absorb light, polarised parallel to the optical axis of the molecule. Orientation of the dichroic guest molecules by the (oriented) host polymer results in macroscopic dichroic behaviour and the typical characteristics of a linear polariser, i.e., in a series arrangement, two parallel polarisers are transparent and this in contrast with two crossed polarisers, which hardly transmit light.

Commercial polarisers are produced since 1928 from drawn, oriented poly(vinyl alcohol) (PVA) films containing dichroic dyes or iodine as a guest molecule. These PVA polarisers possess disadvantages such as a poor long-term stability in humid environments and at elevated temperatures, which limits the applications of LCD's in, for instance, automotive applications.

In recent years, it was shown that absorbance polarisers with a high dichroic ratio (and order parameter) can be produced by introducing dichroic dyes in drawn polyolefins. Moreover, it was shown that these polarisers exhibit an enhanced durability in humid environments and at elevated temperatures.

In the first part of this thesis, a theoretical model is developed to describe the optical properties of polarisers based on drawn, oriented polymer-dye systems. It is assumed that both the host polymer and the guest molecules orient according to the pseudo-affine deformation scheme. These assumptions have been verified on melt-crystallised polyethylenes (Low-Density Polyethylene, Linear-Low-Density Polyethylene, High Density Polyethylene and Ultra-High Molecular Weight Polyethylene) containing dichroic di-azo dyes. In this theoretical model, the development of optical anisotropy with orientation is described using an aggregate of optical elements. The macroscopic optical properties, such as the single-piece transmittance (transparency) and the polarising efficiency (contrast), are calculated assuming a series arrangement of the elements of the aggregate.

The predictive power of the model is tested against experimental results using a model guest-host system (High-Density Polyethylene/Sudan Red B). A good agreement is observed between theoretical predictions and experimental data. The model is used to identify the parameters which determine the optical performance, i.e., polarising efficiency and single-piece transmittance. It was found that the prerequisites for the production of a high performance polariser are: (a) the use of a highly oriented host polymer and, thus, of polymers and production procedures which allow for high draw ratios (>15), (b) a highly anisotropic

dye molecule and, thus, dye molecules with a high aspect ratio, and (c), an optimised film thickness and dye concentration. A direct consequence of (a) is that linear polyolefins are intrinsically superior host polymers in comparison to poly(vinyl alcohol) because of their high maximum attainable draw ratio. Experimental results show indeed that the performance of ultra-drawn polypropylene containing a linear tri-azo dye closely approaches the theoretical limit for a perfect polariser.

An intrinsic problem of both the conventional PVA and the new polyolefin/dye polarisers is that they operate on the principle of anisotropic absorbance of light. This implies that even in a perfect polariser, 50% of the incoming light is absorbed by the guest molecules in the polariser. Consequently, the light (energy) efficiency of LCD displays containing absorbance polarisers is low which limits the brightness of displays. Moreover, in combination with high-intensity light sources (projection displays), the absorbed energy leads to an undesirable temperature increase of the polariser which reduces the lifetime of the device.

In the second part of this thesis a different concept for the polarisation of light is explored: anisotropic scattering of light instead of anisotropic absorbance. These scattering polarisers have been produced from blends of thermoplastic polyesters such as poly(ethylene terephthalate) (PET) or poly(ethylene 2,6-naphthalene dicarboxylate) (PEN) containing isotropic particles (rubbery styrene-butadiene core-shell particles or thermoplastic styrene-methylmethacrylate copolymers). These blends are extruded into tapes, and subsequently drawn in the solid-state to obtain a highly birefringent matrix containing isotropic particles. The materials are chosen with the aim that, after drawing, the ordinary refractive index of the matrix equals the refractive index of the dispersed phase. In the perpendicular direction, a large mismatch is obtained between the extraordinary index of the matrix and the dispersed phase. As a consequence, light polarised perpendicular to the orientation direction is transmitted due to the matched indices and light polarised parallel to the orientation direction is scattered as a result of the refractive index mismatch.

These light-scattering polarisers based on the oriented polyester blends operate in the entire visible wavelength range (400-700 nm). The polarising performance of the scattering polarisers, in terms of polarising efficiency and single-piece transmittance, resembles that of the light absorbing PVA systems. The efficiency and transmittance can be varied within a wide range by adjusting the particle concentration and/or film thickness, i.e., an increase in particle concentration (film thickness) increases the polarising efficiency and decreases the single-piece transmittance and vice versa. The spatial distribution of light scattering is found to be anisotropic for both polyester blends showing excess light scattering perpendicular to the orientation direction of the blends. This anisotropy is a result of the shape of the scattering units in the blends which consists of uniaxially aligned ellipsoids of several core-shell

particles in the case of PET, and cylindrical structures in the case of PEN. The forward to backward scattering ratio is a function of the concentration of the particles, the thickness of the film and the birefringence of the oriented matrix material. For the PET blends a maximum amount of 41% of the incoming radiation is backscattered whereas 75% is backscattered for the PEN blends at an identical particle concentration and tape thickness. Additionally, the contrast ratio in the forward direction is 1000 and 1800 for the PET and PEN blends, respectively. Both the enhanced contrast in the forward direction and the better backscattering properties of the PEN blends are a result of the higher birefringence (i.e., higher refractive-index mismatch) of the oriented PEN blends ($\Delta n_{\text{PEN}} = 0.315$, and $\Delta n_{\text{PET}} = 0.135$).

Potential advantages of the scattering polarisers are that, in a suitable device, all the incoming light is converted into linearly polarised light. This drastically enhances the brightness of conventional displays. The lifetime of projection displays may be expanded because light is polarised without generating heat. Finally, the scattering polarisers presented in this thesis are made from thermoplastic polymers which can be processed on cast-film lines in combination with conventional solid-state drawing equipment.

Chapter 1

General Introduction

1.1 Polarisation of light

Light is understood to be a transversal, electromagnetic wave, i.e., the vibration direction of light is perpendicular to its propagation direction (Figure 1.1). In non-polarised, natural light, the plane of vibration is randomly distributed as is schematically drawn in Figure 1.2a.^{1,2} Mathematically, natural light may be represented as two perpendicular, linearly polarised waves with an equal amplitude for which the phase difference varies rapidly and randomly.¹ (Figure 1.2 b). Light is termed linearly or plane polarised, if it vibrates in a single direction and the vibration direction remains identical along the propagation direction (Figure 1.2c).¹ If light vibrates in a single direction and the vibration direction is not constant along the propagation direction but, for example, makes one complete rotation as the wave advances through one wavelength, light is termed circularly polarised. A schematic representation of (right-handed) circularly polarised light is drawn in Figure 1.2d.

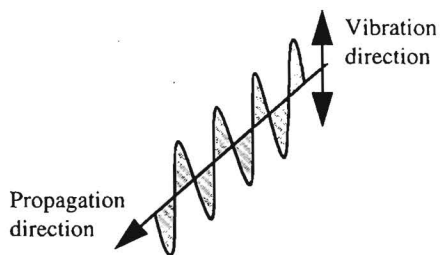


Figure 1.1: Transversal wave-character of light

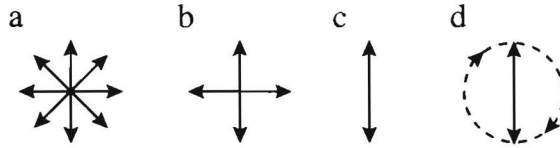


Figure 1.2: a) Natural light, b) Mathematical representation of natural light, c) Linearly polarised light.
d) Right handed circularly polarised light

Linear polarisation phenomena occur frequently in every day life. For instance, both light reflected under oblique angles from a smooth surface and the light from a blue sky are partially, linearly polarised.^{1,3} In the latter case, partially polarised light is obtained due to light scattering by small particles in the atmosphere. In contrast to humans, insects can detect this partial polarisation of light and they use it for navigation purposes.^{4,5,6,7} For instance, on a partly clouded day when the sun is obscured by the clouds, insects can derive the position of the sun from the polarised light pattern in a small blue section in the sky. Visual perception of the polarisation direction by insects starts with the absorbance of light by the pigment rhodopsin which is located in the photoreceptor membranes of the insects' eyes.⁸ This rhodopsin molecule is dichroic, i.e., the incoming light is absorbed by rhodopsin only if the polarisation direction of the light coincides with the optical axis of the molecule.^{5,6,9} In the eyes of insects, the rhodopsin molecules are oriented in a specific direction (Figure 1.3) and, consequently, the light absorbance by their photoreceptor membranes is dependent on the polarisation direction of the incident light.

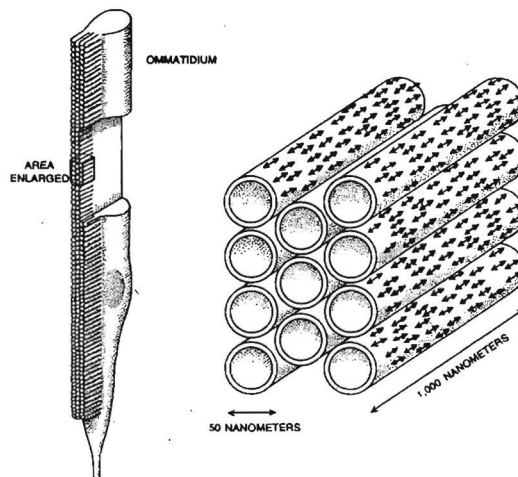


Figure 1.3: Visual cells of insects (Ommatidium) with the arrangement of the rhodopsin molecules (\longleftrightarrow).

Reproduced with permission from: Wehner R., *Scient. Am.*, 1976. 235, 106

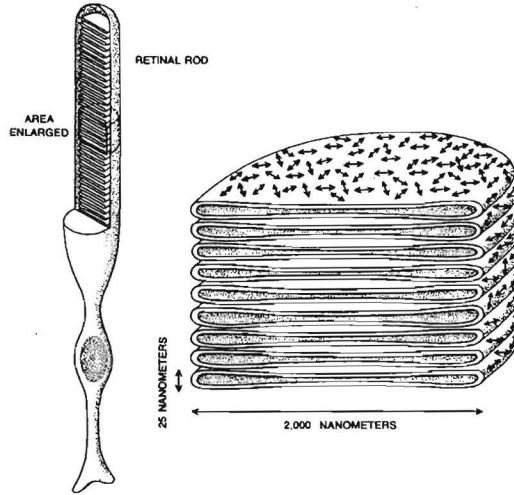


Figure 1.4: Visual cells of humans (Retinal Rods) with the arrangement of the rhodopsin molecules (\longleftrightarrow).

Reproduced with permission from: Wehner R., *Scient. Am.*, 1976, 235, 106

Like the insects, the human eye also contains the rhodopsin molecules but in this case the rhodopsin molecules are randomly distributed in the photoreceptor membranes (Figure 1.4). In this case, the absorbed light intensity is independent of its polarisation direction and, consequently, the human eye is virtually insensitive to light polarisation.¹⁰

The insensitivity of the human eye for the polarisation of light can be circumvented by using polarising filters. The first humans to use polarising filters perhaps were the ancient Vikings.¹¹ They used dichroic cordierite crystals or so-called “sun-stones” for similar purposes as insects, i.e., the filters and the polarisation pattern of the blue sky were used to localise the position of the (obscured) sun which, in turn, was used for navigation at sea.¹¹

The first man-made polarisation filters, which were produced on a large-scale, were manufactured from birefringent, doubly refractive crystals.^{1,2,12} A well-known example of this type of polarising filters is the Nicol prism, which is manufactured from a calcite crystal that is split diagonally and subsequently glued together again with a transparent Canada balsam (Figure 1.5). Unpolarised light entering the crystal is separated into two, linearly polarised, perpendicularly vibrating rays due to the two different (ordinary and extraordinary) refractive indices which each ray encounters at the air-prism interface. The refractive index of the Canada balsam is between the ordinary and extraordinary refractive indices of the prism, which implies that the critical angle for total internal reflection is different for the two light rays. One of the rays, called the ordinary ray (o-ray), is totally internally reflected at the prism-

balsam interface and thereafter absorbed by a black layer painted onto the side of the prism. The other, extraordinary ray (e-ray) is transmitted and linearly polarised light is produced.

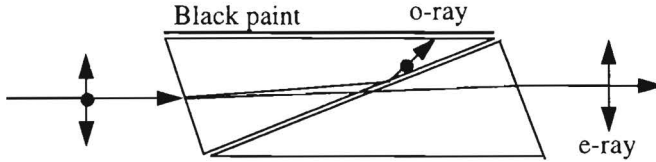


Figure 1.5: Polarisation of light by a Nicol Prism

After the Nicol prism, a variety of other prism polarisers were developed such as the Glan-Foucault or Wollaston prisms.¹ In general, these prism polarisers are bulky, possess a low acceptance angle and are difficult to produce in large areas, which is a serious limitation in applications where size and weight are crucial factors. The first, large area, flexible, thin film polarisers were produced by Land in 1928.^{1,13,14} This co-founder of the Polaroid Corporation discovered that so-called polymeric sheet polarisers can be produced by orienting synthetic polymers which contain dichroic crystals or molecules. To a certain extent, the structure of these materials resembles the photoreceptor membranes of insects. In both cases, dichroic chromophores are uniaxially aligned to detect the polarisation direction of light (or to produce polarised light from natural light).^{5,15} Originally the polymeric sheet polarisers invented by Land were primarily used in applications such as anti-glare sunglasses, anti-glare desk lamps, photography filters, optical instruments (microscopes) and stereoscopic projection devices.^{13,16,17,18} In the early 70's, the so-called Twisted Nematic Display (TN) was invented and commercialised and this broadened the applications of linear polarisers significantly.^{19,20,21,22,23,24} The basic principle of this electro-optical light shutter is briefly discussed below (Figure 1.6). A nematic liquid crystalline material is sandwiched between two glass plates and two crossed sheet polarisers (2). The two glass plates are coated with a transparent electrode of indium tin oxide (ITO), which is covered by an orientation layer consisting of rubbed polyimide (3). The upper and lower orientation layers are oriented parallel to the polarisers, in a crossed position. The nematic liquid crystalline molecules close to the glass walls align parallel to the orientation layers and, due to their crossed position and directed by a small concentration of chiral dopant, force the nematic molecules to perform a 90° twist (4) across the cell gap.

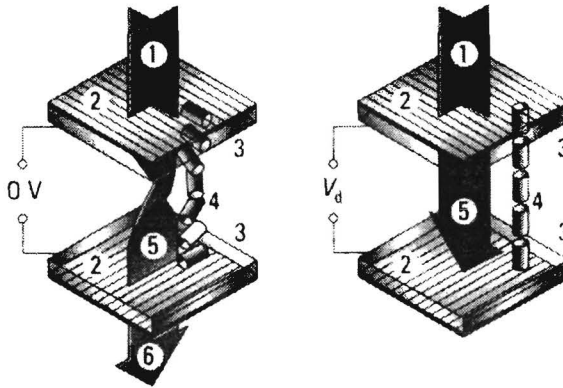


Figure 1.6: Schematic representation of a Twisted Nematic cell in off-state (0V), and on-state (V_d)

If no electric field is applied (0V), the electromagnetic vector of the incident light will also be twisted over 90° and light will therefore pass the second polariser (6) and the LCD appears transparent. However, if an electric field (V_d) is applied via the ITO-electrodes, the nematic molecules tend to align parallel to the electric field (4). Incident light will now encounter the two polarisers in a crossed position (5) and will not be transmitted. Images are produced on the display by selectively addressing the electric field to so-called pixels. Subsequently, other types of displays were developed, for example the Super Twisted Nematic (STN) displays^{22,25} which possesses a larger twist, for instance 270° instead of 90° across the cell gap. Advantages of the STN effect are the steeper transmittance-voltage behaviour and therefore a better multiplexibility (i.e. rows and columns of electrodes can be used to address single pixel elements).

In the past decade, an enormous research effort was devoted to the development of electro-optical shutters like TN or STN displays for applications in, for instance, lap-top computers. Large-scale applications of electro-optical devices are foreseen in dashboards (automotive), desk-top computers, high-definition television and portable telephones.^{25,26,27} In these future applications, the performance of the display with respect to viewing angle, brightness, power consumption, and stability is extremely important. In order to enhance these properties, new and preferentially polymeric polarisation optics are required. For instance, display applications in (automotive) dashboards are limited by the poor high temperature/humidity resistance of the polarisers in TN-displays.^{28,29} The performance of the polarisers deteriorates in time which reduces the lifetime of the device. Moreover, conventional polarisers absorb at least fifty percent of the light and the absorbed energy is transferred into thermal energy. Consequently, to obtain backlit displays with sufficient brightness, the absorbance losses need to be compensated for by increasing the illumination intensity. The extra power consumption and

bulkiness of the backlighting system, adversely affects the size and weight (batteries) of, for example, lap-top computers.^{30,31,32} In the case of projection television, the high intensity of the backlighting in combination with the heating-up of the display causes premature failure of the display.³⁰

1.2 Objectives

In the first part of this thesis, the orientation mechanism and properties of conventional, thin film, polarisation optics based on oriented host-polymers containing dichroic dye molecules are investigated. In these polarisers, one polarisation direction of natural light is selectively absorbed and the other is transmitted. It is attempted to establish experimental relationships between the orientation of the host-polymer, the orientation of the guest-molecule and the resulting optical characteristics of the polarisers in terms of, for instance, dichroic ratio and order parameter. Subsequently, these experimental results are used to derive quantitative structure-property relationships for these materials. The results of these studies are used to select new host-polymers and guest-molecules to produce thin film polarisation optics with an enhanced performance and to predict the ultimate properties of these systems.

The above described polarisers possess several intrinsic disadvantages such as a poor theoretical maximum light efficiency. This inspired us to explore new routes to produce linear polarisers with potentially enhanced properties. In the second part of this thesis, it is attempted to fabricate polarisers which produce linearly polarised light from natural light based on the anisotropic scattering of light (in contrast to anisotropic absorbance of light). The objectives are to fabricate such polarisers from thermoplastic polymers on conventional extrusion equipment in combination with solid-state drawing techniques.

1.3 Scope of the thesis

Part A: Absorbance Polarisers

The relationships between the macroscopic draw ratio of guest-host systems, the orientation of the host-polymer and the guest-molecule, and the optical properties of the films are investigated in Chapter 2. In this Chapter, special attention is devoted to verifying whether the pseudo-affine deformation scheme^{33,34} can be used to describe the development of the orientations of both the host-polymer and guest-molecule as a function of the macroscopic draw ratio. The pseudo-affine deformation scheme is subsequently used in Chapter 3 to

derive a theoretical framework which describes the optical performance of absorbance polarisers based on oriented polymer/dye systems. The optical characteristics of the guest-host systems are calculated as an aggregate of optically anisotropic elements. Verification of the model is performed on a model guest-host system, and finally, the theoretical framework is used to estimate the ultimate optical properties of absorbance polarisers based on oriented host-polymers containing dichroic dyes.

Part B: Scattering Polarisers

Polarisation optics can be produced based on the selective absorbance, reflection and scattering of one polarisation direction of incoming natural light. Light which is reflected or scattered can potentially be recycled and this in contrast to absorbed light which is transferred into heat. In the second part of this thesis, a new route is explored to produce thin-film polarisation optics based on the anisotropic scattering of light. These films consist of a highly birefringent continuous phase containing a dispersed phase which is virtually isotropic. Special care is taken in the selection of both the continuous phase and the dispersed phase to ensure that the refractive indices of the two phases are matched in one direction, while simultaneously a large refractive index mismatch is generated in the perpendicular direction. In Chapter 4, the selection of suitable materials for such a blend is discussed. Moreover, the processing and the properties of these blends are extensively described. Especially the influence of experimental parameters such as the film thickness, blend composition and birefringence of the continuous phase on the polarising performance is evaluated. The angular distribution of light scattering is of practical importance (for example recycling of light) for such a light scattering polariser and is, therefore, discussed in Chapter 5. Light scattering in both the forward and backward mode is investigated and related to the film thickness, morphology and composition of the blends.

Finally, the future perspectives of the polarisers presented in this thesis in terms of potential applications are outlined in the technology assessment. Attention is paid to the question whether it is possible to fabricate large-area, light-scattering polarisers.

This thesis is based on a collection of papers which have been published in, or are submitted to various journals.^{35,36,37,38,39}

1.4 References

- 1 Hecht E., *Optics*, 2nd ed., Addison Wesley: London, 1977
- 2 Driscoll W.G., Vaughan W., *Handbook of Optics*, Mc-Graw Hill: New York, 1988
- 3 Können G.P., *Polarized Light in Nature*; Cambridge University Press: Cambridge, 1985
- 4 von Frisch K., *Experientia*, **1949**, 5, 142
- 5 Wehner R., *Scient. Am.*, **1976**, 235, 106
- 6 Mazokhin-Porshnyakov G.A., *Insect Vision*, Plenum Press: New York, 1969
- 7 Rodieck R.W., *The Vertebrate Retina, Principles of Structure and Function*, W.H. Freeman and Company: San Francisco, 1973
- 8 Matthews R.G., Hubbard R., Brown P.K., Wald G., *J. Gen. Physiol.*, **1963**, 47, 215
- 9 De Vries H.L., Spoor A., Renske J., *Physica*, **1953**, 19, 419
- 10 Some people are able to perceive light with a high degree of polarisation, due to the dichroic properties of the small yellow spot of the retina, this effect is called the Haidingers Brush (references 3 or 9)
- 11 Walker J., *Scient. Am.*, **1978**, 238, 132
- 12 Jenkins F.A., White H.E., *Fundamentals of Optics*, 4th ed. Mc Graw Hill: New York, 1985
- 13 Land E.H., *J. Opt. Soc. Am.*, **1951**, 41, 957
- 14 Land E.H., West C.D., *Colloid Chemistry*, ed. J. Alexander, Vol.6, Reinhold Publishing Corporation, 1946
- 15 Mizoguchi R., Kobayashi K., Shimomura T. Kobayashi S., *Displays*, **1983**, 201
- 16 Grabau M., *J. Appl. Phys.*, **1938**, 9, 215
- 17 West C.D., Clark Jones R., *J. Opt. Soc. Am.*, **1951**, 41, 976
- 18 Land E.H., *J. Opt. Soc. Am.*, **1940**, 30, 230
- 19 Schadt M., Helfrich W., *Appl. Phys. Lett.*, **1971**, 18, 127
- 20 Sobel A., *Scient. Am.*, **1973**, 228, 65
- 21 Scheuble B.S., *Kontakte (Darmstadt)*, **1989**, 1, 35
- 22 Scheffer T.J., Nehring J., *Appl. Phys. Lett.*, **1984**, 45, 1021
- 23 Andoh T., *SID 85 Digest*, **1985**, 71
- 24 Nagatsuka T., Shimomura T., Oishi Y., *SID 85 Digest*, **1985**, 74
- 25 Bahadur B., *Liquid Crystals, Applications and Uses*, Vol.1, World Scientific Publishing: Singapore, 1990
- 26 Drzaic P.S., *Liquid Crystal Dispersions*, Vol.1., World Scientific Publishing: Singapore, 1995
- 27 Morozumi S., *Mol. Cryst Liq. Cryst.*, **1991**, 199, 47
- 28 Mitsubishi Petrochemical CO., *Eur. Pat Appl.*, EP 0348964, 1989
- 29 Bastiaansen C., *Eur. Pat Appl.*, EP 0518425A2, 1992
- 30 Belayev S.V., Schadt M., Barnik M.I., Fünfschilling J., Malimoneko N.V., Schmitt K., *Jap. J. Appl. Phys.*, **1990**, 29, L634
- 31 Schadt M., Fünfschilling J., *Jap. J. Appl. Phys.*, **1990**, 29, 1974
- 32 Broer D.J., Lub J., Mol G.N., *Nature*, **1995**, 378, 467
- 33 Kratky O., *Kolloid Z.*, **1933**, 64, 213

- 34 Kuhn W., Grün F., *Kolloid Z.*, **1942**, 101, 248
- 35 Dirix Y.J.L., *Polarizers Based on Drawn Polyolefins*, IVO. Eindhoven University of Technology. ISBN 90-5282-424-X, 1995
- 36 Dirix Y., Tervoort T.A., Bastiaansen C., *Macromolecules*, **1994**, 28, 486
- 37 Dirix Y., Tervoort T.A., Bastiaansen C.W.M. Lemstra P.J., *J. Text. Inst.*, **1995**, 86, 314
- 38 Dirix Y., Tervoort T.A., Bastiaansen C., *Macromolecules*, **1997**, 30, 2175
- 39 Dirix Y., Jagt H., Hikmet R., Bastiaansen C., submitted to *J. Appl. Phys.*

Part A:
Absorbance Polarisers

Chapter 2*

Orientation Mechanism of Guest-Host Systems

2.1 Introduction

Conventional polymeric sheet polarisers operate on the principle of anisotropic absorbance of light, i.e., one of the two orthogonal components of light is absorbed whereas the other component is transmitted. Often, these polarisers are produced from oriented host polymers containing dichroic guest molecules.^{1,2} The dichroic guest molecules used possess an extinction coefficient along the axis of the molecule which differs significantly from the extinction coefficient perpendicular to this axis. Orientation of the dichroic guests results in macroscopic dichroic behaviour and the typical characteristics of a linear polariser are obtained, i.e., two parallel polarisers are transparent and two crossed polarisers hardly transmit any light. Commercially available polarisers are based on oriented sheets of poly(vinyl alcohol) (PVA). Three different types of PVA based polarisers can be distinguished, depending on the type of dichroic guest molecule: H-sheet, K-sheet and L-sheet polarisers.^{3,4,5,6} The H-sheet polarisers are produced by soaking a pre-stretched PVA sheet in an aqueous iodine solution. Relaxation of the polymer is prevented by fixation of the sheet onto a substrate like cellulose acetate (this substrate remains attached to the PVA sheet as a protective film). After the soaking procedure, the films are dried during which an oriented PVA/poly-Iodine complex is formed.⁷ The oriented poly-Iodine is the dichroic guest and the polarising component of these guest-host systems. K-sheet polarisers are made by dehydration of a stretched PVA sheet. In this case the “guest”-molecule, oriented polyvinylene $-(\text{CH}=\text{CH})_n-$ is not added to the system on beforehand, but is formed in-situ. Finally, the production techniques of the L-sheet polarisers resemble those of the H-sheet polarisers. However, instead of iodine, a solution containing dichroic dyes is used. Dichroic dyes are low

* This chapter is partly reproduced from:

molecular weight, organic molecules with an anisotropic extinction coefficient which generates the polarising properties if the dichroic dyes are oriented.

In the aforementioned sheet polarisers, the dichroic guest molecules are oriented by their host, oriented poly(vinyl alcohol). However, the draw ratio which is employed in practise to orient poly(vinyl alcohol) is relatively low ($\lambda_{\max} < 6$)^{7,8} and, consequently, the attainable degree of orientation of the host polymer and the guest molecules is limited. It is tempting to select other host polymers, possessing enhanced drawing characteristics in comparison with PVA for the orientation of guest molecules. Therefore, in the next paragraph the drawing behaviour and properties of a potential candidate is recapitulated, namely linear polyethylenes.

The drawing characteristics of linear polyolefins were studied extensively in the past.^{9,10,11,12,13} The prime objective of these studies was to introduce an extremely high degree of chain extension and orientation in order to approach the theoretical limits with respect to modulus and strength of the polymer. A variety of processing techniques were developed, including melt-spinning⁹ or solution-casting^{10,11} techniques. With the latter technique it was shown that Ultra-High Molecular Weight Polyethylene (UHMW-PE, $M_w > 10^6$ g/mol) films could be drawn in the solid state to high ($\lambda > 100$) draw ratios, even after removal of the solvent from the films prior to drawing. The oriented UHMW-PE filaments possessed values for the modulus and strength exceeding 150 GPa and 4 GPa, respectively.¹⁰ This value for the modulus approaches the theoretical limit which is approximately 320 GPa.^{14,15} In a comparative study by Schellekens et al.¹⁶ on the solid-state drawing behaviour and properties of solution spun PVA and UHMW-PE fibres, it was shown that the poor drawing characteristics of PVA originate from the presence of hydrogen bridges between the chains of the polymer. These intermolecular interactions prevent the unfolding of crystalline units and consequently limit the maximum attainable draw ratio and degree of orientation of the polymer.

The favourable drawing behaviour of linear polyethylenes in comparison to poly(vinyl alcohol) was used previously for the fabrication of sheet polarisers.^{17,18,19} Basically, the same concept as for the K-sheet polarisers was used, i.e., dichroic dye molecules incorporated in, and oriented by host-polyethylenes. Both melt-processing and solution-casting techniques were used and examples of both will be briefly discussed below. First, in the solution-casting technique, UHMW-PE and a dichroic dye were co-dissolved in a suitable solvent (decaline or xylene) at elevated temperature (130 °C). Subsequently, the solution was cast and, after evaporation of the solvent, a polyolefin/dye film is obtained that can be drawn to high ($\lambda > 30$) draw ratios to orient the polymer and the dichroic dye molecules. The linear dichroism of the films is demonstrated in Figure 2.1, where “ θ ” denotes the angle between the drawing direction of the film and the polarisation direction of the incident light. If the polarisation direction is parallel to the drawing direction ($\theta = 0^\circ$), the absorbance of the dye is at its

maximum and in the crossed position ($\theta = 90^\circ$), the absorbance is negligible which clearly shows the macroscopic dichroic behaviour of the oriented polyolefin/dye system.

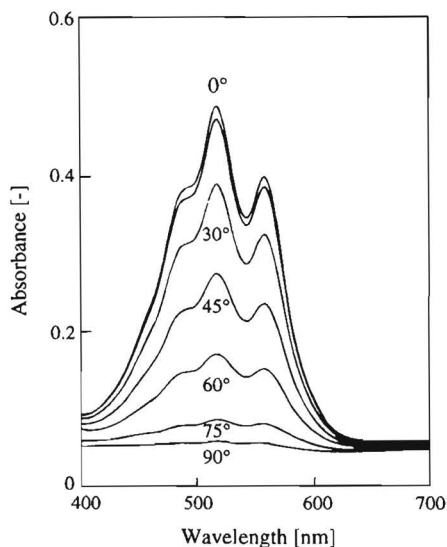


Figure 2.1: Polarised UV/VIS spectra of drawn, solution-cast UHMW-PE containing an anthraquinone dye.

Reproduced with permission from: Bastiaansen C., Schmidt H.W., Nishino T., Smith P., *Polymer*, 1993, 34, 3951

In a second set of experiments, linear High-Density Polyethylene and a dichroic dye were mixed in the melt, compression moulded into films and, finally, drawn in the solid state.¹⁸ The optical properties of these melt-crystallised systems resemble those of the polarisers produced via the solution-casting technique.

In the above described studies, it was shown that certain dichroic dyes can be oriented in ultra-drawn polyolefins. However, the optical performance of these polarisers was not optimised and the parameters which determine the performance of these polarisers were ill-understood. Therefore, a theoretical model has been developed, which will be presented in the next Chapter of this thesis, describing the optical properties of these oriented polymer/dye polarisers. One of the main assumptions in the theoretical framework is that, upon drawing, the orientation mechanism of the host polymer and the dichroic-dye molecules obeys the pseudo-affine deformation scheme. Therefore, in this Chapter, the *orientation mechanism* of these guest-host systems is investigated to verify the above described assumptions. It is attempted to establish an experimental relationship between the draw ratio, the orientation of the host polymer and the orientation of the guest molecule. First, the orientation of the pure and melt-crystallised host polymers (i.e. polyethylenes) is investigated. As model materials,

several polyethylenes are selected and the orientation upon solid-state drawing is evaluated in terms of their birefringence. The prime objective of this study is to verify the validity of the pseudo-affine deformation scheme for a wide range of potential polyolefinic host polymers. Subsequently, the orientation of the guest molecules is investigated to establish a direct link between the orientation of the host polymer and guest molecule. The results of this study are used to illustrate the potential advantages of polyolefins in comparison to poly(vinylalcohol) to produce linear, thin-film polarisers. Moreover, the empirical and/or theoretical relationships between draw ratio, orientation of the host polymer and guest molecule are used to derive quantitative structure-property relationships in these materials (see Chapter 3).

2.2 Experimental

Materials Selection and Preparation of Guest-Host Systems

Four polyethylenes were selected as host polymers: Low-Density Polyethylene (LDPE, DOW type 150), Linear-Low-Density Polyethylene (LLDPE, DSM type 40446), High-Density Polyethylene (HDPE, Hostalen Gur 7255 P, Hoechst Ruhrchemie) and Ultra-High Molecular Weight Polyethylene (UHMW-PE, DSM UH 210). The molecular weights, branch content and type of branches of the polymers are listed in Table 1.

Table 1: Polyethylene grades used as host polymers

Polymer	M_w [g/mol]	Branches
LDPE	195.000	Highly long chain branched
LLDPE	91.000	Short chain (C_6) branched
HDPE	350.000	Linear
UHMW-PE	2.100.000*	Linear

Two different dichroic dyes were used as a guest molecule, Sudan Red B (SR) and Sudan Black B (SB). Both dyes are di-azo compounds and were used as received from Aldrich

* The polyethylene grade used (DSM UH 210), is sold as UHMW-PE. However, according to ASTM D4020, UHMW-PE refers to linear polyethylene with a molecular weight M_w above $3 \cdot 10^6$ g/mol which is higher than the molecular weight used in this study.

(Germany), without further purification. The melting temperatures of the dyes are 173°C and 120°C, respectively. The chemical structures of the chromophores are depicted in Figure 2.2:

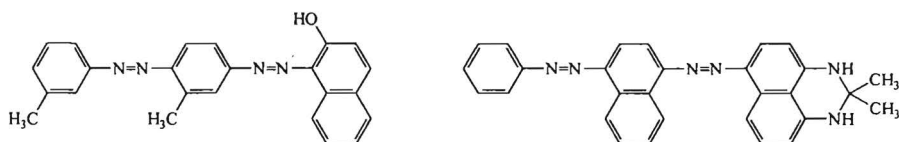


Figure 2.2: Chemical structures of Sudan Red B and Sudan Black B

Melt-crystallised guest-host systems were prepared on a Brabender batch-scale mixing device for 15 minutes at 200°C. The selected combinations of host polymer and guest molecules and the dye contents are listed below in Table 2:

Table 2: Polymer/Dye mixtures and drawing temperatures

Polymer	Dye	Dye Conc % (w/w)	Drawing Temp. (°C)
LDPE	Sudan Red B	0, 0.2, 5, 10, 25	90
LLDPE	Sudan Red B	0, 0.2	100
HDPE	Sudan Red B	0, 0.2, 2.5, 5, 10, 30, 50, 70	120
HDPE	Sudan Black B	0, 0.2	120

Thin films were produced by compression moulding at 210°C for 20 minutes, followed by rapid quenching to room temperature. Only melt-crystallised samples were used to ensure that the polymers and polymer/dye mixtures possessed a random orientation prior to drawing.

Solid-state drawing of the films was performed on thermostatically controlled hot-shoes. The draw ratio was determined by measuring the displacement of ink-marks printed onto the films before drawing. Special care was taken in the drawing experiments to ensure that the drawing temperature of the guest-host system was well below the melting temperature of the polymer (see also Table 2).

Characterisation of Undrawn Host Polymers and Undrawn Guest-Host Systems

Optical microscopy was performed on a Zeiss Universal Polarising microscope. Thin sections ($\approx 5 \mu\text{m}$) of the 0.2% Sudan Red dye-containing HDPE films were cut with a Reichert OM U2 microtome under cryogenic conditions and used for microscopy.

Differential Scanning Calorimetry (DSC) was performed on a Perkin Elmer DSC 7. Undrawn samples (≈ 15 mg) of the pure polymers were heated at a constant heating rate of $10^\circ\text{C}/\text{min}$ from 0 to 210°C . Indium was used as a standard for instrument calibration and only second heating runs were analysed. Melting temperatures were derived from the peak maxima in the thermograms. Mass fraction crystallinities (ω_c) were calculated from the melting peak areas (ΔH), assuming that the heat of fusion of 100% crystalline polyethylene is 289 J/g .²⁰ The thermal behaviour of model guest-host systems (HDPE/Sudan Red B or LDPE/Sudan Red B) with increasing dye concentration was investigated too. Undrawn samples were annealed at 210°C for 5 minutes, cooled to room temperature and heated again to 210°C at $10^\circ\text{C}/\text{min}$ to determine the melting temperatures of the polymer and the dye molecules. In addition to DSC, the melting behaviour of the polyethylene/Sudan Red B mixtures was also examined visually. The HDPE/SR extrudates were filled into test tubes which were put in an oil bath at 210°C for 24 hours, followed by visual detection of the occurrence of phase separation.

Transmission Electron Microscopy (TEM) micrographs were recorded with a JEOL 2000 FX electron microscope operating at 80 kV. Compression-moulded films of the host polymers were treated with rutheniumtetroxide for 16 hours, embedded in an epoxy resin and trimmed for microtoming. Thin sections were cut at room temperature with a Reichert Ultracut E microtome and used for TEM.

Characterisation of Drawn Host Polymers and Drawn Guest-Host Systems

The orientation of the host polymer was characterised by means of birefringence measurements. A Zeiss Universal polarising microscope, equipped with a quartz tilting compensator after Ehringhaus²¹ was used. The measured optical retardation of the drawn tapes was divided by the tape thickness to calculate the birefringence.

The orientation of the dichroic guests was analysed using polarised UV/VIS measurements. Absorbance spectra were recorded with a Perkin-Elmer Lambda 3B double beam UV/VIS spectrometer. The drawn, dye-containing tapes were coated with paraffin oil (spectrometric grade) and sandwiched between two glass slides, to reduce scattering caused by the fibrillar surface texture of the tapes. Subsequently, two linear polarisers were placed in the measuring beam and the reference beam of the spectrometer and a background correction was executed. The coated sample was inserted in the measuring beam and absorbance spectra in the visible wavelength range (400-700 nm) were recorded with the two polarisers positioned parallel, respectively, perpendicular to the drawing direction of the sample. Finally, a standard baseline correction was executed to correct the spectra for surface reflections.^{22,23,24} Specific details concerning the experimental set-up, measuring procedures and positioning of the sample are given in Appendix A.

2.3 Results

The results of the morphological study concerning the melt-crystallised host polymers and the phase behaviour of dye molecules in melt-crystallised guest-host systems will be presented first. Subsequently, the orientations of the host polymers and the guest molecules in drawn guest-host systems are evaluated.

Undrawn, Melt-Crystallised Host Polymers

In Figure 2.3, DSC curves of the four different polyethylenes are shown. The melting temperatures (peak temperatures), heats of fusion and crystallinities of the compression-moulded polyethylenes were determined from the DSC curves. The results of the calorimetric experiments are listed in Table 3 for the four host polymers.

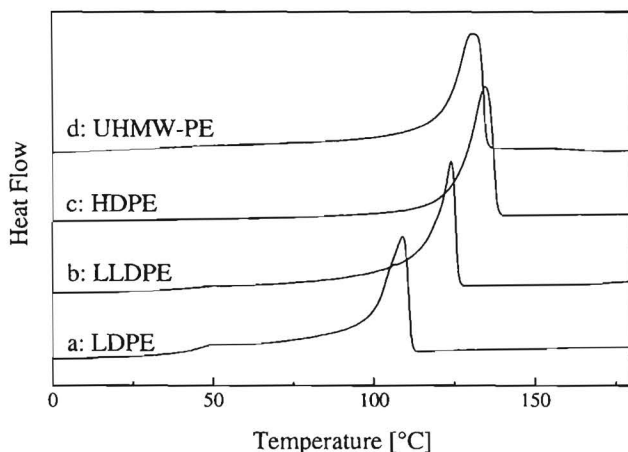


Figure 2.3: DSC thermograms of melt-crystallised polyethylenes: (a) LDPE, (b) LLDPE, (c) HDPE, (d) UHMW-PE

Table 3: Quantitative analysis (DSC and TEM) of the crystalline phase of the undrawn Host-Polyethylenes

Polymer	T_m [°C]	ΔH [J/g]	α_c [-]	d [nm]
LDPE	109	121.2	0.42	6
LLDPE	124	154.7	0.54	7
HDPE	136	166.0	0.57	13
UHMW-PE	130	166.1	0.57	13

In Figure 2.4, TEM micrographs are shown of the four compression moulded polyethylenes. The lamellar thickness (d) of the polyethylene crystals was derived from these TEM micrographs and is also listed in Table 3 (lamellar thicknesses are averaged over approximately 30 lamellae). The increase in lamellar thickness is accompanied by an increase in melting temperature, heat of fusion and crystallinity, respectively.

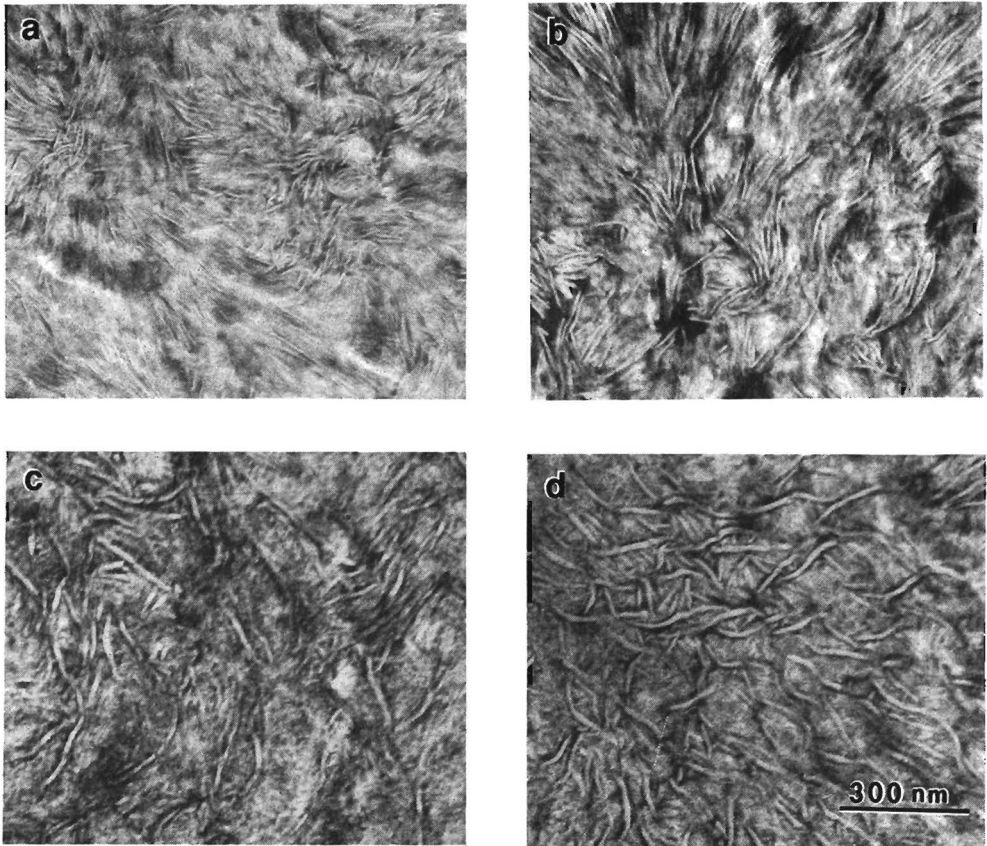


Figure 2.4: Transmission electron micrographs of melt-crystallised polyethylenes:

(a) LDPE, (b) LLDPE, (c) HDPE, (d) UHMW-PE

Undrawn, Melt-Crystallised Guest-Host Systems

The DSC curves of the model guest-host system (HDPE/Sudan Red B) are shown in Figure 2.5. At low dye concentrations (5 % w/w), only the melting endotherm of polyethylene can be distinguished (Figure 2.5-I, curve b). However at higher dye concentrations (>10 % w/w, Figure 2.5-II), two melting endotherms can be observed, one of the polyethylene phase and one of the dye phase. The pure dye possesses two melting endotherms, related to two different crystalline structures, but in the blends only one phase transition can be observed.

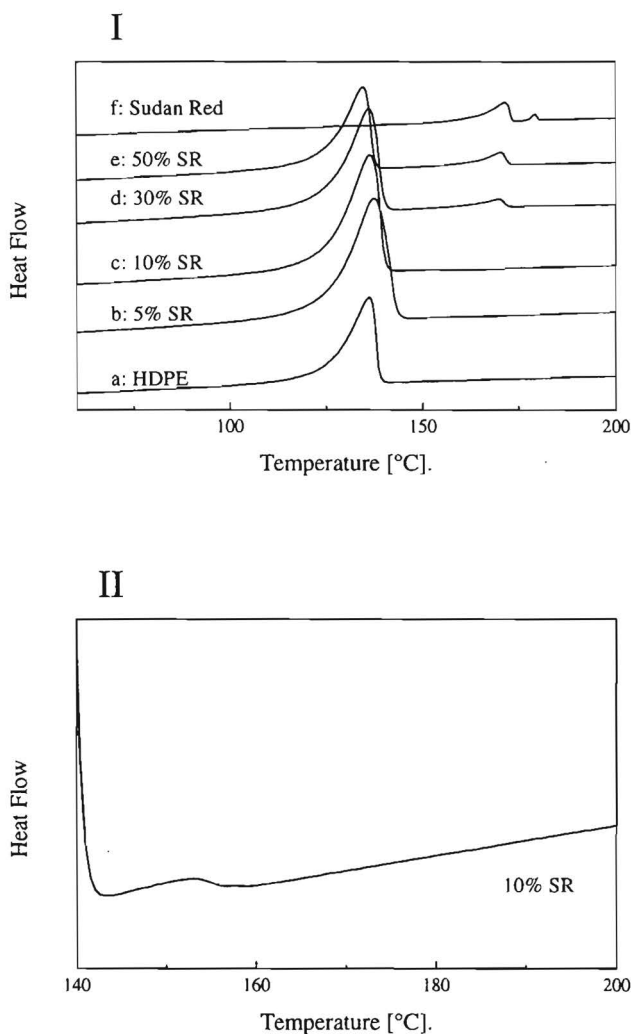


Figure 2.5: DSC thermograms of melt-crystallised HDPE/Sudan Red B systems: **I** all curves: (a) 0% dye; (b) 5% dye; (c) 10% dye; (d) 30% dye; (e) 50% dye; (f) 100% dye; **II** detail of HDPE/SR 10% w/w

The melting point depression of the dye indicates full miscibility in the melt. Also visually, no phase separation could be observed at elevated temperatures (210°C). These observations lead to the following schematic phase diagram:

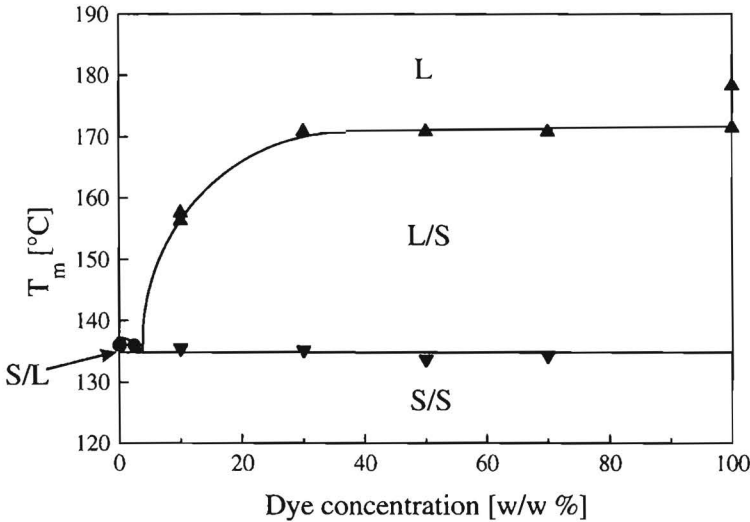


Figure 2.6: Schematic phase diagram of Sudan Red B-HDPE: T_m^{polymer} (●); T_m^{dye} (▲), T_{eutectic} (▼). (no efforts were made to locate the exact position of the eutecticum)

The eutecticum is located at low dye concentrations, and no further efforts were made to derive the exact location of this eutecticum. Full miscibility in the melt was not only observed for the HDPE/Dye system but also in the case of LDPE/Dye system. This melting behaviour of the polymer/dye mixtures is not unusual and agrees well with experimental data found in literature for binary mixtures consisting of polymers (PE or PPO) and other low molecular weight organic molecules (tetrachlorobenzene or anthracene).^{25,26}

In Figure 2.7, an optical micrograph is presented of a cross section of an isotropic Sudan Red B containing HDPE film. The dye concentration of this film (0.2% w/w) should be close to the eutecticum in the phase diagram. The micrograph is taken in polarised light. The red colour of the dye is observed throughout the cross section and no distinct, separate dye crystals can be distinguished.

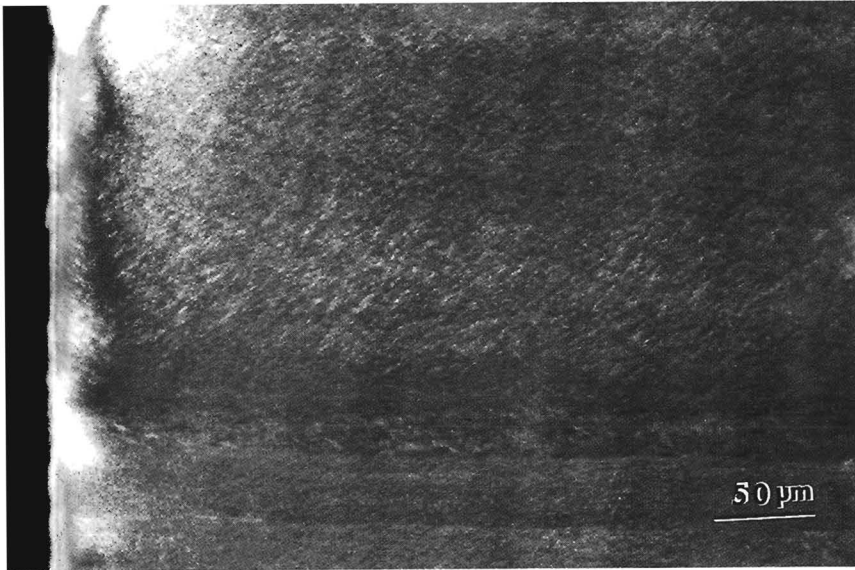


Figure 2.7: Optical micrograph in polarised light of a cross section of a compression moulded HDPE film containing 0.2% w/w Sudan Red B (magnification $\approx 350\times$)

Drawn Host Polymers

The orientation of the host-polyethylenes, expressed in terms of birefringence, is plotted in Figures 2.8 as a function of the draw ratio of the polymer. The birefringence data of Ward²⁷ and Pazur et al.²⁸ for Low-Density Polyethylene are also included in Figure 2.8. The experimental data seem to describe a unique curve as a function of the draw ratio of the polymer.

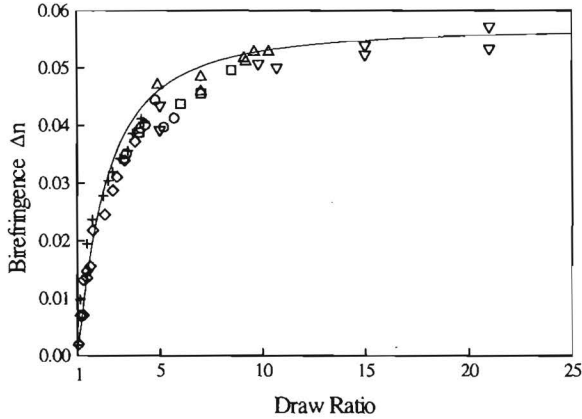


Figure 2.8: Birefringence of drawn polyethylenes: LDPE (O), LLDPE (Δ), HDPE (∇), UHMW-PE (\square), Ward²⁷, LDPE (\diamond), Pazur et al.²⁸; LDPE (+). Theoretical prediction (equations 1 and 2) after the pseudo-affine deformation scheme^{31,32} (—)

The solid line in Figure 2.8 is the theoretical prediction for the birefringence, calculated using equations 1 and 2.²⁹

$$\Delta n = \Delta n_{\max} \cdot f_h^{\text{polymer}} = \Delta n_{\max} \cdot \frac{3 \langle \cos^2 \theta \rangle - 1}{2} \quad (1)$$

$$\langle \cos^2 \theta \rangle = \frac{\lambda^3}{\lambda^3 - 1} - \frac{\lambda^3}{\sqrt{(\lambda^3 - 1)^3}} \cdot \arctan \sqrt{\lambda^3 - 1} \quad (2)$$

In equation (1), Δn_{\max} is the birefringence of the fully oriented sample. It is assumed that the perfectly oriented sample contains only crystalline material, and consequently Δn_{\max} is set equal to the intrinsic birefringence of the crystalline phase Δn_0^c . A value of Δn_0^c of 0.0585 was used.^{28,30} The average orientation of statistical chain segments ($\langle \cos^2 \theta \rangle$) can be calculated assuming the pseudo-affine deformation scheme to be valid. Affine deformation, originating

from the theory of rubber elasticity, implies that the changes in length and orientation of lines joining adjacent cross-links in the molecular network are identical to changes in lines marked on the macroscopic body. The pseudo-affine deformation assumption differs from the affine deformation in ignoring changes in length of the lines, i.e., rigid-rods orienting towards the draw axis. According to the pseudo-affine deformation scheme, the average orientation as a function of the draw ratio is given by equation (2).^{31,32} In this equation, λ is the draw ratio and θ is the angle between a statistical chain segment and the direction of uniaxial deformation. A good agreement is observed between experimental data and theoretical predictions which indicates that the pseudo-affine deformation scheme is valid for the drawn, melt-crystallised polyethylenes.

Drawn Guest-Host Systems

The dichroism of the guest-host system is demonstrated in Figure 2.9 where polarised absorbance spectra are shown for a drawn ($\lambda=10$) High-Density Polyethylene tape containing 0.2% w/w Sudan Red B. The polarisation direction of incident light is parallel (A_{\parallel}), respectively, perpendicular (A_{\perp}) to the orientation direction of the tape. The absorbance of the dye is anisotropic, i.e., depends on the angle between the orientation direction and the polarisation direction.

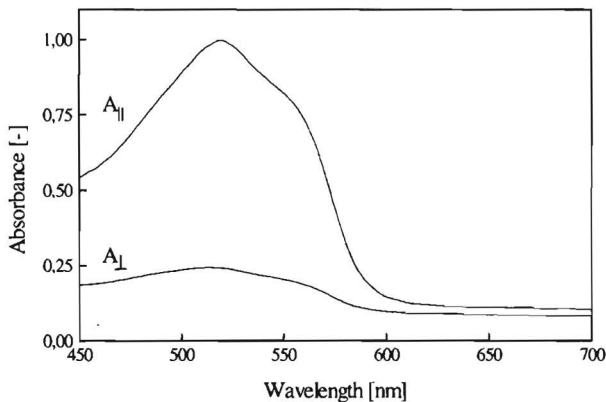


Figure 2.9: Absorbance spectra of drawn ($\lambda=10$) HDPE/Sudan Red B (0.2% w/w) film with incident light polarised parallel (A_{\parallel}) and perpendicular (A_{\perp}) to the drawing direction

The degree of orientation of the dichroic dyes can be quantified in terms of dichroic ratios [R] or order parameters [S]. These parameters are calculated from the polarised UV/VIS spectra using equations 3 and 4:^{33,34}

$$R = \frac{A_{\parallel}}{A_{\perp}} \quad (3)$$

$$S = \frac{(R-1)}{(R+2)} \quad (4)$$

The absorbances in equation 3 are measured at the wavelength of the absorbance maximum. The dichroic ratios and order parameters of the drawn polymer/dye systems containing Sudan Red B (SR) or Sudan Black B (SB) as a guest, are presented in Figure 2.10 as a function of draw ratio. For each guest-host system studied, it can be observed that the orientation of the guest molecules initially increases and levels off at higher (>15) draw ratios.

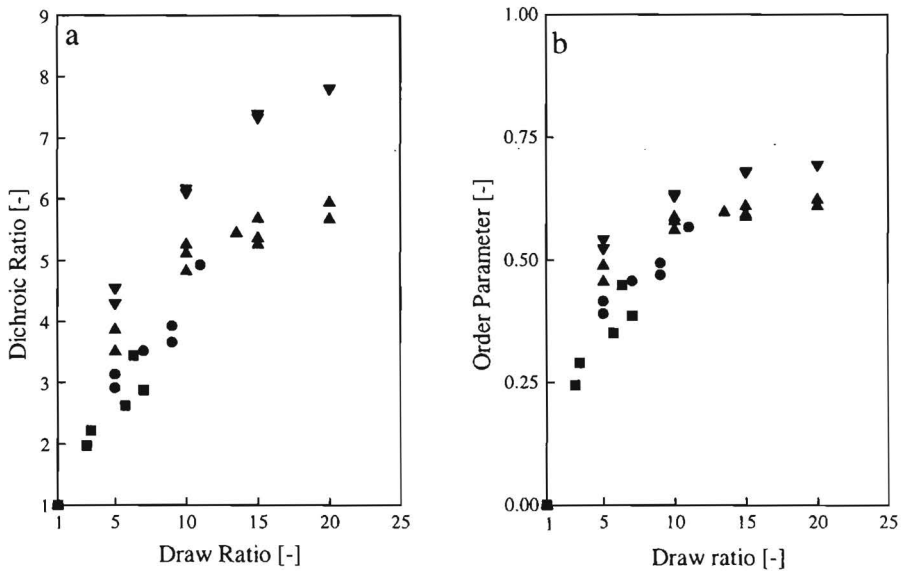


Figure 2.10: (a) Dichroic Ratio and (b) Order Parameter as a function of draw ratio; LDPE-SR (■), LLDPE-SR (●), HDPE-SR (▲), HDPE-SB (▼)

2.4 Discussion

The discussion is subdivided into two parts, first the morphology and drawing behaviour of the host polymers is discussed. Subsequently, the orientation mechanism of guest molecules in drawn guest-host systems is examined.

2.4.1 Orientation of the Host Polymer

In this study host polymers (polyethylenes) have been selected possessing extreme differences in molecular architecture (Table 1). These differences in architecture result, of course, in entirely different morphologies of the melt-crystallised polyethylene samples (DSC and TEM). The calorimetric investigations revealed, for example, that Low Density Polyethylene possesses the lowest melting temperature, heat of fusion, crystallinity and lamellar thickness (Table 3). If the other polyethylenes are examined, subsequently LLDPE, HDPE and UHMW-PE, an increase in melting temperature, crystallinity and lamellar thickness can be observed. The long-chain branches mainly present in LDPE restrict the growth of lamellae during crystallisation from the melt. The lamellar thickness, and consequently the crystallinity and melting temperature, therefore, remain low.^{20,35,36} Going from the less (long-chain) branched LLDPE to the linear polyethylenes (HDPE and UHMW-PE), the crystal growth will be less impeded resulting in higher lamellar thicknesses, melting temperatures and crystallinities (Table 3). However, these rather extreme differences in molecular structure and morphology of the polyethylenes before drawing are not reflected in the orientation after drawing. A unique relationship is found between the experimental birefringence data on one hand and the draw ratio on the other hand. Moreover, the experimental data of the birefringence agree surprisingly well with the theoretical predictions according to the pseudo-affine deformation scheme. To our opinion, these observations support the validity of the pseudo-affine deformation scheme in the description of the orientation of solid-state drawn polyethylenes. It needs to be stated here that the pseudo-affine deformation scheme is only valid under the following experimental conditions: a) the polymer should possess a random configuration prior to drawing, and b) drawing should be performed at temperatures well below the melting temperature of the polymer.³⁷ In the drawing experiments presented in this Chapter, precautions were taken to meet both experimental requirements, i.e., only isotropic, melt-crystallised polyethylenes were drawn at a drawing temperature adjusted to the specific polyethylene grade (section 2.2, Table 2). A direct consequence of the usefulness of the pseudo-affine deformation scheme is that, under the correct experimental conditions, molecular architecture and morphological features are irrelevant for the description of the orientation of drawn semi-crystalline polyethylenes.³⁸

2.4.2 Orientation of the Guest Molecules

From the DSC measurements it is concluded that upon cooling from an isotropic melt, eutectic solidification of the polyethylene and the dye molecules occurs. The eutectic point is located at low dye concentrations. These low dye concentrations (<0.5% w/w) are of practical importance for the production of sheet polarisers. For a good interpretation of the crystallisation behaviour at these low dye concentrations, a schematic drawing of a phase diagram with one eutecticum is shown below in Figure 2.11.

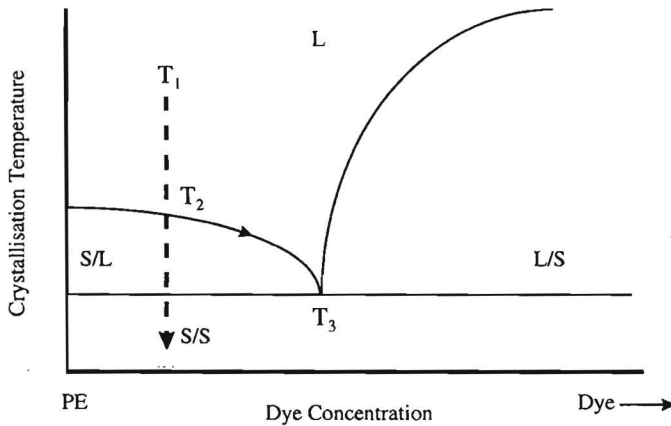


Figure 2.11: Left side of the schematic phase diagram of eutectic polymer/dye system at low dye concentrations.

At elevated temperatures (T_1), a homogeneous solution of the polymer and dye molecules is observed. A decrease in temperature results in phase separation at T_2 in the solid polymer and a liquid polymer/dye phase. Further lowering of the temperature is accompanied by crystallisation of the polyethylene which enriches the liquid phase with dye molecules (liquidus line) until the eutectic temperature is reached (T_3). At the eutectic temperature, both the remaining uncrystallised polymer and dye molecules will crystallise. The eutectic solidification results in a significant melting point depression (from 170°C to 135°C), and a very fine dispersion of small dye crystals in the PE matrix. The latter conclusion agrees well with the optical microscope observations which reveals that no separate dye crystals can be distinguished. The resolution of the optical microscope is limited to approximately 200 nm and, consequently, the dye crystals are smaller than this limit.

In the previous section, the orientation of the host polymer was investigated and found to obey the pseudo-affine deformation scheme. In the next section, we will focus on the orientation of the guest molecules (dichroic dyes) and it is attempted to establish a direct link between the

orientation of the host polymer and the guest molecule via the pseudo-affine deformation scheme.

The degree of orientation of the dye-molecules can be expressed in a Hermans orientation factor (f_H^{dye}). The relation between the Hermans orientation factor of the dye-molecules and the dichroic ratio R or the order parameter S_{dye} is given by equation 5.³⁴ The R_0 in equation 5, denotes the dichroic ratio at infinite draw ratio.

$$f_H^{\text{dye}} = \frac{(R-1)}{(R+2)} \cdot \frac{(R_0+2)}{(R_0-1)} = \frac{(R_0+2)}{(R_0-1)} \cdot S_{\text{dye}} \quad (5)$$

If it is assumed that the host polymer and guest molecule both orient in the affine mode, equations 1 and 5 can be set equal to each other ($f_H^{\text{dye}} = f_H^{\text{polymer}}$), resulting in equation 6:

$$S_{\text{dye}} = \frac{(R_0-1)}{(R_0+2)} \cdot f_H^{\text{polymer}} \quad (6)$$

Equation 6 represents a linear relationship between the order parameter of the dye-molecules and the Hermans orientation factor of the polymer.

Experimental values for the Hermans orientation factor of the polymer can be deduced from the birefringence data in Figure 2.8. Dividing the experimental birefringence by the maximum attainable birefringence directly yields this Hermans orientation factor, f_H^{polymer} (equation 1). Averaged values for the order parameter of the dye molecules S_{dye} (Figure 2.10b), are plotted in Figure 2.12 as a function of the averaged Hermans orientation factor of the polymer.

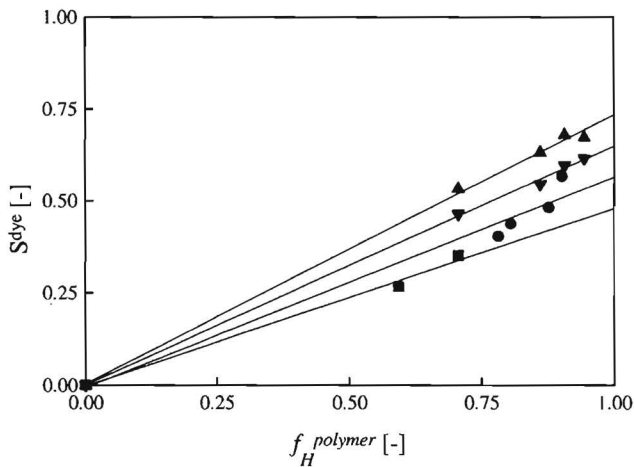


Figure 2.12: Order Parameter (S^{dye}) of the dye versus the Hermans orientation factor of the polymer (f_H^{polymer}): LDPE-SR (■), LLDPE-SR (●), HDPE-SR (▼), HDPE-SB (▲)

Due to localisation phenomena (necking) during solid-state drawing, it is impossible to obtain homogeneously deformed samples at low draw ratios ($\lambda < 3$). Consequently, no experimental data can be obtained at low orientations of the polymer ($f_H^{\text{polymer}} < 0.5$). In the case of the High-Density Polyethylene/Dye systems, linear relationships are observed between the orientation factor of the polymer (f_H^{polymer}) and the order parameter of the dye (S^{dye}), which indicates that the orientation of the host-polymer and guest molecule are indeed identical (equation 6). The orientation of the host-polymer was already found to obey the pseudo-affine deformation scheme, and therefore this deformation scheme is equally applicable for the description of the orientation of dye molecules oriented in High-Density Polyethylene. The eutectic solidification process of the polymer/dye system which occurs before drawing plays an important role during the orientation process. The melting temperature of the dye crystals is lowered (135°) and close to the drawing temperature of the guest-host system (120°C for HDPE/Dye systems). Consequently, also the small dye crystals can deform, just as the host-polymer in the pseudo-affine mode. If the polymer and dye would be immiscible in the melt, crystallisation would result in a morphology consisting of a polyethylene matrix containing large dye crystals with a higher melting temperature. In this case the crystals would probably resist deformation upon drawing and, consequently, would not adopt the same orientation as the host-polymer.

In the case of Low-Density Polyethylene and Linear-Low-Density Polyethylene, the maximum attainable draw ratio is low. Therefore, most of the experimental data have been obtained in the region where the deformation is not homogeneous, which might result in large experimental errors.

Assuming that equation 6 is valid then the slope of the straight lines ($\tan \alpha$) in Figure 2.10 is equal to the quotient $(R_0-1)/(R_0+2)$. The maximum attainable dichroic ratio for perfectly oriented guest-host systems (R_0) can be calculated from this slope using equation 7. The results are listed in Table 5.

$$R_0 = \frac{1 + 2 \tan \alpha}{1 - \tan \alpha} \quad (7)$$

Table 5: R_0 values and mismatch angle γ

Guest-Host system	R_0 [-]	γ [$^\circ$]
LDPE-SR	3.8	36
LLDPE-SR	5.0	32
HDPE-SR	6.6	29
HDPE-SB	9.1	25

For a single chromophore molecule, the electronic transition that accompanies the absorption of light can be represented as a vector attached to the molecule, the electronic dipole transition moment $\bar{\mu}$. The absorbed intensity due to an electric dipole transition process of a set of chromophore molecules (a small crystallite), having all the transition moments oriented in the same direction, is proportional to the square of the scalar product between the electric amplitude vector of light and the transition moment $\bar{\mu}$.³⁹ The absorbance will be at its maximum when the light vector is polarised parallel to the transition moment and zero when the light vector is perpendicular to it. Consequently, this set of aligned chromophores will have an infinite dichroic ratio R . In practise, the dichroic ratio of a guest-host system is not necessarily infinite. For instance, the transition dipole moment of the dye $\bar{\mu}$ is not necessarily parallel to the molecular axis of the chromophore. Consequently, in the case of a perfect match of the molecular orientation of the dye and the polymer, an optical mismatch angle can still be present (Figure 2.11, angle β). Secondly, the molecular axis of the dye molecule does not necessarily adopt a molecular orientation parallel to the polymer chains which also results in an optical mismatch angle (Figure 2.11, angle α).^{40,41} Because of these reasons, even a system of perfectly aligned chromophores may have a finite dichroic ratio R_0 .⁴²

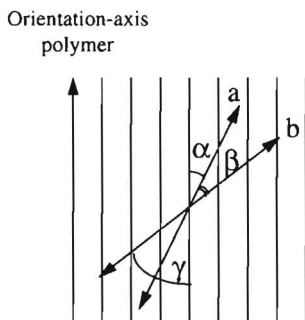


Figure 2.13: Orientation of the polymeric chains versus molecular axis (a) and transition dipole moment $\bar{\mu}$ (b) of the dye molecules

This finite dichroic ratio R_0 is directly related to the total mismatch angle $\gamma (= \alpha + \beta)$ between the polarisation direction of the incoming light and the transition moment $\bar{\mu}$ of the chromophores through equation 8:³⁴

$$R_0 = 2 \cot^2 \gamma \quad (8)$$

The calculated mismatch angles are listed in Table 5 and obviously, a higher R_0 -value is accompanied by a lower off-axis angle γ . The mismatch angle γ is, of course, dependent on the chemical structure of the dye (Table 5). However, it is also observed that the mismatch angle depends on the polyethylene type used. For instance, in the case of HDPE/Sudan Red (SR),

the mismatch angle γ is low in comparison to LDPE/Sudan Red. This experimental observation is somewhat puzzling because, intuitively, one might expect an identical mismatch angle in these guest-host systems. The pseudo-affine deformation scheme describes the overall orientation (i.e. amorphous and crystalline) of the polymer. The fact that this deformation mechanism is equally applicable to the dye molecules suggests that also the dye molecules duplicate the overall orientation of the host-polymer. Consequently it is likely that there exists two dye “populations”; one which copies the crystalline orientation and one which copies the amorphous orientation of the host polymer. Both populations have a specific mismatch angle and, thus, the overall mismatch angle γ which is measured experimentally depends on the distribution of the dye molecules between the amorphous and crystalline material. Therefore, we are inclined to attribute the differences in the mismatch angle γ to differences in the distribution of dye molecules which might depend on, for example, the network topology of the amorphous phase of the host polyethylenes.

The fact that the orientation of the host-polymer and the dichroic dyes can be described by the pseudo-affine deformation scheme indicates that a high draw ratio (>15) is necessary for effective dye orientation. Consequently, the selected host-polymers and chosen production methods should allow for high draw ratios, which implies that linear polyethylenes are intrinsically better host materials (in comparison with poly(vinyl alcohol)) for the orientation of guests, such as dichroic dyes. An additional requirement for a guest-host system with a high optical anisotropy (dichroic ratio) is a low mismatch angle between the transition moment of the dye and the chains of the host-polymer. Therefore, the chemical structure of the dye-molecules is also important to obtain high dichroic ratios.

In previous studies, dichroic dyes with a rod-like shape were used and ultra-drawn guest-host systems were obtained with a high dichroic ratio (>20).^{17,18,43} In the case of high dichroic ratios, the absorbance perpendicular to the drawing direction becomes extremely low and small variations in this absorbance have a large influence on, for instance, the dichroic ratio (equation 3). In this Chapter, dichroic dyes with a less rod-like chemical structure were selected (Figure 2.2), in order to generate drawn guest-host systems with a moderate dichroic ratio which allows accurate experimental characterisation, even at high draw ratios. Of course, this results in rather poor polarisers but makes these guest-host systems a suitable model system for the validation of a theoretical model in the next Chapter. The topic of the ultimate properties of drawn guest-host systems and its relation to the structure of the dichroic dyes is also re-discussed in the next Chapter (Chapter 3, section 3.6).

2.5 Conclusions

The orientation mechanism of guest-host systems based on oriented polyethylene/dichroic dye systems was investigated. It is shown that, due to eutectic solidification, small dichroic dye crystals are intimately mixed with the host-polymer. Upon solid-state drawing, the orientation of both the host-polyethylene and the dichroic dyes (Sudan Red B, Sudan Black B) can be accurately described by the pseudo-affine deformation scheme. The direct link between the orientation of the polymer and dichroic guest molecule indicates that high maximum attainable draw ratios (>15) are a prerequisite for obtaining high performance polarisers. This implies also that linear polyethylenes are intrinsically better host materials (in comparison with PVA) for the orientation of guests such as dichroic dyes. Moreover, it is also shown that the chemical structure (and shape) of the dye molecule also has a profound influence on the dichroism and order parameter of these guest-host systems.

2.6 References

- 1 Driscoll W.G. Vaughan W., *Handbook of Optics*, Mc Graw-Hill: New York, 1987
- 2 Hecht E., *Optics*, 2nd ed., Addison Wesley: London, 1977
- 3 Land E.H., West C.D., *Colloid Chemistry*, ed. J. Alexander, Vol. 6, Reinhold Publishing Corporation, 1946
- 4 Land E.H., *J. Opt. Soc. Am.*, **1940**, *30*, 230
- 5 Mizoguchi R., Kobayashi K., Shimomura T., Kobayashi S., *Displays*, **1983**, 201
- 6 Originally there were four types of sheet polarisers, the J,H,K and L-sheet polariser. However, the J-sheet polariser containing oriented dichroic herapathite crystals is of historical interest only.
- 7 Miyasaka K., *Adv. Polym. Sci.*, **1992**, *108*, 91
- 8 Nagatsuka T., Shimomura T., Oishi Y., *SID 85 Digest*, **1985**, 74
- 9 Capaccio G., Ward I.M., *Polymer*, **1974**, *15*, 233
- 10 Smith P., Lemstra P.J., Booij H.C., *J. Polym. Sci. Polym. Phys. Ed.*, **1981**, *19*, 877
- 11 Smith P., Lemstra P.J., *J. Polym. Sci. Polym. Phys. Ed.*, **1981**, *19*, 1007
- 12 Zwijnenburg A., Pennings A.J., *Coll. Polym. Sci.*, **1976**, *254*, 868
- 13 Peterlin A., *Coll. Polym. Sci.*, **1987**, *48*, 4099
- 14 Tashiro K., Kobayashi M., Tadokoro H., *Macromolecules*, **1978**, *11*, 914
- 15 Kelly A., Macmillan N.H., *Strong Solids*, 3th ed., Clarendon Press: Oxford, 1986
- 16 Schellekens R., Bastiaansen C., *J. Appl. Polym. Sci.*, **1991**, *43*, 2311
- 17 Bastiaansen C., Schmidt H.W., Nishino T., Smith P., *Polymer*, **1993**, *34*, 3951
- 18 Bastiaansen C., Schmidt H.W., Govaert L., Smith P., *Polym. Prep.*, **1993**, *34*, 776
- 19 Dirix Y., Tervoort T.A., Bastiaansen C., *Macromolecules*, **1995**, 28,486
- 20 Wunderlich B., *Macromolecular Physics*, Academic Press: New York, 1973
- 21 Ehringhaus A., *Zeitschr. F. Kristallogr.*, **1931**, *76*, 315
- 22 Wold E., Bremer J., Hunderi O., *J. Polym. Sci. Polym. Phys.*, **1993**, *31*, 579
- 23 Borsdorf R., Scholz M. *Spektroskopische Methoden (IR, UV/VIS) in der Organischen Chemie*, Akademie-Verlag: Berlin, 1989
- 24 Cunningham A., Ward I.M., Willis H.A., Zichy V., *Polymer*, **1974**, *15*, 749
- 25 Aerts L., Berghmans H., *Bull. Soc. Chim. Belg.*, **1990**, *99*, 931

- 26 Smith P., Pennings A.J., *J. Mat. Sci.*, **1976**, *11*, 1450
- 27 Ward I.M., *Mechanical Properties of Solid Polymers*. 2nd ed., John Wiley & Sons: New York, 1985
- 28 Pazur R.J., Ajji A., Prud'homme R.E., *Polymer*, **1993**, *34*, 4004
- 29 Hermans P.H., Heikens D., *Rec. Trav. Chem. Pays-Bas*, **1952**, *71*, 49
- 30 Wedgewood A.R., Seferis J.C., *Polym. Eng. Sci.*, **1984**, *24*, 328
- 31 Kratky O., *Kolloid Z.*, **1933**, *64*, 213
- 32 Kuhn W., Grün F., *Kolloid Z.*, **1942**, *101*, 248
- 33 Driscoll W.G., Vaughan W., *Handbook of Optics*, Mc Graw-Hill: New York, 1987
- 34 Read B.E., Stein R.S., *Macromolecules*, **1968**, *1*, 116
- 35 Wunderlich B., Poland D., *J. Polym. Sci. Part A*, **1963**, *1*, 357
- 36 Willbourn A.H., *J. Polym. Sci.*, **1959**, *34*, 569
- 37 Irvine P.A., Smith P., *Macromolecules*, **1986**, *19*, 240
- 38 Dirix Y., Tervoort T.A., Bastiaansen C.W.M., Lemstra P.J., *J. Text Inst.*, **1995**, *86*, 314
- 39 Norden B., *Appl. Spectroscop. Rev.*, **1978**, *14(2)*, 157
- 40 Philips P.J., *Chem. Rev.*, **1990**, *90*, 425
- 41 Sagiv J., *Isr. J. Chem.*, **1979**, *18*, 339
- 42 Fraser R.D.B., *J. Chem. Phys.*, **1953**, *21(9)*, 1511
- 43 Bastiaansen C.W.M., *PhD thesis*, Eindhoven University of Technology, 1991

Chapter 3*

Modelling of the Optical Properties of Dichroic Polarisers

3.1 Introduction

In the previous Chapter, the orientation mechanisms of the host polymer and guest molecules in dye-containing polyolefins were investigated. It was shown that the orientations of host and guest can be described accurately by the pseudo-affine deformation scheme. The properties of these drawn guest-host systems are commonly expressed in a variety of optical characteristics, which can roughly be subdivided into two classes: a) parameters related to the orientation and optical characteristics of the guest molecules only, and b) parameters related to the polarising performance of the guest-host system. The dichroic ratio (R) and order parameter (S), already introduced in Chapter 2, belong to the former category. The polarising efficiency (PE) and single-piece transmittance (T_{sp}) are application criteria and are related to, respectively, the contrast ratio (in transmittance) between two parallel and two crossed polarisers, and to the transmittance of a single polariser in non-polarised light.^{1,2,3} As pointed out in the general introduction, images are formed in LCD-cells (TN and STN) by electrically switching of the liquid crystalline molecules in combination with the top and bottom polarisers. For the transparent regions of the display, where light passes the bottom polariser (Figure 1.6), a high single-piece transmittance is required. The dark regions, where light encounters the polarisers in a crossed position, demand a high polarising efficiency. Consequently, to obtain good contrast in the display, polarisers are needed which possess a combination of both a high single-piece transmittance and a high polarising efficiency (preferentially $PE > 0.95$, $T_{sp} > 0.35$).

* This chapter is reproduced in part from:

Dirix Y., Tervoort T.A., Bastiaansen C., *Macromolecules*, **1995**, 28, 486

Dirix Y., Tervoort T.A., Bastiaansen C., *Macromolecules*, **1997**, 30, 2175

The dichroic ratio and polarising efficiency of a model system (HDPE/Sudan Red B) which was also used in the previous Chapter, are plotted in Figure 3.1 as a function of the draw ratio of the films. The experimental data indicate that the dichroic ratio increases with increasing draw ratio, but, by contrast and seemingly contradictory, the polarising efficiency decreases at high draw ratios. These observations seem to contradict because, at first sight, a highly oriented guest-host system (high dichroic ratio) results in a low contrast ratio (PE) of the polariser.

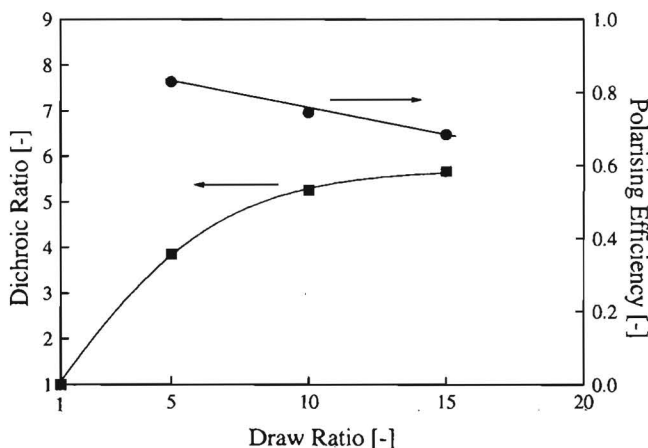


Figure 3.1: Dichroic ratio (■) and polarising efficiency (●) as a function of draw ratio

The principal objectives of this Chapter are: (i) to derive a theoretical framework for the development of optical characteristics of these polarisers and to analyse the above mentioned apparent discrepancy, (ii) to study the influence of parameters like the drawability or dye anisotropy of the guest-host system on the polarising properties, (iii) to predict the ultimate optical properties of oriented polymer/dye polarisers and to compare the predictions with experimental data on polymer/dye polarisers based on poly(vinyl alcohol) and polypropylene.

3.2 Theoretical section

According to the pseudo-affine deformation scheme, the average orientation of statistical chain segments ($\langle \cos^2 \theta \rangle$) with respect to the direction of (uniaxial) deformation is given by equation 1:^{4,5,6}

$$\langle \cos^2 \theta \rangle = \frac{\lambda^3}{\lambda^3 - 1} - \frac{\lambda^3}{\sqrt{(\lambda^3 - 1)^3}} \cdot \arctan \sqrt{(\lambda^3 - 1)} \quad (1)$$

In equation 1, λ is the draw ratio and θ the angle between a statistical chain segment and the draw ratio. It was shown previously that the pseudo-affine deformation scheme reasonably describes the development of orientation upon drawing of semi-crystalline polymers.^{7,8,9,10} In chapter 2 of this thesis, it was established that the development of orientation of the dichroic dyes during tensile deformation is identical to that of the host-polymer, as is represented by equation 2, where the subscripts “dye” and “pol” refer to the dichroic dyes and the polymer, respectively:

$$\langle \cos^2 \theta \rangle_{dye} = \langle \cos^2 \theta \rangle_{pol} \quad (2)$$

In section 2.4.3, it was pointed out already that the electronic dipole transition moment $\bar{\mu}$ does not necessarily adopt the same orientation as the polymeric chains (angles α , β , and γ , Figure 2.13). Unfortunately, the off-axis angles α and β are usually unknown which complicates the derivation of the optical properties of drawn guest-host systems from first principles.

In this study it is therefore assumed that the present systems are comprised of optically transverse-isotropic elements, ignoring physical details like the angles α and β . The extinction coefficient tensor, ϵ_{ij} , of such an element is represented by equation 3, where the subscripts “ \perp ” and “ \parallel ” denote the directions perpendicular and parallel to the axis of transverse isotropy of the elements.^{11,12}

$$\epsilon_{ij} = \begin{bmatrix} \epsilon_{\perp} & 0 & 0 \\ 0 & \epsilon_{\perp} & 0 \\ 0 & 0 & \epsilon_{\parallel} \end{bmatrix} \quad (3)$$

In fact, the ratio between the extinction coefficients parallel and perpendicular ($\epsilon_{\parallel}/\epsilon_{\perp}$), is the dichroic ratio at infinite draw ratio, R_0 , which was introduced already in chapter 2.

The macroscopic molar extinction coefficients (E_{\parallel} and E_{\perp}) of an aggregate of optically anisotropic elements (where the subscripts “ \parallel ” and “ \perp ” now denote the directions parallel and perpendicular to the drawing direction) can be calculated from the extinction coefficient tensor ϵ_{ij} by a coordinate transformation from the microscopic frame to the laboratory frame, followed by an averaging procedure.¹¹ For fibre symmetry this results in equations 4 and 5, where $\langle \cos^2 \theta \rangle$ is the average orientation of the elements with respect to the drawing direction.

$$E_{\parallel} = \langle \sin^2 \theta \rangle \epsilon_{\perp} + \langle \cos^2 \theta \rangle \epsilon_{\parallel} \quad (4)$$

$$E_{\perp} = \frac{1}{2}(\langle \cos^2 \theta \rangle + 1)\epsilon_{\perp} + \frac{1}{2}\langle \sin^2 \theta \rangle \epsilon_{\parallel} \quad (5)$$

Substitution of equation 1 in equations 4 and 5, directly yields the relationships between the draw ratio (λ) applied to the guest-host system, and the macroscopic extinction coefficients parallel ($E_{||}$) and perpendicular (E_{\perp}) to the direction of draw.*

The absorbance parallel and perpendicular to the direction of draw ($A_{||}$ and A_{\perp}) can be calculated from equations 4 and 5 using Lambert-Beer's Law (equations 6 and 7, see also Appendix B):^{15,16}

$$A_{||} = E_{||} \cdot c \cdot d \quad (6)$$

$$A_{\perp} = E_{\perp} \cdot c \cdot d \quad (7)$$

In equations 6 and 7, c and d denote, respectively, the specimen thickness (cm) and the concentration of the dichroic dye (mol/l) in the host polymer. The corresponding transmissions (T) are calculated using equations 8 and 9:¹⁵

$$T_{||} = 10^{-A_{||}} \quad (8)$$

$$T_{\perp} = 10^{-A_{\perp}} \quad (9)$$

From the respective absorbances and transmittances, all relevant optical properties of the polariser can be calculated. The equations for the dichroic ratio (R), order parameter (S), polarising efficiency (PE) and single-piece transmittance (T_{sp}) are given below:^{1,2,3}

$$R = \frac{A_{||}}{A_{\perp}} \quad (10)$$

$$S = \frac{R-1}{R+2} \quad (11)$$

$$PE = \frac{T_{\perp} - T_{||}}{T_{\perp} + T_{||}} \quad (12)$$

* Verification of equations 4 and 5 can be performed by substitution of these equations in the Hermans orientation function (f_h):¹⁴

$$f_h = \frac{R-1}{R+2} \cdot \frac{R_0+2}{R_0-1} = \frac{\left(\frac{E_{||}}{E_{\perp}}\right) - 1}{\left(\frac{E_{\perp}}{E_{||}}\right) + 2} \cdot \frac{\left(\frac{\varepsilon_{||}}{\varepsilon_{\perp}}\right) + 2}{\left(\frac{\varepsilon_{\perp}}{\varepsilon_{||}}\right) - 1} = \frac{3 \langle \cos^2 \theta \rangle - 1}{2}$$

This substitution correctly results in the well-known expression for the Hermans orientation function.¹³

3.3 Model predictions

The material and experimental parameters in the equations of the previous paragraph are: (i) the extinction coefficient tensor ϵ_{ij} of the optical elements, (ii) the dye concentration (c), and (iii) the thickness (d) of the polariser. For illustrative purposes only, the following (arbitrarily chosen) values for these parameters are used to demonstrate some of the properties of the model:

$$\begin{aligned} \epsilon_{||} &= 100 \times 10^3 \quad [\text{l.mol}^{-1}.\text{cm}^{-1}] & \epsilon_{\perp} &= 2.5 \times 10^3 \quad [\text{l.mol}^{-1}.\text{cm}^{-1}] \\ R_0 &= 40 \quad [-] & c &= 2 \times 10^{-3} \quad [\text{mol.l}^{-1}] \\ d_0 &= 0.5, 1, 2 \quad [\times 10^{-2} \text{ cm}] \end{aligned}$$

here, d_0 is the initial thickness of the film prior to drawing. During tensile deformation, the values of $\epsilon_{||}$, ϵ_{\perp} and c remain, of course, constant. By contrast, the thickness of the films decreases with increasing draw ratio. In the case of uniaxial deformation, assuming isotropic lateral contraction and deformation at constant volume, the thickness of the film d as a function of draw ratio can be described by:

$$d = \frac{d_0}{\sqrt{\lambda}} \quad (14)$$

The effect of decreasing thickness on the optical properties can now be calculated by substitution of equation 14 into equations 6 and 7.

In Figure 3.2, the model predictions for the dichroic ratio are plotted as a function of the draw ratio. In accordance with expectations, it is found that the dichroic ratio increases with increasing draw ratio and is independent of the initial thickness of the films. The polarising efficiency passes through a maximum and decreases at high draw ratios (Figure 3.3). Moreover, the polarising efficiency strongly depends on the original thickness of the films. Clearly, in contrast to the dichroic ratio, the polarising efficiency is not normalised with respect to parameters such as film thickness (or dye-concentration)

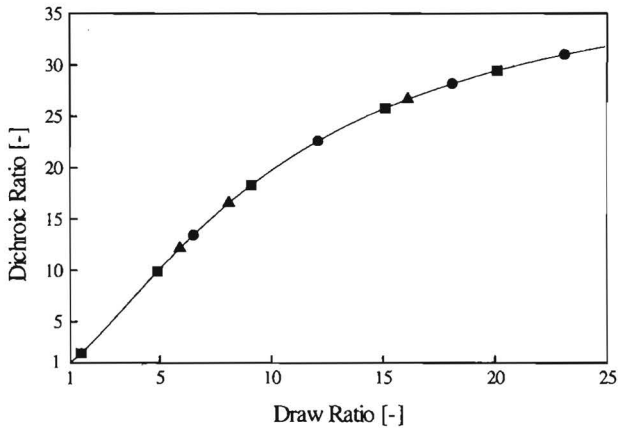


Figure 3.2: Dichroic ratio (R) as a function of draw ratio and initial film thickness; $d_0 = 0.005$ cm (■), $d_0 = 0.01$ cm (▲), $d_0 = 0.02$ cm (●)

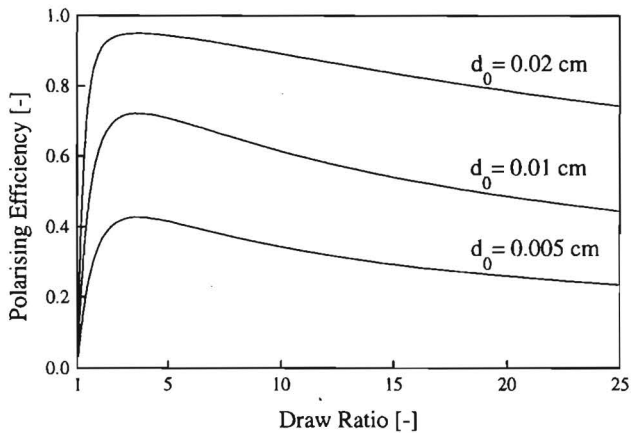


Figure 3.3: Polarising Efficiency (PE) as a function of draw ratio and initial film thickness

The single-piece transmittance is plotted in Figure 3.4 as a function of draw ratio and initial film thickness. The predictions in this figure show that the single-piece transmittance increases with increasing draw ratio and decreasing film thickness. The polarising efficiency and single-piece transmittance appear to be mutually dependent, and oppositely affected by variations of the initial film thickness. For instance, increasing the thickness at a given draw ratio, enhances the polarising efficiency (Figure 3.3), but simultaneously reduces the single-piece transmittance (Figure 3.4).

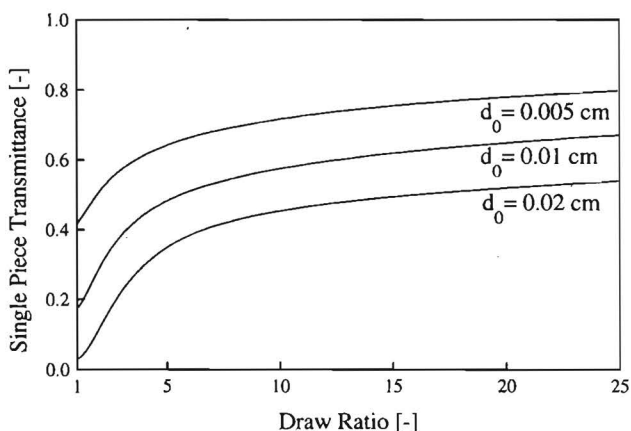


Figure 3.4: Single-piece transmittance (T_{sp}) as a function of draw ratio and initial film thickness

In the next paragraphs it is attempted to verify the usefulness of the theoretical model by comparing experimental data on drawn polyethylene/dye systems with the theoretical predictions of the model.

3.4 Experimental

Preparation of polymer/dye films

Linear High-Density Polyethylene (HDPE, Hostalen Gur 7255P, Hoechst Ruhrchemie, Germany; $M_w = 350.000$ g/mol) was used in combination with a di-azo dye Sudan Red B (Figure 3.5a). Melt-crystallised films with an initial thickness of 0.01 cm and 0.007 cm and a dye concentration of 0.2 % w/w (5.2×10^{-3} mol/l) were produced and drawn at 120 °C after standard procedures described in section 2.2.

Isotactic Polypropylene (i-PP) used in this study was Stamyilan 14M10 (DSM Geleen, The Netherlands). The dichroic dye was a linear tri-azo dye (BASF/Germany) with a melting temperature of 124 °C. The chemical structure of the tri-azo dye is shown in Figure 3.5b.

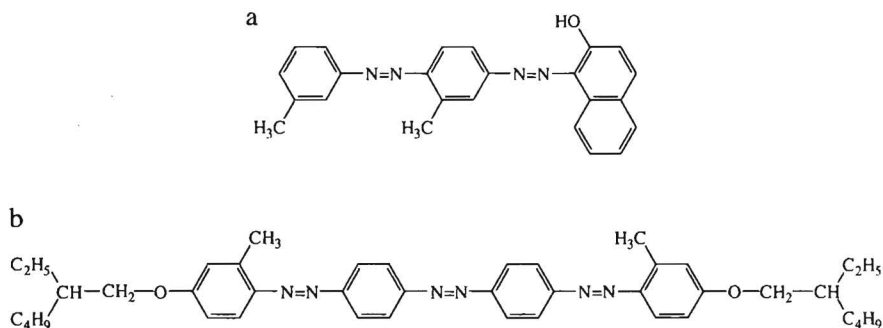


Figure 3.5: Chemical structures of a) Sudan Red B and b) linear tri-azo dye

A mixture of *i*-polypropylene containing 0.25% (w/w) tri-azo dye was fed into a twin screw extruder equipped with a sheet extrusion dye. Tapes were cut from the cast films (30×15×0.33 mm) and subsequently drawn on thermostatically controlled hot-shoes. The tapes were pre-drawn at 135 °C and finally post-drawn at 150 °C. The draw ratio was determined as the displacement of ink-marks.

Characterisation of polarising performance

Two different experimental procedures were used in this Chapter to determine the optical performance of oriented polymer/dye polarisers. The main difference between these methods is that in the first one reference polarisers are used, whereas in the second method no auxiliary polarisers are required. Specific details about both measuring procedures can be found in Appendix A.

For the HDPE/Sudan Red B system possessing moderate optical anisotropy, a Perkin-Elmer Lambda 3B double beam UV-VIS spectrometer was used. To reduce scattering at the (fibrillar) film surface, the drawn tapes were coated with a thin layer of paraffin oil and placed between glass slides.¹⁷ Absorbance spectra in the visible wavelength range (400-700 nm) were recorded with two reference polarisers positioned in the measuring and reference beam of the spectrometer. The coated sample was inserted in the measuring beam and absorbance spectra were obtained with the two reference polarisers positioned parallel and perpendicular, respectively, to the draw direction of the sample. A standard base-line correction was performed to correct the spectra for surface reflections etc.^{18,19,20}

The drawn *i*-PP/tri-azo tapes were also coated with paraffin oil and sandwiched between glass slides. The optical anisotropy of the tapes was analysed with a Perkin Elmer Lambda 900 double beam UV/VIS spectrometer. For these highly anisotropic systems, a special measuring procedure was adopted to determine the polarising performance without using auxiliary polarisers. In this method special care is also taken to avoid influences of the instrumental

polarisation and reflections at the glass/air interfaces. Four transmittances were measured: no sample in the measuring beam (T_0), the drawn sample positioned horizontal (T_h), respectively, vertical (T_v) in the measuring beam, and, finally, two crossed samples in the measuring beam (T_{hv}). From these transmittances the polarising efficiency and single-piece transmittance can be calculated using equations A.9 and A.10 (the equations are derived in Appendix A):

$$PE = \sqrt{1 - \frac{4T_0 T_{hv}}{(T_h + T_v)^2}} \quad (\text{A.9})$$

$$T_{sp} = \frac{T_h + T_v}{2T_0} \quad (\text{A.10})$$

3.5 Model verification

The thickness of the HDPE/Sudan Red B tapes is shown in Figure 3.6 as a function of the draw ratio. According to equation 14, the thickness should be inversely proportional to the square root of the macroscopic draw ratio. However, it is observed that the thickness after drawing deviates significantly from the values according to equation 14; the measured thickness is systematically above the expected value.

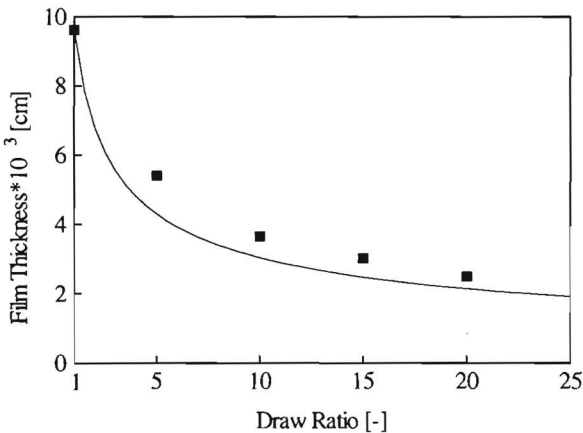


Figure 3.6: Film thickness after drawing; experimental (■), calculated after equation 14 (—)

The experimental values of the dichroic ratio, polarising efficiency and single-piece transmittance for a model system based on HDPE/Sudan Red B are depicted in Figures 3.7, 3.8 and 3.9 (open symbols). The data are derived from the absorbance maximum of the dye (520 nm). The experimental transmittances ($T_{||}$ and T_{\perp}) necessary to calculate the polarising efficiency and single-piece transmittance were derived from the corresponding absorbances (after baseline correction!) with equations 8 and 9, respectively.

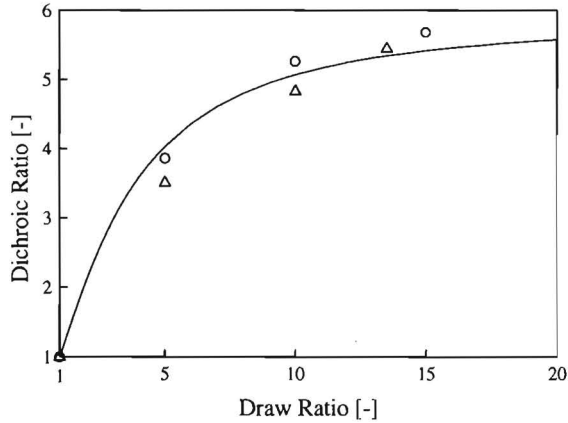


Figure 3.7: Dichroic ratio as a function of draw ratio and initial film thickness, $d_0 = 0.01$ cm (Δ), $d_0 = 0.007$ cm (O); theoretical (—)

Comparison of the experimental data with the theoretical predictions in Figures 3.2, 3.3 and 3.4 indicates that the general trends are correctly predicted. The absolute values, of course, deviate due to the arbitrary selection of the values for $\epsilon_{||}$, ϵ_{\perp} , d_0 and c in the previous section.

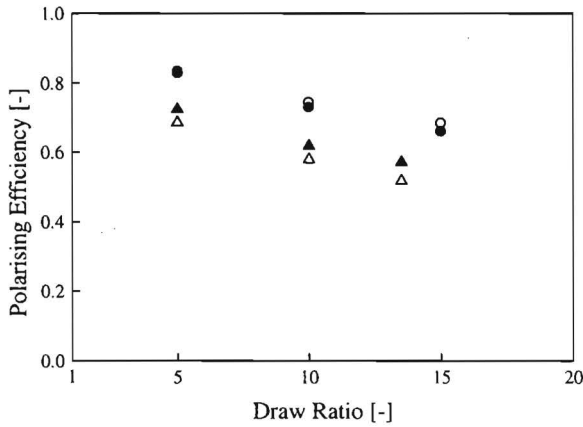


Figure 3.8: Polarising efficiency (PE) as a function of the draw ratio and initial film thickness: experimental, $d_0 = 0.01$ cm (O), $d_0 = 0.007$ cm (Δ); calculated, $d_0 = 0.01$ cm (\bullet), $d_0 = 0.007$ cm (\blacktriangle)

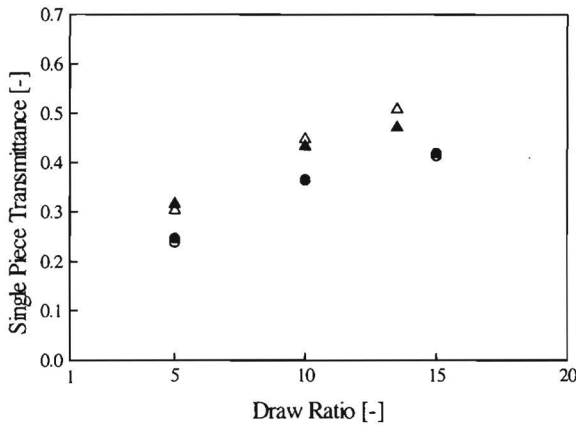


Figure 3.9: Single-piece transmittance (T_{sp}) as a function of the draw ratio and initial film thickness: experimental, $d_0 = 0.01$ cm (O), $d_0 = 0.007$ cm (Δ); calculated, $d_0 = 0.01$ cm (\bullet), $d_0 = 0.007$ cm (\blacktriangle)

To obtain a more accurate description of the various characteristics of the polarising films, the correct values of the above mentioned parameters need to be substituted in the relevant equations. In the theoretical section it was discussed that the absolute values of ϵ_{ij} and ϵ_{\perp} cannot be derived from first principles. Therefore, an experimental procedure was used to estimate the values for the extinction tensor ϵ_{ij} . This method was first used by Ward et al. in modelling the mechanical properties of drawn semi-crystalline polymers.^{9,11} It employs

experimental data of an oriented aggregate for the estimation of the characteristics of the constituting elements. In this particular case, the absorbances ($A_{||}$ and A_{\perp}) of a particular specimen are measured (here $d_0 = 0.01$ cm, $c = 5.2 \times 10^{-3}$, $\lambda = 10$) and the macroscopic extinction coefficients ($E_{||}$ and E_{\perp}) are calculated using equations 6 and 7. In this calculation the thickness should be inversely proportional to the square root of the draw ratio. Invariably, the thickness of the drawn films was found to be above that expected (Figure 3.6). Therefore, these experimental values for the film thickness after drawing were used in the calculation of the macroscopic extinction coefficients ($E_{||}$ and E_{\perp}) of the tape. From $E_{||}$, E_{\perp} and the average orientation ($\langle \cos^2\theta \rangle$, equation 1), the values of the microscopic extinction coefficients $\epsilon_{||}$ and ϵ_{\perp} are calculated using equations 4 and 5. The extinction tensor ϵ_{ij} ($\epsilon_{||} = 54.5 \times 10^3$ [l.mol.cm⁻¹] and $\epsilon_{\perp} = 9.2 \times 10^3$ [l.mol.cm⁻¹]) thus obtained is used to calculate the optical properties with the model.

The results of the calculations are shown in Figures 3.7, 3.8 and 3.9 (closed symbols). A good agreement is observed between theoretical predictions and experimental data which, in our view, strongly supports the validity of the present approach.

3.6 Ultimate optical properties

The present model can be used to predict the optical characteristics and, by methodically varying the input parameters, find the prerequisites for the production of a high-performance polariser ($PE > 0.95$, $T_{sp} > 0.35$).

In Figure 3.10, the predicted values for the polarising efficiency as a function of the single-piece transmittance are depicted. The curve is obtained by increasing the initial film thickness at a constant draw ratio ($\lambda = 5$) and the combinations of PE and T_{sp} are calculated with the identical input parameters of section 3.3 (extinction coefficients $\epsilon_{||}$, ϵ_{\perp} and concentration c).

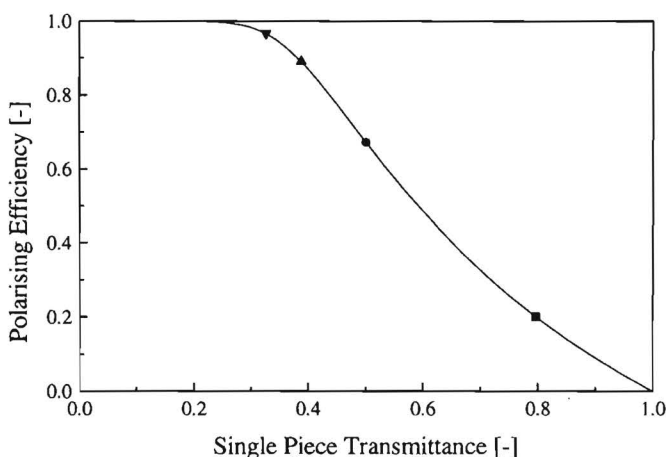


Figure 3.10: Polarising efficiency versus single-piece transmittance as a function of initial film thickness at a constant draw ratios ($\lambda = 5$) and constant optical anisotropy of the dye ($\epsilon_{||} / \epsilon_{\perp} = 40$); $d_0 = 10^{-3}$ cm (■), $d_0 = 4 \times 10^{-3}$ cm (●), $d_0 = 7 \times 10^{-3}$ cm (▲), $d_0 = 10^{-2}$ cm (▼)

This figure illustrates that the values of PE and T_{sp} can be varied within a wide range simply by adjusting the initial film thickness. Identical curves can be drawn for variations of the dye-concentration in the films because in Lambert-Beers law (equations 6 and 7), the thickness (d) and concentration (c) are equivalent. Moreover, in Figure 3.11 it is shown that both the polarising efficiency and single-piece transmittance are enhanced by increasing the draw ratio of the films. For each draw ratio, the curve is again obtained by increasing the initial film thickness at a constant optical anisotropy of the dye ($\epsilon_{||} / \epsilon_{\perp} = 40$).

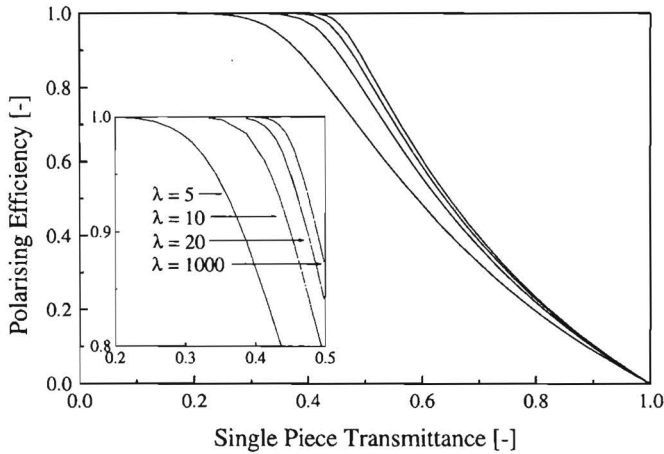


Figure 3.11: Polarising efficiency versus single-piece transmittance as a function of draw ratio (λ) at a constant optical anisotropy of the dye ($\epsilon_{||} / \epsilon_{\perp} = 40$)

In Figure 3.12, the influence of the optical anisotropy of the dichroic dye is demonstrated by increasing the ratio between the extraordinary and ordinary extinction coefficients of the element ($\epsilon_{||}/\epsilon_{\perp} = R_0$, at a constant draw ratio $\lambda=20$). Identical to the predictions of Figure 3.10, the initial film thickness is again the running parameter on each curve of Figure 3.12. Obviously, increasing the anisotropy of the dye-molecule, shifts the PE- T_{sp} curve to higher values.

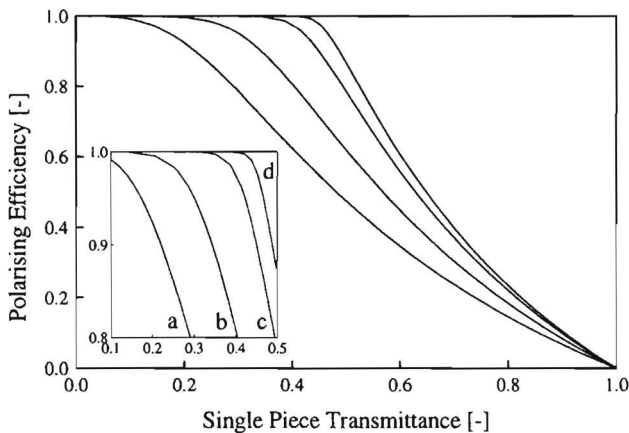


Figure 3.12: Polarising efficiency versus single-piece transmittance as a function of the anisotropy of the dye ($\epsilon_{||}/\epsilon_{\perp}$) at a constant draw ratio ($\lambda=20$); $\epsilon_{||}/\epsilon_{\perp}=5$ (a), $\epsilon_{||}/\epsilon_{\perp}=10$ (b), $\epsilon_{||}/\epsilon_{\perp}=40$ (c), $\epsilon_{||}/\epsilon_{\perp}=10^3$ (d)

From Figures 3.11 and 3.12 it can be concluded that the attainable combinations of a high PE and T_{sp} can be expanded by: (i) a high draw ratio and (ii) a highly anisotropic dye molecule. The ultimate properties for a guest-host system at infinite draw ratio ($\lambda = \infty$) and infinite dye anisotropy ($\epsilon_{||}/\epsilon_{\perp} = \infty$, i.e., mismatch angle $\gamma = 0$) are calculated and the results are presented in Figure 3.13. The drawn curve is again obtained by varying the dye-concentration or film thickness, assuming Lambert Beer's law to hold at high absorbances (a more detailed description of the validity of Lambert-Beer's law is given in appendix B). The polarising efficiency and single-piece transmittance for a perfect polariser are 1 and 0.5, respectively, i.e. no light passes two crossed polarisers, whereas fifty percent will be transmitted by a single polariser.^{1,2,3} This value is the upper limit of the theoretical curve in Figure 3.13, at high dye concentrations and/or film thicknesses.

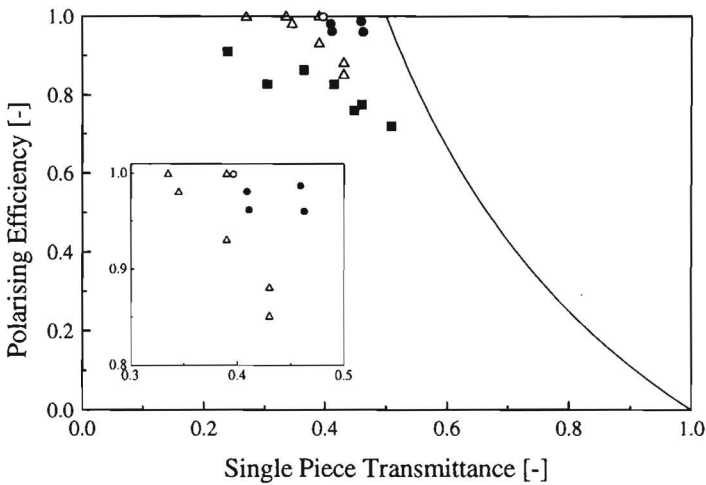


Figure 3.13: Polarising efficiency as a function of single-piece transmittance; theoretical curve at infinite draw ratio and extinction coefficient ratio $\epsilon_{||}/\epsilon_{\perp} \rightarrow \infty$ (—), HDPE/Sudan Red B polarisers (■), PVA/Dye polarisers literature values²¹ (Δ), PVA-iodine polariser (○), i-PP/tri-azo dye polarisers (●)

In Figure 3.13, the theoretical predictions are compared with experimental data on a commercial poly(vinyl alcohol)/iodine polariser and with literature values of poly(vinyl alcohol)/dye polarisers.²¹ The polarising efficiency of the poly(vinyl alcohol) polarisers ranges from 0.8 to almost fully contrast ($PE \approx 1$). However, the single-piece transmittance is rather low in comparison with the theoretical limit ($T_{sp} \leq 0.40$). Experimental data on polyolefinic based polarisers are included as well. The performance of the model system HDPE/Sudan Red, which was used in the previous Chapter for the elucidation of the orientation mechanism, is low in comparison with the PVA based systems. The polarising efficiency of drawn ($\lambda=15$)

i-polypropylene films containing a tri-azo dye is drastically enhanced compared to the HDPE/Sudan Red system. A closer look at the chemical structures of the dyes used in both systems (Figure 3.5) reveals that aspect ratio of the linear tri-azo dye is substantially higher than for Sudan Red B, a di-azo dye. The more rod-like structure of the tri-azo dyes provides for the enhanced orientation in drawn polypropylene. This reconfirms the observations by Michl and Thulstrup²² who studied the relation between the shape of organic solute molecules and its orientation in low-density polyethylene. They concluded that rod-like molecules possessing high aspect ratios, most efficiently duplicate the orientation of the host polymer during the drawing process. Moreover, the experimental data in Figure 3.13 indicate that the polyolefinic polarisers based on polypropylene/tri-azo dyes have an enhanced single-piece transmittance in comparison to PVA at an identical polarising efficiency. At first sight, the gain in single-piece transmittance is small (< 4 %) with respect to commercial poly(vinyl alcohol) polarisers. However, these few percentages increase in transmittance, significantly enhance the brightness of displays in which such polarisers are applied.

3.7 Discussion

In this Chapter, a simple model was presented for the description of the optical properties of drawn semi-crystalline polymers containing a dichroic dye. The model is based on the following assumptions: (i) the material is unoriented prior to drawing, (ii) deformation of the polymer and orientation of the dichroic dye occurs in an affine mode, (iii) the uniaxial drawn films possess fibre symmetry, (iv) the properties of drawn systems can be described with an aggregate type model, and (v) Lambert-Beer's law is valid. The validity of the first four assumptions has been verified thoroughly, not only in Chapter 2 of this thesis, but also in a large number of theoretical and experimental studies, mainly related to mechanical properties of oriented polymers.^{7,8,9,11,23,24} The reader is referred to Appendix B for the verification of the last assumption, i.e., the validity of Lambert-Beer's law. A good agreement is observed between experimental data and theoretical predictions for the dichroic ratio, polarising efficiency and single-piece transmittance, respectively (Figures 3.7, 3.8 and 3.9). Although experimental verification of the theory was performed with only one model system (HDPE/Sudan Red B), it is expected to be equally applicable to other guest-host systems, provided that the principal assumptions presented above are met.

The main attribute of the present model is that the influence of a wide variety of experimental parameters, such as the draw ratio, dye characteristics, film thickness and dye concentration on the polarising performance can be quantitatively predicted. The apparent inconsistency in certain experimental observations, pointed out in the introduction of this Chapter, is predicted accurately by the model. It is demonstrated that enhanced performance with respect to PE and

T_{sp} can be achieved through proper optimisation of the film thickness and dye concentration (Figure 3.10).

The maximum draw ratio which is applied for the production of sheet polarisers from poly(vinyl alcohol) is relatively low ($\lambda_{max} < 6$)^{25,26}. This is a result of the intermolecular interactions (hydrogen bonds) between the chains of the polymer which restrict the unfolding of lamellae upon solid-state drawing.²⁷ In linear polyolefins, strong intermolecular interactions are absent and high draw ratios ($\lambda \gg 10$) can be obtained. The experimental results on ultra-drawn i-PP/tri-azo dye polarisers indicate that this enhanced drawability results in an enhanced orientation of the guest molecules and an improved performance of the polariser. An additional, and essential requirement for a high-performance polariser, is that the dichroic dye is highly anisotropic. The linear tri-azo dye used (Figure 3.5), possessing a high aspect ratio fulfils this requirement. These i-PP/tri-azo dye polarisers possess an improved balance between polarising efficiency and single-piece transmittance in comparison with conventional poly(vinyl alcohol)/dye polarisers (Figure 3.13). To summarise, the combination of anisotropic dye molecules and ultra-drawable polyolefins results in polarisers with an optical performance close to the theoretical limit set at infinite draw ratio and infinite dye anisotropy. Moreover, these polyolefin polarisers have some additional advantages in comparison with poly(vinyl alcohol) based systems with respect to temperature and/or humidity resistance.^{28,29} This improved resistance to rough conditions is a potential advantage in, for instance, automotive (e.g. dashboard) applications of Liquid Crystalline Displays.

A few critical remarks concerning the theoretical model and experimental data are in order. First, it is common practise in the determination of the polarising efficiency and single-piece transmittance to perform an averaging procedure over the entire visible wavelength range. The calculations and experimental data presented in this Chapter are, by contrast, limited to a single wavelength (the absorbance maximum of the dye). Second, in the present calculations, background scattering due to reflection losses at the polymer-air interfaces are not included. In the absorbance measurements for the model-system, the background scattering is eliminated by standard baseline corrections. Another comment is that in the guest-host systems a single dye was used and consequently the polarisers are effective in a rather narrow region (≈ 100 nm) of the visible wavelength range. Production of so-called neutral grey, polyolefin based polarisers which cover the entire visible wavelength range is problematic because of the poor compatibility of most current dichroic dyes with apolar host-polyolefins (examination of Figure 3.5 reveals that in this study dye molecules have been selected with alkyl side chains and/or the absence of bulky polar side-groups).³⁰ As a final comment, the theoretical model was derived for polymeric sheet polarisers produced by uniaxial deformation. In industrial processes, polymer films are often constrained in the lateral direction³¹, which results, of course, in deviations from the simple uniaxial deformation scheme used in this Chapter.

3.8 Conclusions

A theoretical framework was derived to describe the optical properties of polymer/dye polarisers. Experimental data on a model HDPE/Sudan Red B system agree well with the theoretical predictions of the model. The apparent discrepancy in experimental data between the dichroic ratio and the polarising efficiency, is accurately described by the model. The ultimate performance of polymer/dye polarisers with respect to polarising efficiency and single-piece transmittance can be predicted quantitatively by the aggregate model. From the theoretical considerations it is obvious that the prerequisites for the production of a high-performance polariser are: i) highly oriented guest-host systems and thus polymers and production procedures which allow for high draw ratios ($\lambda \geq 15$), and ii) highly anisotropic dye molecules. These prerequisites imply that highly drawable, linear polyolefins are not only better host-materials (in comparison with Poly(vinyl alcohol)) for the orientation of guest molecules (Chapter 2), but intrinsically should result in polarisers with an enhanced optical performance. The theoretical ultimate properties are compared with experimental data on commercial poly(vinyl alcohol) based polarisers and with polarisers based on i-polypropylene/tri-azo dye systems. It is shown that indeed the enhanced drawability of the latter system in combination with a linear, rod-like tri-azo dye, results in polarisers with an improved balance with respect to polarising efficiency and single-piece transmittance. Moreover, the performance of these polarisers closely approaches the theoretical limit.

3.9 References

- 1 Driscoll W.G., Vaughan W., *Handbook of Optics*, Mc Graw-Hill: New York, Chapter 10, 1987
- 2 Hecht E., *Optics*, 2nd ed., Addison-Wesley: London, 1987
- 3 Mathieu J.P., *Optics*, Pergamon Press: Oxford, 1975
- 4 Kratky O., *Kolloid Z.*, **1933**, *64*, 213
- 5 Crawford S.M., Kolsky H., *Proc. Phys. Soc. B*, **1951**, *64*, 119
- 6 Kuhn W., Grün F., *Kolloid Z.*, **1942**, *101*, 248
- 7 This thesis Chapter 2
- 8 Irvine P.A., Smith P., *Macromolecules*, **1986**, *19*, 240
- 9 Ward I.M., *Mechanical Properties of Solid Polymers*, 2nd ed., John Wiley & Sons: New York, 1985
- 10 Hadley D.W., Pinnock P.R., Ward I.M., *J. Mater. Sci.*, **1969**, *4*, 152
- 11 Ward I.M., *Proc. Phys. Soc.*, **1962**, *80*, 1176
- 12 Norden B., *Appl. Spectrosc. Rev.*, **1978**, *14(2)*, 157
- 13 Hermans P.H., Heikens D., *Recl. Trav. Chem. Pays Bas*, **1952**, *71*, 49
- 14 Read B.E., Stein R.S., *Macromolecules*, **1968**, *1*, 116
- 15 Vogel I., *Textbook of Quantitative Inorganic Analysis*, 5th ed., Longman Scientific: London, 1989
- 16 The validity of the Lambert-Beer's Law approximation for the model guest-host system (HDPE/Sudan Red B) has been verified in Appendix B
- 17 Bastiaansen C., Schmidt H.W., Nishino T., Smith P., *Polymer*, **1993**, *34*, 3951
- 18 Wold E., Bremer J., Hunderi O., *J. Polym. Sci. Part B; Polym. Phys.*, **1993**, *31*, 579
- 19 Borsdorf R., Scholz M., *Spektroskopische Methoden (IR, UV/VIS) in der Organischen Chemie*; Akademie Verlag: Berlin, 1989
- 20 Cunningham A., Ward I.M., Willis H.A., Zichy V., *Polymer*, **1974**, *15*, 749
- 21 Nitto Denko product info on transmissive PVAL/Dye polarisers
- 22 Michl J., Thulstrup E.W., *Acc. Chem. Res.*, **1987**, *20*, 192
- 23 Postema A.R., Smith P., *Macromolecules*, **1990**, *23*, 3296
- 24 Motamedi F., Bastiaansen C., Smith P., *Macromolecules*, **1992**, *25*, 1006
- 25 Miyasaka K., *Adv. Polym. Sci.*, **1992**, *108*, 91

- 26 Nagatsuka T., Shimomura T., Oishi Y., *SID 85 DIGEST*, **1985**, 74
- 27 Schellekens R., Bastiaansen C., *J. Appl. Polym. Sci.*, **1991**, 43, 2311
- 28 Bastiaansen C.W.M., *Eur. Pat. Appl.* EP 0518 425, 1992
- 29 Mitsubishi Petrochemical CO., *Eur. Pat. Appl.* EP 0348964, 1989
- 30 For the production of neutral grey dye polarisers, combinations of at least three dyes are required which absorb in a specific wavelength region, see for example: Scheffer T.J., *J. Appl. Phys.*, **1982**, 53, 257;
Land E.H., West C.D., *Colloid Chemistry*, ed. J. Alexander, Vol. 6, Reinhold Publishing Corporation, 1946
- 31 *Encyclopedia of Polymer Science and Engineering*, 2nd ed., Vol. 7, John Wiley&Sons: New York, 1985

Part B:
Scattering Polarisers

Chapter 4

Light-Scattering Polarisers

4.1 Introduction

The polarising properties of guest-host systems based on oriented polyolefins containing dichroic dyes were investigated in the previous Chapters. It was found that high-performance polarisers can be produced from oriented polyolefin/dye systems. The ultimate optical properties of the polyolefin/dye polarisers, with respect to the single-piece transmittance, were systematically enhanced in comparison with conventional poly(vinyl alcohol) polarisers. It was also shown that for a perfect dichroic polariser, with a polarising efficiency of unity, the single-piece transmittance is limited to a theoretical maximum of 50% (disregarding reflection losses). This upper limit is inherently related to the operating principle of these polarisers, i.e., linearly polarised light is generated by absorption of one polarisation direction and by transmission of the other polarisation direction.¹ These polarisers are used in Liquid Crystalline Displays (LCD) where the plane of polarisation of light is modulated by electrically switching of the liquid crystalline molecules (Figure 1.6). Two linear sheet polarisers are required to generate linearly polarised light and to obtain visual perception of the electro-optical switching of the liquid crystalline molecules. A standard LCD display contains neutral grey polarisers (for example, H-sheet polarisers) which absorb light in the entire visible wavelength range and as a result, the displays switch from grey to black. For the fabrication of a full colour LCD, additional colour filters are added to each pixel which transmit one of the three primary colours, either red, green or blue.

As a consequence of the use of absorbance polarisers, the output intensity of a standard LCD in the off-state cannot exceed 50% of the input light intensity. In the case of colour LCDs, the colour filters absorb an additional 60% of the incident light.² Therefore, and because of reflection losses between the several layers of the device, the output intensity of colour LCDs is below 20%.³ In direct-view displays, a backlighting system consisting of a light source, reflector and a waveguide is necessary to illuminate the display. For these backlit direct-view displays, the absorbance losses are compensated for by increasing the illumination intensity of the light source. The extra power consumption of the light source reduces the battery lifetime

of, for example, portable computers. In projection LCDs which require high intensity light sources, the absorbed energy of the conventional polarisers is transformed into heat. The heating-up of the polarisers reduces the life-time of the display due to thermal degradation of the polarisers.

In the past, it was already attempted to produce polarised light without absorbing one polarisation direction of natural light. In these polarisers, reflection^{3,4,5,6} or scattering^{7,8,9,10,11,12,13} of light is used to generate polarised light. A schematic drawing of a polariser based on anisotropic scattering is shown in Figure 4.1. The system consists of particles dispersed in a continuous matrix (Figure 4.1a). In one direction (x) the refractive indices of matrix and dispersed particles are matched whereas in the other direction (y), which is perpendicular to the x-direction, there is a large mismatch in refractive indices (Figure 4.1a). Consequently, incident light which is polarised in the direction of the matched refractive indices (s-polarised) is transmitted and light which is polarised in the mismatch direction (p-polarised) is scattered (Figures 4.1b and 4.1c). With this anisotropic scattering principle, linearly polarised light is produced.

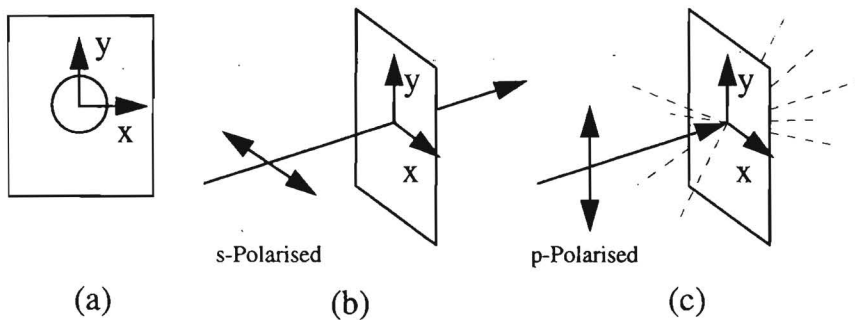


Figure 4.1: a) Operating principle of light-scattering polariser, x = match of refractive indices; y= mismatch of refractive indices; b) non-scattering state (s-Polarised light); c) scattering state (p-Polarised light)

The first polarisers which operate on the above described principle were reported by Edwin H. Land⁷ who was also the inventor of the first absorbance polarisers. These polarisers were produced by coating a (isotropic) polymeric sheet with a dispersion of birefringent crystals. The birefringent crystals were oriented in a strong magnetic field (10,000 Gauss) and allowed to dry in the magnetic field. One of the two principle refractive indices of the crystals was matched with the refractive index of the polymeric sheet and a linear polariser was experimentally obtained. The production method for these light-scattering polarisers was laborious and restricted to small areas. Moreover, at that moment (twenty years before the

invention of liquid crystalline displays) E.H. Land did not recognise the full potential of his invention, as is illustrated by one of his conclusions which is depicted below:

THE SCATTERING POLARISER

“We have developed an entirely different kind of polariser, which very few people indeed have ever seen and for which there seems to be no obvious use. In this polariser we use doubly refracting crystals, and we deliberately make the crystals with a size several times the wavelength of light. Furthermore, the refractive index of the plastic matrix is made equal to one of the two principal indexes of the birefringent crystals. What is then obtained is quite a beautiful product: when the sheet is examined with an analyser, it is as transparent as glass for one position of the polariser, but when the analyser is turned 90°, the sheet is turbid and highly diffusing”⁷

More recently, several new light-scattering polarisers were developed based on liquid crystalline materials.^{8,9,10,11,12,13} For instance, polarisers were manufactured by photopolymerisation of a liquid crystalline mixture present in a glass cell. This mixture consists of a reactive (cross-linkable) and a non-reactive nematic liquid crystalline (LC) material. Prior to polymerisation, the liquid crystalline mixture is oriented by orientation layers present at the glass walls. After the UV-initiated polymerisation, an oriented polymer network is formed in which the non-reactive LC material is dispersed. Both the crosslinked and the free LC molecules are highly birefringent and, by a proper selection of materials, it is possible to achieve the desired match and mismatch of refractive indices parallel or perpendicular to the orientation direction. These anisotropic gels act as a permanent light-scattering polariser,⁸ or as an electrically switchable polariser.^{9,11} In the latter case, the gels can be switched electrically from a transparent, non-polarising state to a scattering, polarising state. With the anisotropic gel technique, the degrees of freedom in selection and chemical modification of the LC materials are numerous, and the orientation and photopolymerisation conditions can be varied within a wide range. For example, cholesteric liquid crystals can be introduced in the gels and a reflectance polariser is produced.^{4,5,14} The cholesteric LC molecules reflect circularly polarised light with the same handedness as the cholesteric helix of the molecules and this circularly polarised light is converted into linearly polarised light using a quarter wave foil.

The above described polarisers are manufactured from relative expensive liquid crystalline materials, a constant driving voltage is often required to generate permanent polarisation of light^{9,10,11} and/or additional optical components such as quarter wave foils are required to produce linearly polarised light.^{3,5,6,14} Moreover, the experimental procedures used are

laborious and these polarisers are difficult to produce in large areas. In this Chapter, a new route is explored for the production of polarisers which operate on the selective scattering of one polarisation direction of natural light. It is attempted to produce these polarisers based on polymeric blends of commercial engineering polymers. The blends are oriented by solid-state drawing to generate birefringence in the continuous phase and it is attempted to match one of the refractive indices of the continuous phase with the refractive index of the dispersed phase. Special attention is devoted to the selection of proper materials, the drawing behaviour of the blends and the properties of the films in terms of their polarising efficiency and single-piece transmittance.

4.2 Experimental

Materials

Two polyesters, poly(ethylene terephthalate) (PET) and poly(ethylene-2,6-naphthalene dicarboxylate) (PEN) were selected as the high birefringent matrix material. The chemical structures of the two polyesters are depicted in Figure 4.2. The PET grade used in this study was DSM ARNITE D02 300 ($M_w = 51.500$ g/mol). The PEN grade used was kindly supplied by Akzo Nobel Arnhem.

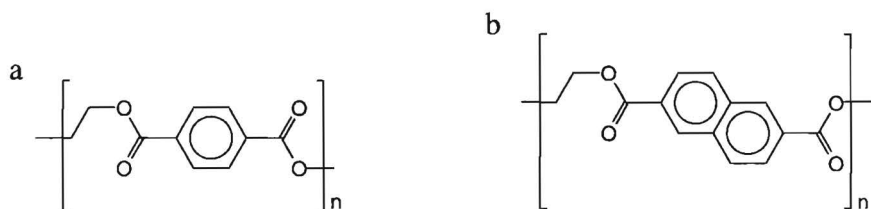


Figure 4.2: Chemical structures of a) poly(ethylene terephthalate) PET, and b) poly(ethylene-2,6-naphthalene dicarboxylate) PEN

For the dispersed phase, crosslinked latex particles and a thermoplastic copolymer were used:

- Rubbery core-shell particles with a diameter of 200 nm consisting of a styrene-butadiene rubber (S-BR) core and a (cross-linked) PMMA shell (Rohm and Haas Paraloid EXL3647).¹⁵
- A Styrene/Methylmethacrylate copolymer with a styrene content of 60% v/v (NAS 30, Polysar Inc.)

The isotropic refractive indices and the glass transition temperatures of the dispersed phases and the isotropic refractive indices of the matrix polyesters are listed below (Table 1):

Table 1: Glass transition temperatures and isotropic refractive index of dispersed phases

Material	T_g [°C]	n [-]	ref.
S-BR Core-Shell Particles	-76	1.530	15, 16
NAS 30	100	1.560	17
PET	75	1.585	21
PEN	125	1.645	21

Tape extrusion and solid-state drawing

The polyesters were dried for 24 hours at 150 °C. Subsequently, blends were prepared on a Haake counterrotating twin-screw extruder. The blend compositions and extrusion temperatures are listed below.

Table 2: Blend compositions and extrusion temperatures

Matrix	Dispersed Phase	Composition % [w/w]	Extrusion Temp. [°C]
PET	S-BR Core-Shell	0,2,4,6,8,10,20, 30	270
PEN	NAS 30	0,10	290

The extrudates were granulated, dried again and extruded into tapes ($\approx 12 \times 0.4 \text{ mm}^2$) on a Haake extruder equipped with a tape-extrusion die. The tapes were quenched in a water/ice bath, and subsequently drawn uniaxially on a tensile tester submitted with a thermostatically controlled oven. The PET core-shell tapes with an initial length of 40mm were drawn at 68°C and 85°C with cross-head speeds of 5 and 600 mm/min, respectively. The PEN/NAS 30 blends were drawn at 130°C and 300 mm/min. Before drawing, the tapes were heated for 2 minutes at the desired temperature to obtain thermal equilibrium. The drawn tapes were finally quenched to room temperature. Draw ratios were determined by measuring the displacement of ink-marks.

Characterisation

Refractive indices of the drawn, oriented polyesters were measured using a Abbe refractometer. The so-called trirefringence technique¹⁸ was used to determine the three refractive indices (indicatrix) of the material, i.e., parallel and perpendicular to the direction of draw, and in the thickness direction.

The birefringence of the oriented polyester blends was also measured using a Zeiss universal polarising microscope in combination with a tilting compensator after Ehringhaus.¹⁹ Cross sections (2–20 μm) were cut edge-on from the oriented tapes under cryogenic conditions with a Reichert Ultracut E microtome. The birefringence of the sections was calculated by dividing the optical retardation by the sample thickness. The sample thickness was measured by Scanning Electron Microscopy. The birefringences were averaged over 5 measurements.

Wide-Angle X-Ray Scattering (WAXS) of the undrawn and drawn poly(ethylene terephthalate) was performed using a Statton camera. Ni-filtered Cu-K α radiation was generated at 40 kV and 35 mA.

The morphology of the drawn blends was investigated with Scanning Electron Microscopy (SEM, Cambridge Stereoscan 200). Fracture surfaces of the drawn tapes were prepared perpendicular (Figure 4.3 plane a), respectively parallel (Figure 4.3 plane b) to the orientation direction. The drawn samples were cooled in liquid nitrogen to ensure brittle fracture. The fracture surfaces were etched for 10 minutes in an oxygen plasma and subsequently coated with a gold/palladium layer.

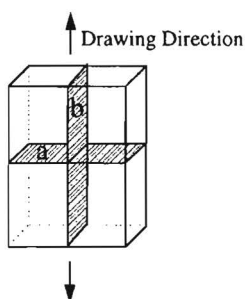


Figure 4.3: Schematic representation of fracture surfaces perpendicular (a) respectively parallel (b) to the direction of draw

The polarising performance of the oriented polyester blends was characterised using polarised UV/VIS measurements. The samples were coated with paraffin oil to reduce surface scattering.²⁰ The measuring procedure which was adopted is described in detail in section 3.4 and Appendix A (measuring the polarising performance of polarisers with moderate optical anisotropy).

4.3 Results

Orientation of the matrix polymers

In Figure 4.4, the refractive indices of drawn poly(ethylene terephthalate) tapes are depicted as a function of the draw ratio. The results are shown for tapes drawn slowly (5 mm/min; $T_d = 68^\circ\text{C}$) below the glass transition temperature of PET (70°C)²¹ and for tapes drawn at higher speeds (600 mm/min; $T_d = 85^\circ\text{C}$) above the glass transition temperature. The experimental data of Lorenzo et al.²², drawn at 85°C and the refractive index of the S-BR Core-Shell particles (Table 1) are included as well.

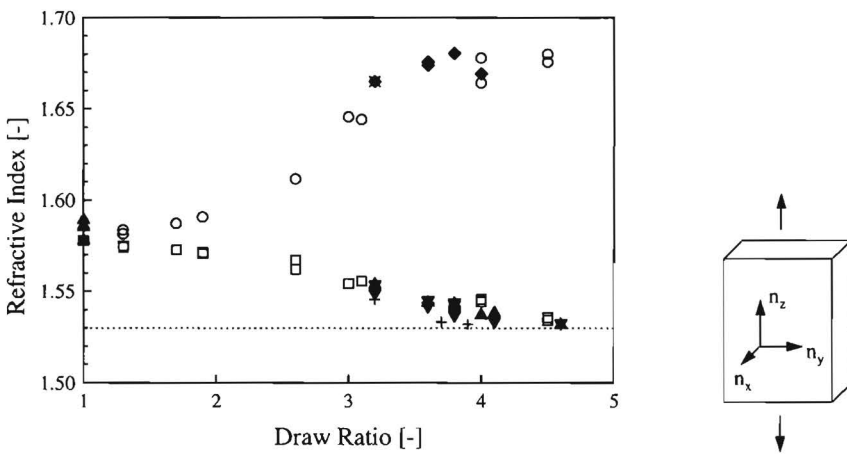


Figure 4.4: Refractive index of uniaxially drawn PET as a function of draw ratio and drawing temperature:

n_x , $T_d = 85^\circ\text{C}$ (\blacktriangle); n_y , $T_d = 85^\circ\text{C}$ (\blacktriangledown); n_z , $T_d = 85^\circ\text{C}$ (\blacklozenge); n_x , $T_d = 68^\circ\text{C}$ (+);
 n_z , $T_d = 68^\circ\text{C}$ (\times); Literature data of Lorenzo et al.:²² n_y , $T_d = 85^\circ\text{C}$ (\square); n_z , $T_d = 85^\circ\text{C}$ (\circ).
 (.....) Isotropic refractive index of S-BR Core-Shell particles

The refractive indices parallel (n_z) to the drawing direction increase upon drawing whereas the respective indices n_x and n_y , perpendicular to the direction of draw decrease which clearly shows the positively birefringent character of PET. The absolute birefringence values ($\Delta n_{zy} = n_z - n_y$) of PET drawn in this narrow temperature region around the glass transition temperature are identical. The refractive indices n_y and n_x , perpendicular to the direction of draw are identical too, which illustrates the fibre symmetry in the material.

The refractive indices for uniaxially drawn PEN tapes are depicted in Figure 4.5 as a function of draw ratio. Tapes were drawn at 130°C which is above the glass transition temperature of PEN ($T_g = 125^\circ\text{C}$).²¹ The drawn PEN tapes are also fibre symmetrical and are extremely

birefringent. The isotropic refractive index of the NAS 30 copolymer is shown as well (Table 1).

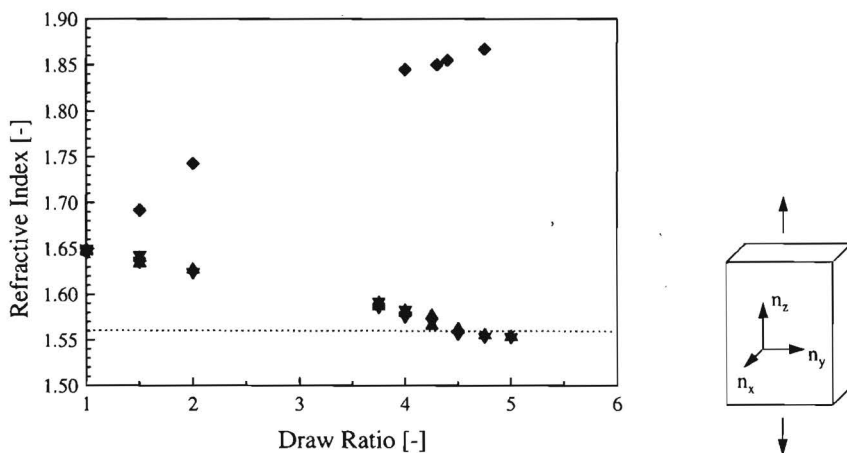


Figure 4.5: Refractive index of uniaxially drawn PEN at 130 °C as a function of draw ratio: n_x (▲); n_y (▼); n_z (◆). (.....) Isotropic refractive index of NAS 30, styrene-mma copolymer

The refractive index perpendicular (n_y) and the maximum birefringence (Δn_{yz}) of the drawn polymers are crucial criteria for the production of a light-scattering system, i.e., the perpendicular refractive index needs to be matched with the refractive index of the dispersed phase, whereas the maximum birefringence determines the degree of mismatching in the perpendicular direction. The experimental values of the perpendicular refractive index and the maximum birefringence are presented in Table 3 for the pure polyesters as obtained with the Abbe refractometer (trirefringence technique).

Table 3: Refractive index n_y and maximum birefringence Δn_{yz} after drawing of the pure polyesters as measured with the Abbe refractometer.

Material	Drawing	Draw Temp [°C]	Draw Ratio [-]	n_y [-]	n_z [-]	Δn_{yz} [-]
PET	uniaxial	85	4 - 4.5	1.535	1.670	0.135
PET	uniaxial	68	3.5 - 4	1.535	1.670	0.135
PEN	uniaxial	130	5	1.555	1.870	0.315

Wide Angle X-ray (WAXS) patterns of the polyester films are shown in Figure 4.6. Prior to drawing (Figure 4.6 a), the extruded PET tapes possess an isotropic diffuse x-ray pattern. The absence of crystalline reflections indicates that the quenched poly(ethylene terephthalate) film are predominantly amorphous. The PET tape drawn above the glass transition temperature shows distinct crystalline reflections (Figure 4.6 b) which indicates that the material is oriented and partially crystalline. From literature it is known that fast (600 mm/min) drawing above the glass transition temperature of (initially amorphous) PET results in stress induced crystallisation.²³ If drawing is performed at a low speed (5 mm/min) below the glass transition temperature, the oriented polyester film is still predominantly amorphous (Figure 4.6 c). The WAXS results for the PEN tapes are identical, i.e., prior to drawing the material is amorphous and after drawing above the glass transition temperature it is partially crystalline (Figures 4.6 d and e). The WAXS observations on the drawn polyester tapes with respect to drawing temperature/speed agree well with data found in literature for PET^{23,24,25,26,27} and PEN^{28,29}, respectively.

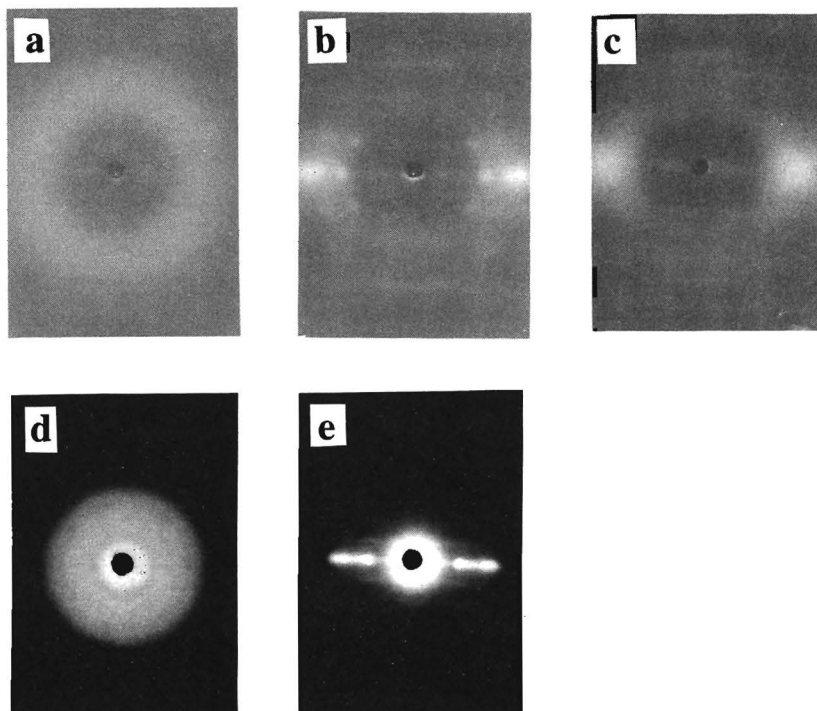


Figure 4.6: WAXS patterns: a) Undrawn (quenched) PET-tape, b) PET drawn at 85 °C ($v = 600$ mm/min; $\lambda = 4.0$), c) PET drawn at 68 °C ($v = 5$ mm/min; $\lambda = 3.8$), d) Undrawn (quenched) PEN-tape, e) PEN drawn at 130°C ($v = 300$ mm/min; $\lambda = 5.0$). Distance between sample and film is 7 cm for WAXS patterns a, b and c, respectively 5 cm for WAXS patterns d and e.

Orientation of the blends

In the previous paragraph, the refractive indices of drawn, *pure* polyesters are described and the birefringence (refractive indices) was measured using the Abbe refractometer. In this section it is attempted to characterise the birefringence of the polyester matrix in the drawn polyester *blends*. These blends scatter light and, consequently, it is impossible to measure the birefringence with the Abbe refractometer. Therefore, the birefringence was quantified on thin cross sections taken along the drawing direction of the blends using the tilting compensator. The birefringence data of the uniaxially drawn polyester blends and of the pure polyesters (also measured with the compensator) are shown in Table 4. The measured values represent the birefringence of the cross sections in the x-z plane but are, from fibre symmetry considerations (Figures 4.4 and 4.5), identical to the birefringence in the y-z plane.

Table 4: Birefringence (Δn) of pure polyesters and oriented polyester blends (10 % w/w) as measured with tilting compensator

Material	Draw Temp [°C]	Draw Ratio[-]	Δn_{xz} [-]	Δn^*_{xz} [-]
PET	85	4.0	0.123	-
PET/S-Br	85	4.0	0.100	0.115
PEN	130	4.6	0.252	-
PEN/NAS 30	130	4.6	0.232	0.266

The birefringence of the polyester blends (Δn_{xz}) is lower than the birefringence of the pure polyesters at an identical draw ratio. The birefringence of the matrix polymer in the blend can be calculated by dividing the measured birefringence by the volume fraction of the matrix polymer, assuming that the dispersed phase is isotropic. In the last column of Table 4, these corrected birefringences (Δn^*_{xz}) are tabulated. It is observed that these corrected matrix birefringences are almost identical to the birefringence of the pure polymers (Δn_{xz} , Table 4). The measured values for the birefringence of the matrix and for the pure polyesters agree well with compensator data found in literature for drawn PET³⁰ and PEN.^{28,30} However, comparison of Tables 3 and 4 reveals that the birefringences measured with the tilting compensator are systematically below the values measured with the Abbe refractometer. Similar inconsistencies between experimental data were found by Ward and co-workers on solid state drawn PET films.³¹ A possible explanation is that the Abbe refractometer data refer to the surface of the sample whereas the compensator data refer to an average over the sample thickness. Solid-state drawing is performed in a thermostatted oven followed by a rapid quench to room temperature. Relaxation phenomena which decrease the orientation of the polymer are more pronounced in the core of the tape because the quench to room

temperature is slower in the core than in the skin of the tape. This implies that the drawn samples may possess a layered structure with a skin that is more oriented than the core of the tape which is in agreement with the experimental observations.

Morphology of the oriented polyester blends

In Figure 4.7, SEM micrographs are shown of a uniaxially drawn PET blend containing 10% w/w S-BR core-shell particles. Etched fracture surfaces are presented which are cut in a plane parallel (Figure 4.3, plane b), respectively perpendicular (Figure 4.3, plane a) to the direction of draw.

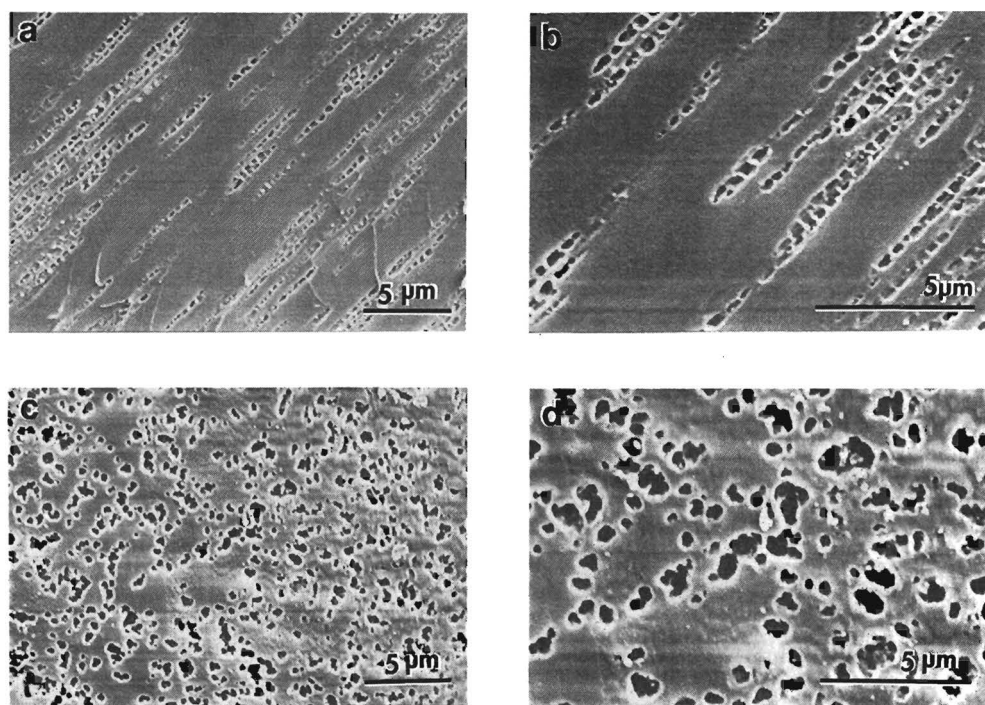


Figure 4.7: SEM micrographs of fracture surfaces of 10% w/w* PET/Core-Shell blends, uniaxially drawn at 85 °C, $\lambda=4.0$, parallel (a) and (b), respectively perpendicular (c) and (d) to orientation direction

* **Comment:** At first sight the particle concentration in Figures 4.7 c and d appears to be higher than 10% w/w. This is due to the etching procedure which not only reacts with the rubbery core-shell particles, but also removes matrix polyester situated between the particles.

The dark regions represent the original location of the dispersed core-shell particles which disappeared due to their preferential reaction with the etching plasma. In the perpendicular cross section (c and d), the core-shell particles are randomly distributed in the films. The fracture surface parallel (a and b) to the orientation direction shows elongated strings of agglomerated core-shell particles, and the original particles (200 nm) can still be discerned. Consequently, from both cross sections it is concluded that the morphology consists of arrays of core-shell particles and these arrays are oriented towards the drawing direction of the tape. Apparently, during solid-state drawing, agglomerates of core-shell particles are deformed into strings consisting of several discrete core-shell particles, which we will call pearl-necklace structures. The aspect ratio (l/d) of the rows is approximately 20, and the width is identical to the diameter of the particles (200 nm). The pearl necklace structure is also observed at higher particle concentrations, as is shown in Figure 4.8 for 20% and 30% blends drawn at 85 °C.

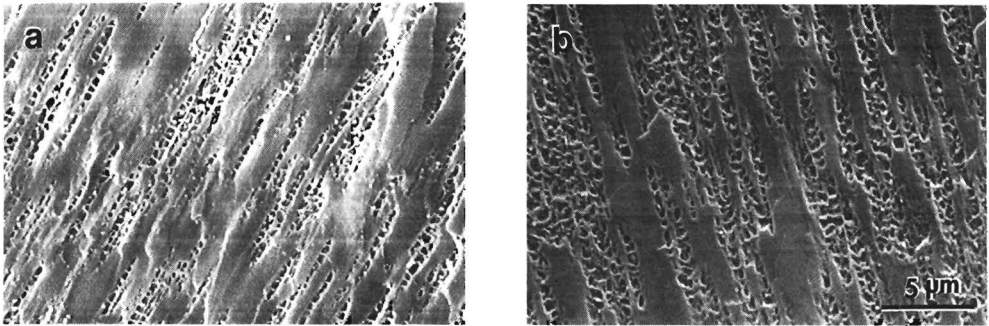


Figure 4.8: SEM micrographs of PET blends, fracture surface parallel to the orientation direction, uniaxially drawn at 85°C: a) 20 % S-BR core-shell particles, b) 30% S-BR core-shell particles

The observed morphology is independent of the temperature of drawing, i.e., the pearl-necklace morphology is also present in the PET blends drawn below T_g at 68 °C.

Fracture surfaces of the oriented PEN/NAS 30 blends are depicted in Figure 4.9. The morphology of the blends consists of extremely long NAS 30 ellipsoids ($30 \times 0.4 \mu\text{m}$) which are embedded in the PEN matrix. The aspect ratio of the NAS 30 particles is high ($l/d \approx 70$) and the particles resemble to long fibrils.

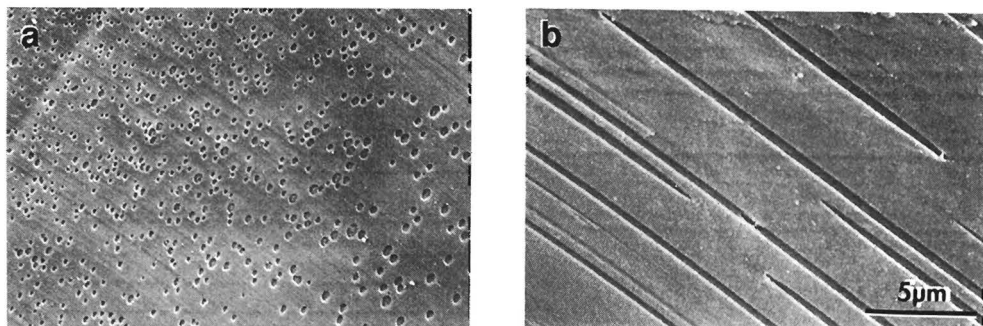


Figure 4.9: SEM micrographs of fracture surfaces of 10% w/w PEN/NAS 30 blends, drawn uniaxially at 130°C . (a) perpendicular, and (b) parallel to orientation direction

Optical properties

In Figure 4.10, photographs are shown of the oriented PET and PEN blends in polarised light with the polarisation direction parallel respectively perpendicular to the orientation direction. For both polyesters, the tapes are optically transparent in s-polarised light, i.e., if the polarisation direction of light is perpendicular to the drawing direction of the tape. However, in p-polarised light, polarised parallel to the direction of draw, the tapes are opaque and light is scattered. (The terms s-polarised and p-polarised are German abbreviations for, respectively, “Senkrecht”-polarised and “Parallel”-polarised).³²

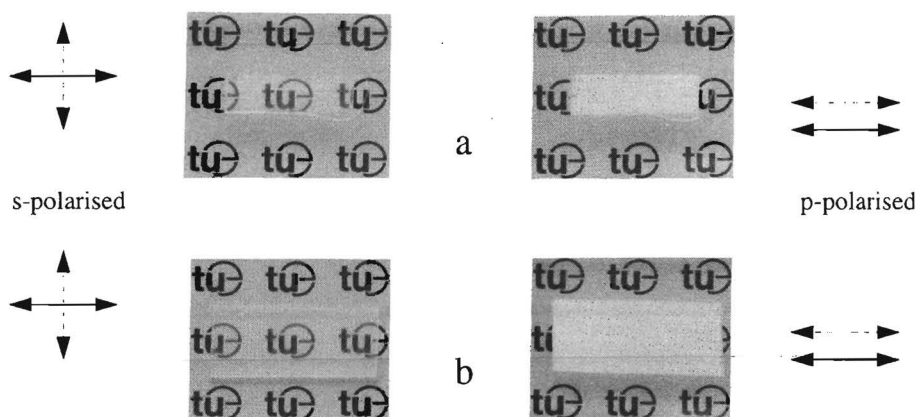


Figure 4.10: Photographs of oriented polyester blends in polarised light, orientation direction of tape (\longleftrightarrow), polarisation direction of light ($\dashv\dashv$): (a) PET/Core-Shell 6% w/w, uniaxially drawn at 85 °C, $\lambda = 4.0$, $d = 0.19$ mm; (b) PEN/NAS 30, 10% w/w, uniaxially drawn at 130 °C, $\lambda = 5.5$, $d = 0.11$ mm. Distance between logo and tape is 5 mm.

The difference in transmitted light intensity, as observed above, is quantified by polarised UV/VIS measurements. The transmittance as a function of wavelength is plotted in Figure 4.11 for a 10% w/w PET/Core-Shell tape. The transmitted light intensity is low (<5%, curve a) over the entire visible wavelength range for p-polarised light (scattering state). In s-polarised light (transparent state) the transmittance is substantially higher (> 60%, curve b) and slightly increases with increasing wavelength of light. This increase in transmittance in the transparent state of the polariser is due to a non-perfect index match. The (unwanted) light scattering is more effectively at lower wavelengths, resulting in a lower transmittance for blue light in comparison with red light.

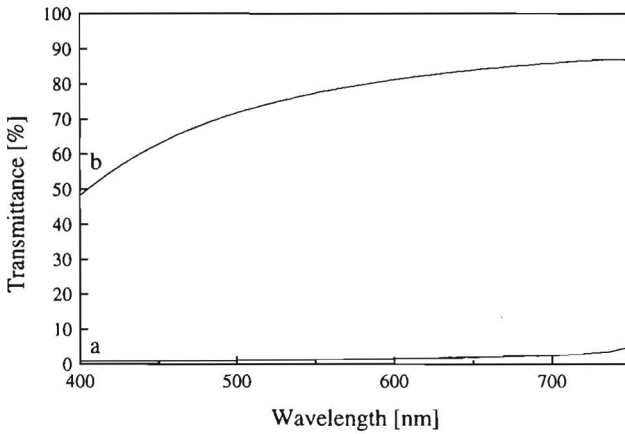


Figure 4.11: Transmittance as a function of wavelength of a PET/Core-Shell tape 10% w/w $d= 0.24$ mm: (a) p-polarised light, (b) s-polarised light

From these two principal transmittances the performance as a polariser, expressed in terms of single-piece transmittance (transparency) and polarising efficiency (contrast), is calculated using equations 12 and 13 of Chapter 3. The results are shown in Figure 4.12.

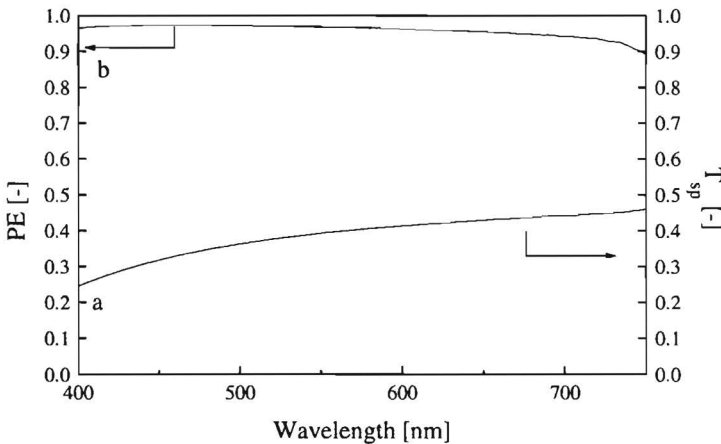


Figure 4.12: Polarising performance as a function of wavelength of a PET/Core-Shell 10% w/w tape, $d = 0.24$ mm: (a) Single-Piece Transmittance (T_{sp}); (b) Polarising Efficiency (PE)

The polarising efficiency remains at a constant level (>0.95 , Figure 4.12 curve b) over a relatively broad wavelength range (400-700 nm). The single-piece transmittance gradually increases with increasing wavelength (Figure 4.12, curve a). The single-piece transmittance is

calculated as the mean sum of the parallel and perpendicular transmittances (Chapter 3, equation 13). For a light scattering polariser, the parallel transmittance (Figure 4.11, curve a) is virtually zero and, as a consequence, the single-piece transmittance is mainly determined by the perpendicular transmittance of the transparent state (Figure 4.11, curve b). The latter transmittance increases with increasing wavelength and thus accounts for the increase in single-piece transmittance. The principal transmittances and polarising performance as a function of wavelength show similar trends for the uniaxially drawn PEN/NAS30 tapes. For all systems, the polarising performance is listed below in Table 5, at a fixed wavelength (600nm), concentration and tape thickness.

Table 5: Polarising performance at 600 nm for the polyester blends (10% w/w)

System	T_{dr} [°C]	λ [-]	c [% w/w]	d [mm]	T_{sp} [-]	PE [-]
PET/S-Br	85	4.4	10	0.16	0.347	0.969
PET/S-Br	68	3.8	10	0.15	0.356	0.975
PEN/NAS	130	5.0	10	0.15	0.317	0.973

The performances of the PET/S-Br core-shell tapes which are drawn at temperatures slightly above or below the glass transition temperature of the matrix are identical. The properties of the PEN system resemble those of the uniaxially drawn PET tapes with respect to the polarising efficiency, although the single-piece transmittance is lower.

The influence of the particle concentration and thickness (d) of the drawn tapes on the optical properties are shown in Figures 4.13 and 4.14, respectively.

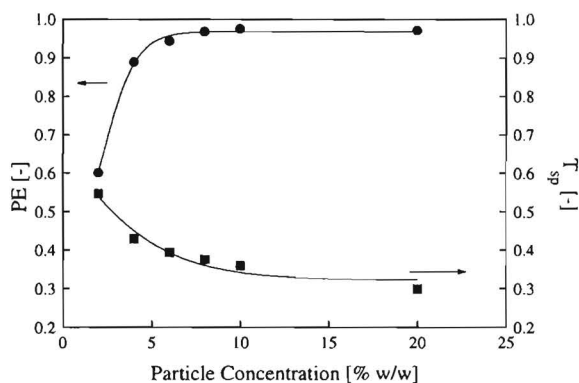


Figure 4.13: Polarising performance at 600 nm as a function of particle concentration of uniaxially drawn PET/S-Br core-shell blends ($T_d = 68$ °C, $d = 0.17 \pm 0.02$ mm, $\lambda = 3.8$): Polarising Efficiency (●); Single-Piece Transmittance (■)

Increasing the particle concentration at a fixed thickness and draw ratio, reduces the single-piece transmittance but enhances the polarising efficiency. Both the efficiency and transmittance level off to a constant value at high particle concentrations (>10% w/w, Figure 4.13).

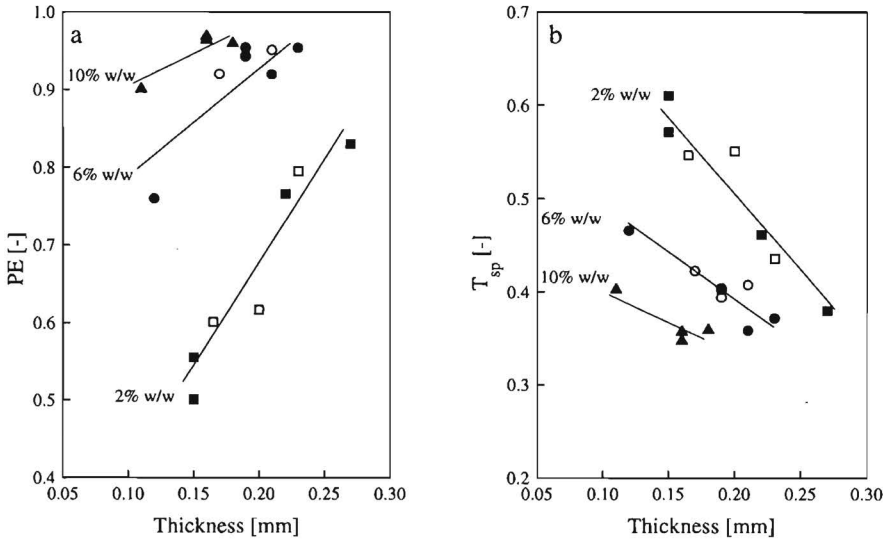


Figure 4.14: (a) Polarising Efficiency (PE) and (b) Single-Piece Transmittance (T_{sp}) as a function of tape thickness for drawn PET/S-Br Core-Shell tapes at a fixed draw ratio ($\lambda = 4.0$):

- (■) 2% Core-Shell, $T_d = 85\text{ }^\circ\text{C}$; (□) 2% Core-Shell, $T_d = 68\text{ }^\circ\text{C}$; (●) 6% Core-Shell, $T_d = 85\text{ }^\circ\text{C}$;
- (○) 6% Core-Shell, $T_d = 68\text{ }^\circ\text{C}$; (▲) 10% Core-Shell, $T_d = 85\text{ }^\circ\text{C}$.

At a low (2% w/w) particle concentration an increase in tape thickness improves the polarising efficiency but at the same time reduces the single-piece transmittance (Figure 4.14). However, at a particle concentration of 10% w/w, the thickness dependence is less and the polarising efficiency and single-piece transmittance level off to a constant value. Consequently, from Figures 4.14 and 4.13 it can be concluded that at high particle concentrations and/or tape thicknesses, the performance of scattering polarisers becomes constant. There is no influence of the drawing temperature on the polarising performance, the tapes which are drawn around the glass transition temperature of PET have identical optical properties (68 °C and 85 °C, indicated with open and closed markers, respectively).

4.4 Discussion

The PET/core-shell and PEN/NAS 30 blends function as a linear polariser, i.e., the intensity of the transmitted light depends on the polarisation direction of incident radiation, which is clearly demonstrated in Figure 4.10. In the transparent state, the polarisation direction of light is perpendicular to the direction of draw. In this direction the refractive indices (n_y) of the oriented matrix polyesters are almost completely matched with the isotropic refractive indices of the dispersed phases (Figures 4.4 and 4.5). During drawing, the polyesters become highly birefringent which is retained in the polyester blends (Table 4). The obtained index mismatch of the blend, parallel to the orientation direction results in excess scattering and a milky appearance of the tape (Figure 4.10). The blends scatter light over the entire visible wavelength range as illustrated by the photographs and by the polarised UV/VIS measurements. The UV/VIS measurements are used to quantify the polarising performance, which is, in contrast to the polymer/dye polarisers presented in the previous Chapter, constant over a broad wavelength range (400-700nm, Figure 4.12).

The results of the WAXS experiments showed that the oriented PET matrix can be predominantly amorphous or partially crystalline depending on the specific drawing conditions. The crystallites present in oriented semi-crystalline PET may cause additional and undesired scattering of light. However, it was shown that the present difference in the crystallinity of the matrix did not have any influence on the final polarising performance: slowly drawing of the PET blends below, or fast drawing above the glass transition temperature yields identical polarisers (at comparable concentration and film thickness). From this observation, it is concluded that the crystallinity of the oriented matrix is too low to influence the scattering behaviour of the blends or that the size of the PET crystallites is too small for light scattering.³³

In the previous Chapter it was stated that, for conventional display applications, polarisers are required possessing an optimum balance between efficiency and transmittance. Therefore, and to get a comparison with the absorbance polarisers, the polarising efficiency is plotted as a function of the single-piece transmittance for the PET/Core-Shell tapes and the conventional PVAL absorbing polarisers (Figure 4.15):

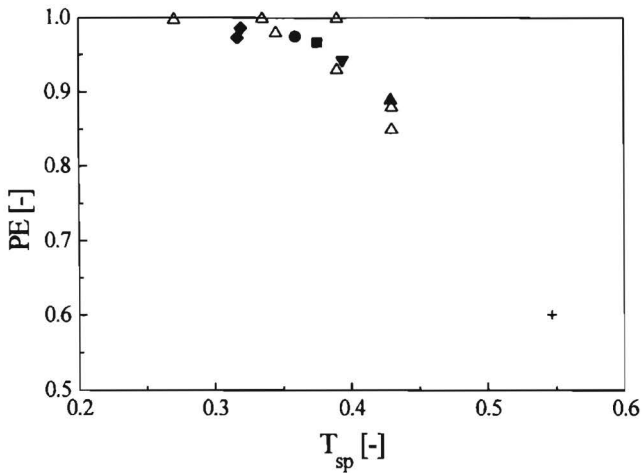


Figure 4.15: Polarising Efficiency (PE) as a function of Single-Piece Transmittance (T_{sp}) at 600 nm:

PET/S-Br Core-Shell, $d = 0.17$ mm, particle concentration is 2% (+); 4% (\blacktriangle); 6% (\blacktriangledown); 8% (\blacksquare); 10% (\bullet), PEN/NAS 30 particle concentration is 10%, $d = 0.15$ mm (\blacklozenge); Absorbance polarisers based on PVAL/dye systems (Δ)³⁴

The performance of the scattering polarisers can be optimised by varying the particle concentration (or film thickness), i.e., an increase in particle concentration enhances the polarising efficiency and simultaneously reduces the single-piece transmittance. In comparison with the conventional absorbance polarisers, the scattering PET/Core-Shell tapes can compete with respect to the single-piece transmittance. However, the polarising efficiency of the scattering systems does not yet reach full contrast (PE=1). A polarising efficiency of unity is reached if the parallel transmittance of the polariser is zero (Chapter 3, equation 13). Apparently, for the scattering polarisers presented in this Chapter, light which has been (multiple) scattered in the tape can still pass the tape, and the parallel transmittance is not zero.

The PEN/NAS 30 polarisers are also included in Figure 4.15, with an identical efficiency but a reduced transmittance in comparison with their PET counterparts. The single-piece transmittance is mainly determined by the transmittance of the transparent state which depends on the match of refractive indices. The refractive index of the drawn matrix (n_y) is identical to the isotropic refractive index of NAS 30 (Tables 1 and 3) which should, in principle, result in transmittances comparable with the PET systems. However, the morphology of the two polyester blends differs significantly from each other. In the case of PET/core-shell systems, original particle size (200 nm) is retained in the drawn blends (Figure

4.6). During the melt-blending process, the (cross-linked) shell of the rubbery core-shell particles prevents redistribution of the particle size. Upon solid-state drawing, agglomerates of core-shell particles are deformed into the observed pearl-necklace structures consisting of isotropic, spherical particles. With respect to the PEN/NAS 30 systems, the morphology consists of extremely elongated ellipsoidal particles after drawing (Figure 4.8). Although the drawing temperature of the blend (130°C) is well above the glass transition temperature of the dispersed phase (100°C), the molecular orientation in the dispersed phase is not likely to be zero. Consequently, these ellipsoidal particles could be birefringent too, leading to an imperfect index match with the matrix. As for the PET system, the individual and isotropic core-shell particles are still present in the oriented polyester matrix.

The birefringence of drawn PEN ($\Delta n = 0.315$) is twice as high as the birefringence of drawn PET ($\Delta n = 0.135$). The higher birefringence of PEN is a result of the different chemical structure of the polymer (Figure 4.2). The higher anisotropy in polarisability of the electrons in the 2,6-naphthalenedicarboxylate units, in comparison with the terephthalate units, accounts for this higher birefringence.^{21,35} However, from the polarised UV/VIS results it is not possible to see a dramatic influence of the matrix birefringence on the polarising performance.

It is important to note here that the comparison of scattering and absorbing polarisers based on the polarising efficiency and single-piece transmittance is the only similarity between those two systems. The differences are obvious, the scattering systems polarise light without the formation of heat and no light is lost in the material. Secondly, the light-absorbing polarisers presented in the previous Chapter operate in a relatively narrow wavelength range (100 nm) which implies that there are at least three different dyes necessary to produce a neutral grey polariser. The scattering blends contain only one dispersed phase and cover already the entire visible wavelength range. Finally, the visual appearance of the scattering polariser (white) is different from the absorbing polarisers (grey or coloured). In a conventional direct-view display which uses two neutral grey polarisers, images are formed as black numbers on a grey background. The visual perception of images on a display consisting of, for example, one absorbance and one scattering polariser is completely different, i.e., white numbers on a grey background.

In this Chapter, the concept of a permanent light-scattering polariser based on oriented polymer blends was introduced (this in contrast to electrically switchable polarisers^{9,10,11}). Linearly polarised light is produced by selectively matching and mismatching of refractive indices between the continuous and dispersed phase of the blend. The refractive indices of the continuous phase perpendicular to the orientation direction which needs to be matched with the index of the dispersed phase was measured with the Abbe refractometer using (non-monochromatic) white light. The refractive indices of both the matrix and the dispersed phase depend, of course, on the wavelength of light and therefore the measured values are averages

over the visible wavelength range. Consequently, perfect index matching may not be accomplished over the entire wavelength range. Furthermore, it was concluded, from the comparison of the Abbe data with the compensator data, that the orientation of the core of the tapes is less than the orientation of the skin. This might also be a complicating factor for a perfect index matching over the thickness of the tape. Finally, the most important comment is that the polarising performance was characterised using polarised UV/VIS measurements which are restricted to scattering in the forward direction and to relatively small collection angles. The measured transmittances and, consequently, the single-piece transmittance and polarising efficiency depend on the aperture of the UV/VIS spectrometer. Therefore, a full description of the light-scattering polarisers is required with a complete picture of the angular distribution of light scattering in the forward and backward mode. This subject which will be discussed in the next Chapter.

4.5 Conclusions

Light-scattering polarisers have been produced based on a thermoplastic polyester matrix (poly(ethylene terephthalate) or poly(ethylene-2,6-naphthalenedicarboxylate)) containing dispersed particles (Rubbery S-BR Core-Shell particles, or S-MMA copolymers). The polyester blends are subsequently oriented in the solid state to obtain the desired match and mismatch in refractive index between the polyester matrix and dispersed particles. After orientation, linear polarisers are obtained that scatter light polarised parallel to the orientation direction over a broad wavelength range (300 nm), but transmit light polarised perpendicular to the direction of draw. The polarising performance in terms of polarising efficiency and single-piece transmittance can be optimised by varying the concentration of particles and/or the thickness of the tape. Thus, light-scattering polarisers have been produced possessing optical properties which enter the high-performance regime of the traditional absorbance polarisers, but due to their scattering principle are potentially useful for liquid crystalline displays in projection applications (see technology assessment).

4.6 References

- 1 Driscoll W.G., Vaughan W., *Handbook of Optics*, Mc Graw-Hill: New York, Chapter 10, 1987
- 2 Drzaic P.J., *Liquid Crystal Dispersions*, World Scientific Publishing: Singapore, Vol. 1, 1995
- 3 Belayev S.V., Schadt M., Barnik M.I., Fünfschilling J., Malimoneko N.V., Schmitt K., *Jap. J. Appl. Phys.*, **1990**, 29, L634
- 4 Broer D., Hikmet R., Lub J., Seppen A., *Chemisch Magazine*, **1994**, 28, 486
- 5 Broer D.J., Lub J., Mol G.N., *Nature*, **1995**, 378, 467
- 6 Schadt M., Fünfschilling J., *Jap. J. Appl. Phys.*, **1990**, 29, 1974
- 7 Land E.H., *J. Opt. Soc. Am.*, **1951**, 41, 957
- 8 Hikmet R.A.M., *Eur. Pat. Appl.*, EP 0 506 176 A1, 1991
- 9 Hikmet R.A.M., *Mol. Cryst. Liq. Cryst.*, **1991**, 198, 357
- 10 Bloisi F., Ruocchio C., Terrecuso P., Vicari L., *Liq. Cryst.*, **1996**, 20, 377
- 11 Hikmet R.A.M., *J. Appl. Phys.*, **1990**, 68, 4406
- 12 Zyryanov V.Y., Smorgon S.L., Shabanov V.F., *Mol. Eng.*, **1992**, 1, 305
- 13 Aphonin O.A., Panina Y.V., Pravdin A.B., Yakovlev D.A., *Liq. Cryst.*, **1993**, 15, 395
- 14 Broer D.J., Lub J., *United States Patent*, 5-506-704, 1996
- 15 The average refractive index of the particles is controlled by varying the copolymer compositions of the rubbery core and the (thin) cross-linked shell. Commercially available core-shell particles are added to, for example, poly(vinyl chloride)* or poly(methyl methacrylate)** to obtain optically transparent, rubber-toughened materials. * Breuer H., Haaf F., Stabenow J., *J. Macromol. Sci. Phys.*, **1977**, B14, 387 and Haaf F., Breuer H., Stabenow J., *Angew. Makrom. Chem.*, **1977**, 58/59, 95; ** Bucknall C.B., *Comprehensive Polymer Science*, Pergamon Press: Oxford, Chapter 2, 1989
- 16 Rohm and Haas product information
- 17 Polysar Inc. Product information
- 18 Samuels R.G., *J. Appl. Polym. Sci.*, **1981**, 26, 1383
- 19 Ehringhaus A., *Zeitschr. f. Kristallogr.*, **1931**, 76, 315
- 20 Bastiaansen C., Schmidt H.W., Nishino T., Smith P., *Polymer*, **1993**, 34, 3951
- 21 Huijts R.A., Peters S.M., *Polymer*, **1994**, 35, 3119
- 22 Lorenzo V., Pereña J.M., *J. Appl. Polym. Sci.*, **1990**, 39, 1467
- 23 Blundell D.J., MacKerron D.H., Fuller W., Mahendrasingam A., Martin C., Oldman R.J., Rule R.J., Riekel C., *Polymer*, **1996**, 37, 3303
- 24 Allison S.W., Ward I.M., *Brit. J. Appl. Phys.*, **1967**, 18, 1151
- 25 Pereira J.R.C., Porter R.S., *J. Polym. Sci. Polym. Phys. Phys. Ed.*, **1983**, 21, 1133
- 26 Chang H., Schultz J.M., Gohil R.M., **1993**, B32(1), 99
- 27 Göschel U., Deutscher K., Abetz V., *Polymer*, **1996**, 37, 1
- 28 Cakmak M., Lee S.W., *Polymer*, **1995**, 36, 4039
- 29 Cakmak M., Wang Y.D., Simhambhatla M., *Polym. Eng. Sci.*, **1990**, 30, 721

- 30 Jager J., Juijn J.A., Van den Heuvel C.J.M., Huijts R.A., *J. Appl. Polym. Sci.*, **1995**, 57, 1429
- 31 Bower D.I., Jarvis D.A., Ward I.M., *J. Polym. Sci.:Part B. Polym Phys.*, **1986**, 24, 1459
- 32 Born M., *Optik*, Springer Verlag: Berlin, 1985
- 33 *Encyclopedia of Polymer Science and Engineering*, John Wiley & Sons, 2nd ed., Vol. 10, 1985
- 34 Nitto Denko product info on transmissive PVAL/Dye polarisers
- 35 Karplus M., Porter R.N., *Atoms and Molecules*, Benjamin Cummings: Amsterdam, 1970

Chapter 5

Angular Distribution of Light Scattering

5.1 Introduction

In the previous Chapter, the processing and properties of light-scattering polarisers based on blends of thermoplastic polymers were described. The performance of these scattering polarisers was expressed in terms of polarising efficiency (~contrast) and single-piece transmittance (~transparency).¹ It was shown that the polarising performance of the scattering systems enters the regime of the high-performance dichroic polarisers. These properties were determined using a UV/VIS spectrometer which measures transmittances (or absorbances) whereas the polarisers presented in the previous Chapter scatter light instead of absorb light. The polarising performance of the scattering systems which is actually measured with a UV/VIS spectrometer depends on the numerical aperture of the measurement, for example the distance between the sample and the detector (the collection cone of detection is approximately 10°). Moreover, the UV/VIS measurements are restricted to transmitted light intensities in the forward direction whereas the scattering polarisers scatter light in both the forward and backward direction. For many practical (potential) applications of such polarisers the full scattering pattern and the ratio of forward to backward scattered light are important. In direct-view displays, for example, this knowledge is useful in designing a display configuration possessing an enhanced brightness and/or energy efficiency. For these applications, which are discussed in the epilogue of this thesis, the full scattering pattern at larger viewing angles, both in the forward and backward direction needs to be determined. Furthermore, it is important to know if the scattering polarisers change the plane of polarisation of the scattered ray, i.e., is the plane of polarisation of the incoming ray identical to the scattered ray ?

Therefore, the spatial scattering distribution of the scattering polarisers is investigated in this Chapter. Attention is paid to the question whether polarisation shifts do occur upon scattering. The general features of the light-scattering distributions will be discussed using the oriented PET/S-BR core-shell blends. The influence of the particle concentration, tape thickness and wavelength of incident radiation on the scattering patterns is examined. Finally, the properties

of the PEN/NAS 30 polarisers are evaluated and compared with the PET/S-BR core-shell polarisers.

5.2 Experimental

The light-scattering polarisers used in this Chapter are based on oriented blends of PET/S-BR/core-shell particles or PEN/NAS 30 systems. The production techniques and drawing conditions are described in detail in § 4.2 of the previous Chapter.

The experimental arrangement (autronic-Melchers corporation) to measure the angular distribution of light scattering is depicted in Figure 5.1.

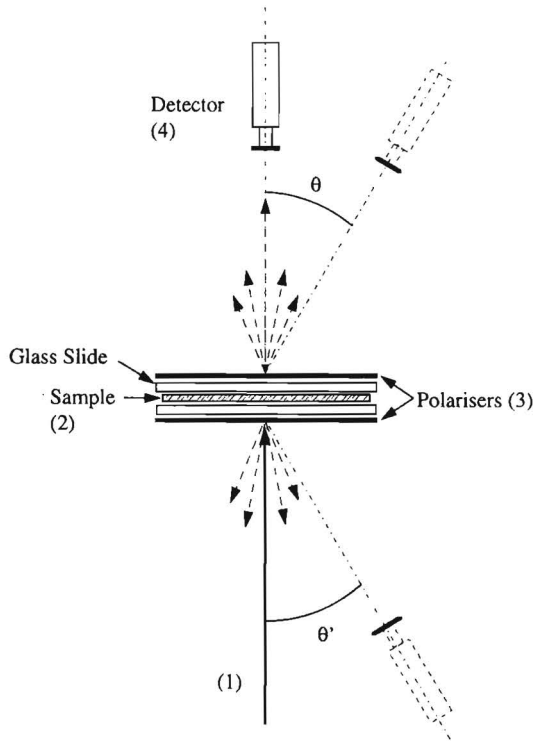


Figure 5.1: Experimental set-up to determine the angular distribution of light scattering

A collimated beam of light (1), originating from a halogen light source, illuminates the sample via a glass optical fibre. The drawn sample is coated with mineral oil ($n_d^{20} = 1.467$) and placed between two glass slides (2) to reduce surface scattering.² The measurements are performed using a green bandpass filter with a central wavelength of 561 nm and a full width at half maximum (FWHM) of 21 nm. The beam diameter is 1.5 mm and the divergence of the beam

is approximately 0.75° . Two linear sheet polarisers (3) are placed below and above the sample to control the polarisation direction of the incoming beam, and to determine the polarisation direction of the scattered radiation. The scattered radiation is collected by a measuring microscope (4) which is connected to a Photo Multiplier Tube (PMT). The PMT quantitatively measures the intensity of the scattered light in terms of absolute luminances (Cd/m^2). The measuring microscope (4) can rotate in a vertical plane over angle θ (forward scattering) from 0° to 70° . In the backward direction, scattered light over angle θ' ranging from 14° to 66° can be measured (angles below 14° are impossible because the microscope will coincide with the incoming light beam). The rotating stage consisting of the sampleholder, polarisers, and light source, can rotate in a horizontal plane over angle ϕ ranging from 0° to 360° . Consequently, all combinations of angles θ (θ') and ϕ represent the surface of a sphere and enables the determination of the spatial distribution of the scattered light in the forward and backward mode.

In the measurements, the two polarisers below and above the sample are arranged in four specific combinations with respect to the orientation direction of the film (Figure 5.2). In the **ss** and **pp** configurations the polarisation direction of the two polarisers are parallel to each other. For the **ss** configuration (transparent state) the polarisation directions of the two polarisers are perpendicular to the orientation direction of the tapes, whereas in the **pp** configuration (scattering state) the polarisation directions are parallel to the orientation direction. The crossed arrangements of the two polarisers, **sp** and **ps** are necessary to determine changes in the state of polarisation of the scattered beam.

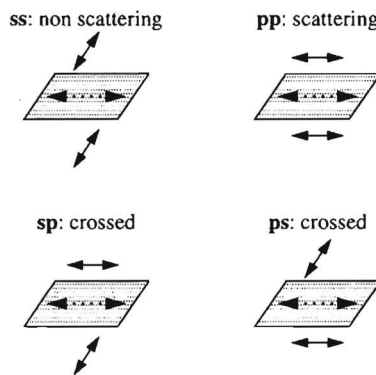


Figure 5.2: Arrangement of polarisers below and above the drawn sample: dotted arrows represent orientation direction of the tape, full arrows represent polarisation directions of bottom and top polarisers

A reference measurement without a tape between the oil-coated glass slides is executed before each measurement. The measuring microscope has a circular aperture stop, and consequently the area from which light is detected is only a circle in the direct forward direction, at angle $\theta = 0^\circ$. At angles deviating from 0° , the area from which light is detected (an ellipsoid) increases and therefore, the measured intensities are multiplied by a factor $\cos\theta$ (or $\cos^2\theta$) to compensate for this effect.^{3,4}

Integrating sphere measurements are performed to determine the absolute values of the total amount of light which has been scattered in the forward or backward direction. The experimental set-ups for the integrating sphere measurements are depicted in Figure 5.3.

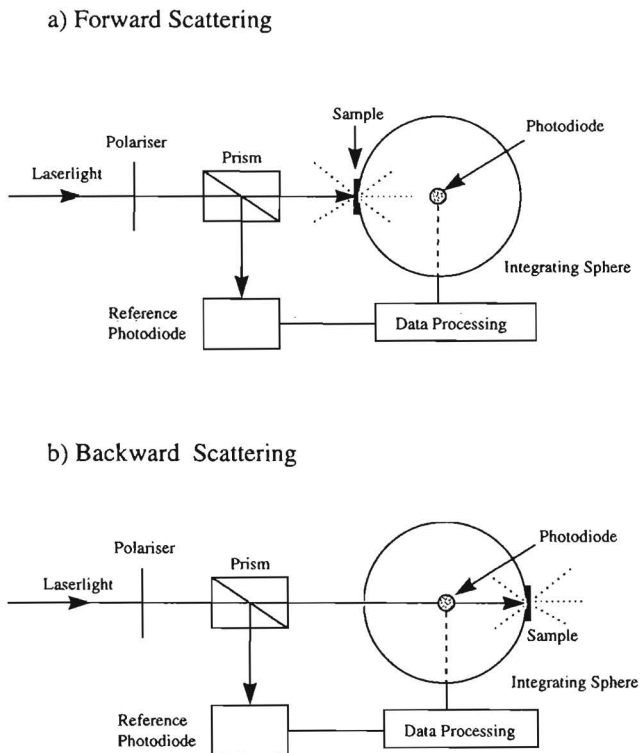


Figure 5.3: Experimental set-ups for integrating sphere measurements in a) the forward and b) the backward direction

Laser light is polarised (s or p) using a H-sheet polariser and subsequently split into two beams by a prism, one beam is directed to the integrating sphere, the other (reference) beam goes directly to a photodiode. In the forward scattering mode (a), the laser light hits the sample and the scattered radiation is collected by a photodiode after multiple reflections at the

inner surface of the integrating sphere. Light which is scattered by the sample is depolarised due to the diffusive reflections at the inner surface of the sphere and, consequently, no polarisation shifts are determined. Therefore, no second polariser is used and the measurements are defined as *s*-polarised or *p*-polarised. In the backscattering measurements (b), the laserlight first passes the integrating sphere before scattering occurs by the sample. In both the forward and backward measurements, the intensity of the scattered radiation in the sphere is divided by the intensity of the reference beam. This is done to compensate for intensity fluctuations of the laser. The dependence of the scattered intensity on the wavelength of light is investigated using three different lasers:

- Red light 650 nm (Spectra Physics 4mW helium-neon Class IIIb laser)
- Green light 540 nm (Spectra Physics 2mW helium-neon Class III laser)
- Blue light 410 nm (Spectra Physics 2020 0.3W argon-krypton Class IV laser)

5.3 Results and discussion

In Figure 5.4, a two-dimensional (2-D) plot of the forward scattered light for a drawn, 10% w/w (13% v/v) PET/core-shell tape is plotted on a logarithmic scale as a function of scattering angle θ . The two-dimensional plot is obtained by rotating the detector (measuring microscope) over angle θ (Figure 5.1) in a plane parallel to the drawing direction of the blend. The absolute intensities are normalised by dividing the measured intensities of the tape by the peak value at $\theta = 0^\circ$ of the reference measurement, i.e., without a scattering tape in the beam.

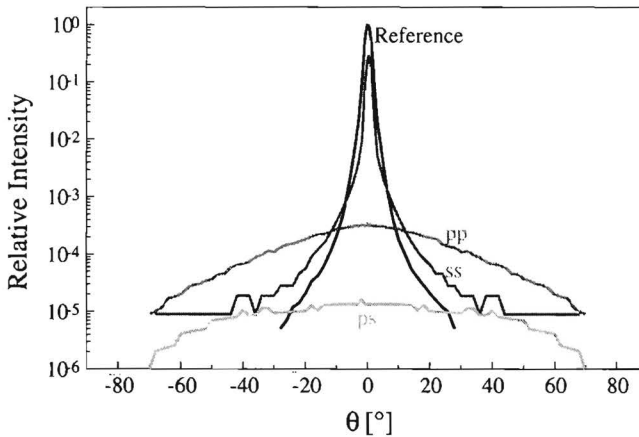


Figure 5.4: Forward 2-D scattering profiles of a drawn ($\lambda=3.7$, $T_{\text{draw}} = 85^\circ\text{C}$, $d = 0.37$ mm) PET/Core-Shell tape (10% w/w) for *ss* (—), *pp* (—) and *ps* (—) polarised light (560 nm) together with the reference profile of the incoming beam (—).

A collimated beam is transmitted in *ss*-polarised light, the transparent state of the polariser. The reference measurement without a sample between the coated glass slides (section 5.2) is also included and the shape of the *ss*- and reference curve are comparable. The absolute value for the transmittance of the tape in the direct forward direction ($\theta = 0^\circ$) is, however, lower than the reference measurement (log-scale!). This effect is caused by a combination of reflection and scattering losses at the (fibrillar) tape surface and of an imperfect refractive index match between the oriented PET matrix and the core-shell particles. In *pp*-polarised light (scattering state), the scattered light is evenly distributed over larger ($>30^\circ$) angles, and no transmittance peak can be observed in the forward direction. The absence of a direct transmittance peak, which consists of light that has not been scattered in the tape, indicates that all of the incoming light is scattered in the tape. The contrast ratio in the forward direction

(I_{ss}/I_{pp}) for small scattering angles is approximately 1000 for $\theta = 0^\circ$, but decreases rapidly at higher angles.

The transmittance with the two polarisers above and below the sample arranged in a crossed position (**ps**) is also included in Figure 5.4. The intensity of the **sp**-profile is identical to the **ps**-profile. If part of the incoming, linearly polarised light is depolarised after scattering, this should result in crossed transmittances deviating from zero. However, the measured intensities with crossed polarisers are negligible which indicates that the plane of polarisation is identical for the incoming and scattered radiation, i.e., polarisation shifts can be neglected. For a mathematical explanation for the absence of polarisation shifts, the reader is referred to Appendix C.

The influence of tape thickness on the scattering profiles for the PET/Core-Shell system (10% w/w) is demonstrated in Figures 5.5 and 5.6 for, respectively, the transparent (**ss**-polarised) and scattering state (**pp**-polarised). The thickness is increased by stacking identical tapes which are coated with mineral oil ($n_d^{20} = 1.467$) to reduce scattering between the layers. The detector is, just as in the results presented above, rotated in a plane parallel to the direction of draw. In the transparent state (Figure 5.5), the shape of the scattering profiles are identical at low (0.24 mm) or high (0.48 mm) thicknesses, i.e., a collimated beam of light passes the tape. In the direct forward direction, the intensity decreases with increasing thickness, due to imperfect index matching and/or reflection losses between the stacked tapes.

In the scattering state, a direct transmittance peak is only observed at the lowest tape thickness (0.12 mm, Figure 5.6 curve b), which is superimposed onto a broad background of scattered light. At lower particle concentrations (2% w/w instead of 10% w/w) the direct transmittance peak of non-scattered radiation can be observed even at higher tape thicknesses (Figure 5.7, curves b-e).

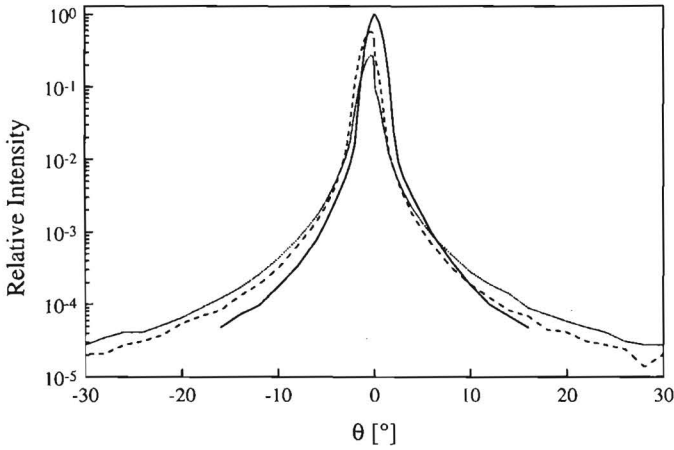


Figure 5.5: Forward scattering profiles of drawn ($\lambda=3.9$, $T_{\text{draw}} = 85$ °C) PET/Core-Shell tapes (10% w/w) for **ss** polarised light (560 nm) as a function of tape thickness: reference (—); $d = 0.24$ mm (---); $d = 0.48$ mm (.....)

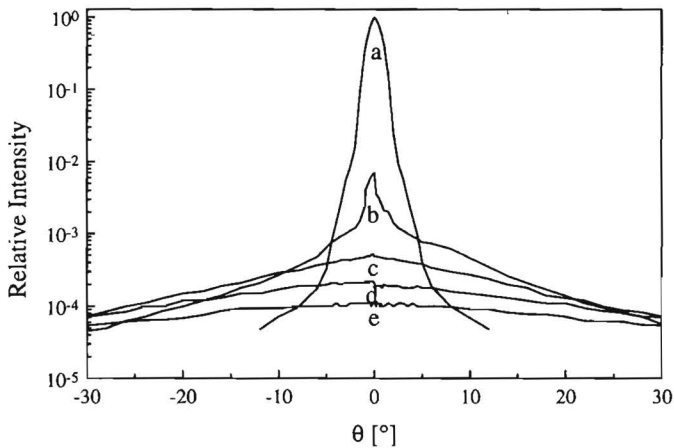


Figure 5.6: Forward scattering profiles of drawn ($\lambda=3.9$, $T_{\text{draw}} = 85$ °C) PET/Core-Shell tapes (10% w/w) for **pp** polarised light (560 nm) as a function of tape thickness: a) reference; b) 0.12 mm; c) 0.24 mm; d) 0.36 mm; e) 0.48 mm

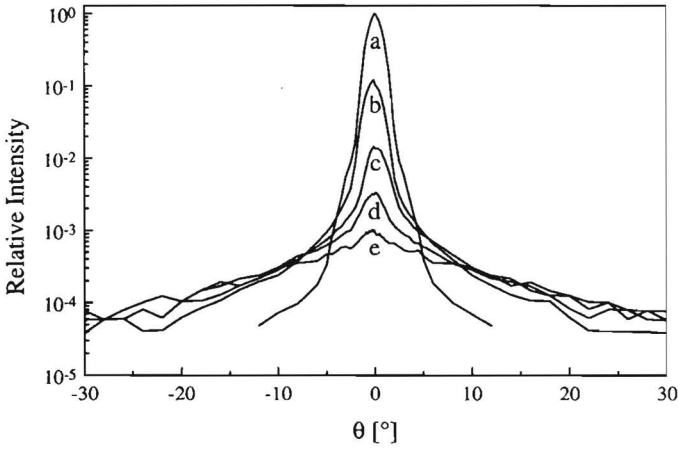


Figure 5.7: Forward scattering profiles of drawn ($\lambda=4.1$, $T_{\text{draw}} = 85 \text{ }^\circ\text{C}$) PET/Core-Shell tapes (2 % w/w) for pp polarised light (560 nm) as a function of tape thickness: a) reference; b) 0.15 mm; c) 0.30 mm; d) 0.45 mm; e) 0.60 mm

The direct transmittance peak consists of light which passes the tape without being scattered by the particles in the tape. The intensity of the direct transmittance peak as taken from Figure 5.7 (but corrected for the scattered background intensity) is plotted below on a log scale as a function of the tape thickness.

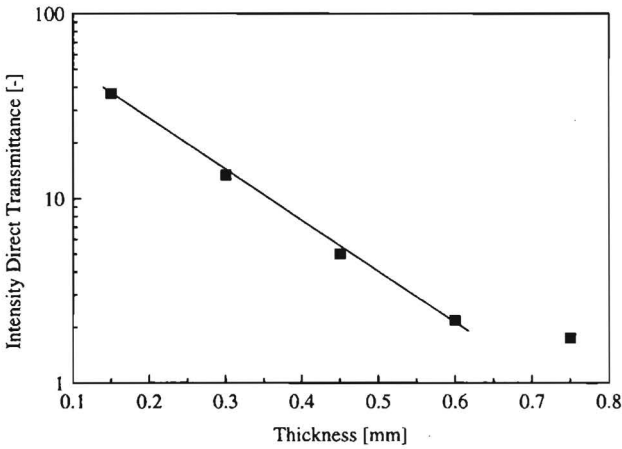


Figure 5.8: Direct transmittance at 560 nm of a 2% w/w PET/Core-Shell tape as a function of tape thickness

A linear relationship is observed which indicates that the decay in direct transmittance can be described with an (exponential) Lambert-Beer's law:^{3,5,6}

$$T_{direct} = e^{-d\beta\sigma} \quad (1)$$

In this equation, d (mm) is the sample thickness, β ($1/\text{mm}^3$) is the number density of particles, σ (mm^2) is the effective scattering cross section of a particle. At thicknesses below 0.6 mm (Figure 5.8), the linear relationship according to equation 1 is observed which indicates that single scattering occurs. Above 0.6 mm, the decrease in transmittance is less than expected due to multiple scattering phenomena. If single scattering is dominant, light which has been scattered once cannot contribute to the direct transmittance peak. However, in the multiple scattering domain, light which has been scattered several times can be transmitted into the direction of the incoming beam. This extra contribution to the direct transmittance leads to deviations from the Lambert-Beer decay. At concentrations exceeding 10% w/w, the direct transmittance peak already disappears at a small thickness (0.24 mm, Figure 5.6) which indicates that, in almost all systems studied here, multiple scattering of light occurs. As the thickness increases or the number density of particles (concentration) increases, the amount of scattering units increases too and, consequently, the probability for light to pass the tape without being scattered will decrease. As a result, not only the direct transmittance peak disappears, but also the intensity of the forward scattered light decreases (Figure 5.6, curves c, d and e). The input light intensity (reference beam) is, of course, identical in all systems presented above. Because no light is lost in the tape by the scattering polariser, the next section focusses on the other part of the spatial scattering distribution, i.e., backward scattering.

The two-dimensional scattering profiles in the backward direction are plotted in Figure 5.9, also on a logarithmic scale. The measuring microscope is, identical to all the forward scattering profiles presented above, rotated in a plane parallel to the drawing direction of the tapes.

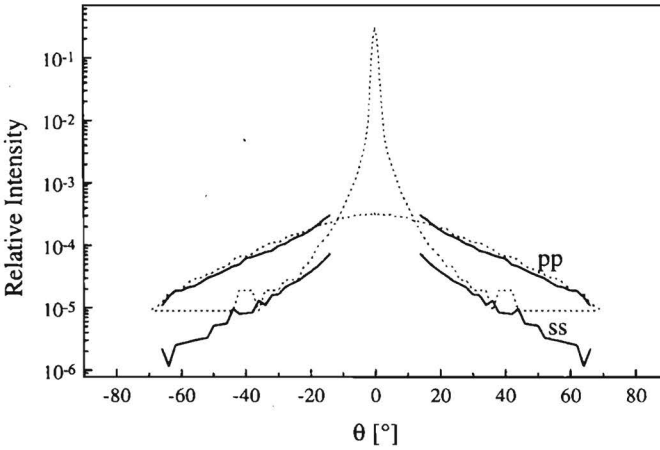


Figure 5.9: Backward scattering profiles (solid lines) of a drawn ($\lambda=3.7$, $d=0.37$ mm) PET/Core-Shell tape for **ss** and **pp** polarised light (560 nm). The corresponding forward scattering profiles are also included (dotted lines)

With the experimental set-up used in this study, it is impossible to measure scattered intensities in the direct backward direction ($\theta = 0^\circ$), but only at angles above 14° . Consequently, no contrast ratio in the backward direction can be determined. Both in **ss**- and **pp**-polarised light, the backward scattered radiation is distributed over large angles θ . In the scattering state of the polariser (**pp**-polarised), light is more backscattered than in the transparent state (**ss**-polarised). If the refractive indices of the matrix and dispersed phase are exactly matched, a collimated beam of (**ss**-polarised) light is transmitted into the forward direction and (almost) no light is backscattered. Light polarised in the mismatch direction (**pp**-polarised), is multiple scattered in the tape and can leave the tape either in the forward or backward direction. A comparison of the backward and forward scattering profiles (Figure 5.9, dotted lines) reveals that, for this specific tape, the shape and the absolute intensities of the forward and backward profiles are identical.

The above described experimental results represent light scattering in a two-dimensional plane parallel to the drawing direction of the tapes. For a graphical representation of the complete three-dimensional scattering distributions, it is essential to convert the spherical co-ordinates θ (θ') and ϕ into Cartesian co-ordinates x and y ($x = \sin(\theta)\cos(\phi)$, $y = \sin(\theta)\sin(\phi)$). The measured intensity (related to a specific combination of θ (θ') and ϕ) is plotted on the z -axis. The intensities are normalised with respect to the peak value of the reference measurement and plotted on a logarithmic scale. A schematic representation of such a three dimensional plot is drawn in Figure 5.10. The Cartesian co-ordinate frame is shown together with the

spherical co-ordinates (θ and ϕ) and the drawing direction of the films. The centre of the plot ($x = y = 0$) corresponds with the location of the incoming light beam.

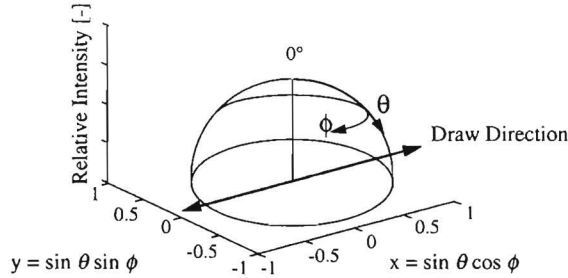


Figure 5.10: Cartesian x,y,z -frame with spherical co-ordinates (θ,ϕ) and drawing direction of tape

Typical examples of the three dimensional (3-D) scattering distributions for oriented PET/S-BR Core-Shell blends (10% w/w) are depicted in Figure 5.11 for forward scattering. The two-dimensional plots presented in Figures 5.4-5.9 are cross sections taken at $y = 0$. The absolute intensity of the transmitted light in the forward direction is high for **ss**-polarised light (transparent state), compared to **pp**-polarised light (scattering state). The drawing direction of the tapes is parallel to the x -axis of the co-ordinate frame. It is observed that the scattering of light is more intense along the y -axis, perpendicular to the orientation direction of the tapes. This anisotropy refers to the intensity of the scattered radiation, not to the polarisation direction, i.e., the anisotropic scattering patterns are present in both **ss** and **pp**-polarised light (the anisotropy in the **pp**-plot appears less as a result of the identical log scales for the **ss** and **pp** plots). It was mentioned previously that the contrast ratio (I_{ss}/I_{pp}) of the PET polariser is high (≈ 1000) in the forward direction and decreases rapidly with increasing scattering angle θ . However, due to the anisotropy in the scattering patterns, the contrast reduction is faster in a plane parallel to the direction of draw ($y = 0$) in comparison to a plane perpendicular to the direction of draw ($x = 0$).

In the corresponding backward profiles (Figure 5.12, note different log-scale !), the reversed is the case: the intensity of **pp**-polarised light is higher than for **ss**-polarised light. The anisotropy in scattered light intensity perpendicular to the orientation direction of the tapes is also present in the backward direction.

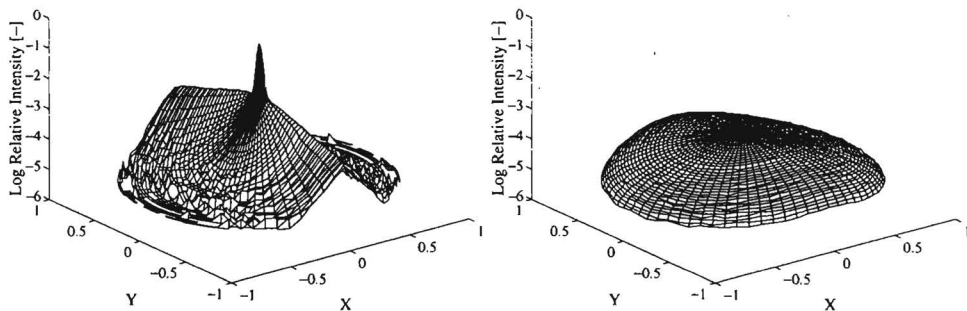


Figure 5.11: 3-D Forward scattering profiles for a drawn PET/S-BR Core-Shell tape (10% w/w, $d=0.36$ mm, $T_{\text{draw}} = 85^{\circ}\text{C}$, $\lambda=3.8$) a) in **ss**-polarised light, and b) in **pp**-polarised light. $x = \sin\theta \cos\phi$; $y = \sin\theta \sin\phi$

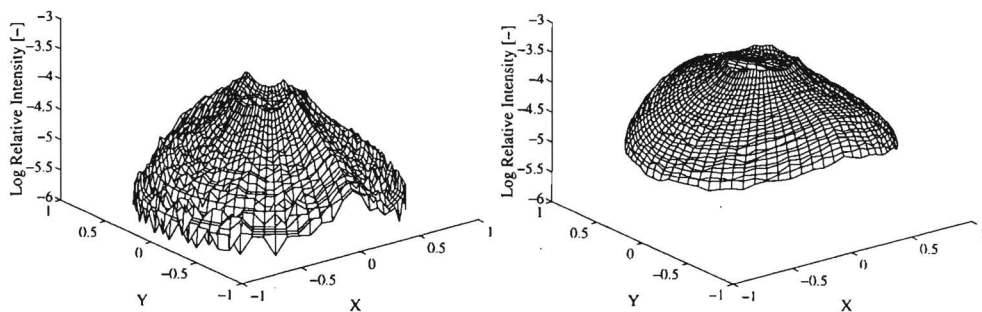


Figure 5.12: 3-D Backward scattering profiles for a drawn PET/S-BR Core-Shell tape (10% w/w, $d=0.36$ mm, $T_{\text{draw}} = 85^{\circ}\text{C}$, $\lambda=3.8$) a) in **ss**-polarised light, and b) in **pp**-polarised light. $x = \sin\theta \cos\phi$; $y = \sin\theta \sin\phi$

The anisotropy in the scattering patterns can be explained by the shape of the scattering units, which consists in the oriented PET/Core-Shell blends of elongated agglomerates of Core-Shell particles oriented towards the direction of draw (“pearl necklace structures”, § 4.3). Other experimental observations, mainly related to oriented semi-crystalline polymers showed similar anisotropic scattering behaviour, although scattering was confined to the Small Angle Light Scattering region, $\theta < 10^{\circ}$.⁷ The anisotropy was explained in terms of scattering from oriented, elongated crystalline structures (cylinders) surrounded by an amorphous matrix.^{8,9,10} Therefore, as a first approximation, the pearl-necklace morphology in the PET blends is assumed to consist of long cylinders composed of an isotropic material, but the cylinders are uniaxially aligned in a continuous, birefringent matrix. The theoretical

description of the scattering from such oriented cylinders is well documented in the literature.^{11,12,13} The scattering behaviour of oriented rods was described using the Rayleigh-Gans approximation. In the Rayleigh-Gans approach it is assumed that: a) scattering occurs by weakly refracting particles ($|n_{\text{particle}}/n_{\text{matrix}} - 1| \ll 1$), and b) the particles are small ($< 0.5\mu\text{m}$) with respect to the wavelength of light.¹⁴ The equations of the Rayleigh-Gans approach will be used here for a qualitative interpretation of the results, despite the fact that both assumptions are not exactly met in the oriented blends ($|n_{\text{particle}}/n_{\text{matrix}} - 1| \approx 0.2$ and the length of the rods is in the order of micrometers).

For single scattering from a cylinder with length L , the following correlation can be derived for the electric field strength E_s of the scattered light (the intensity is proportional to the square of the electric field):^{11,15}

$$E_s \approx \frac{\sin\left(k_{s,x} L/2\right)}{\left(k_{s,x} L/2\right)} \quad (2)$$

In this equation, $k_{s,x}$ is the projected length of the scattered wavevector \mathbf{k}_s onto the x-axis which is parallel to the long axis of the cylinder (Figure 5.13). The projected length $k_{s,x}$ is zero for scattering in the y-z plane and the limit of equation 2 goes to unity. However $k_{s,x}$ can attain substantial values for scattering in the x-z plane and the denominator in equation 1 reduces the field strength (and thus the scattered intensity). Consequently, the light-scattering distribution of oriented, rod-like particles is more intense in the y-z plane, perpendicular to the cylinder axis.

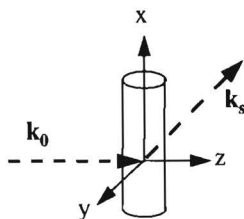


Figure 5.13: Scattering by a cylinder: \mathbf{k}_0 is incoming wavevector, \mathbf{k}_s is scattered wavevector

The 3-D scattering profiles for drawn PET/S-BR core-shell tapes as a function of the particle concentration are depicted below in Figure 5.14. Light scattering in the forward direction is regarded for tapes with identical thicknesses.

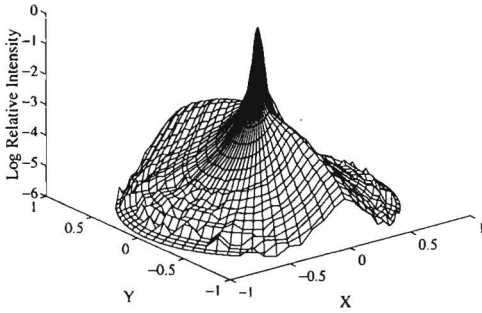
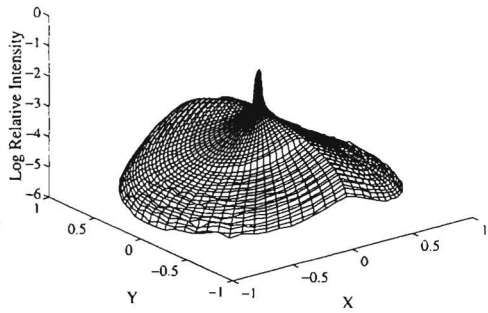
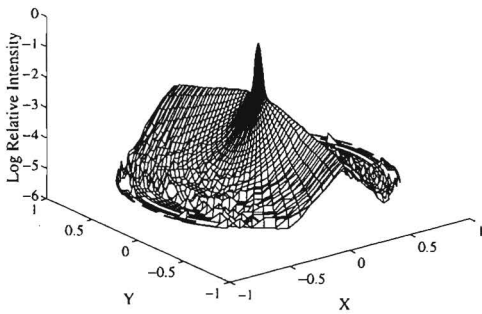
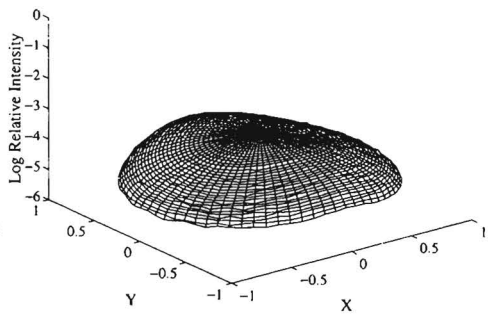
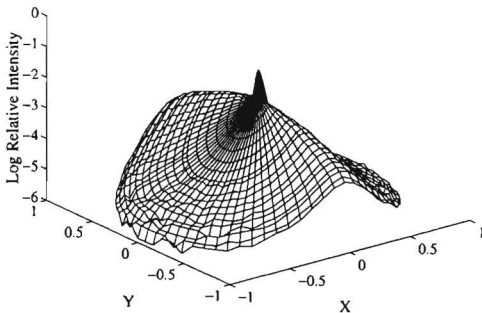
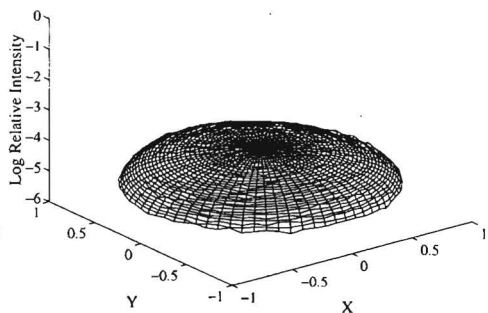
a: 5% w/w, **ss**-polarised**b:** 5% w/w, **pp**-polarised**c:** 10% w/w, **ss**-polarised**d:** 10% w/w, **pp**-polarised**e:** 20% w/w, **ss**-polarised**f:** 20% w/w, **pp**-polarised

Figure 5.14: Forward light scattering profiles for PET/Core-Shell tapes ($\lambda = 3.7$, $d = 0.36$ mm, $T_{\text{draw}} = 85^\circ\text{C}$) as a function of particle concentration: a) 5% w/w **ss**-polarised light; b) 5% w/w **pp**-polarised light; c) 10% w/w **ss**-polarised light; d) 10% w/w **pp**-polarised light; e) 20% w/w **ss**-polarised light; f) 20% w/w **pp**-polarised light

In **ss**-polarised light (Figures 5.14 a,c,e), the direct transmittance peak decreases with increasing particle concentration. This indicates that at high (20% w/w) concentrations, in the transparent state of the polariser, a considerable amount of light is scattered. Apparently, there is no perfect match of the refractive indices perpendicular to the orientation direction of the

blends. In pp-polarised light (scattering state, Figures 5.14 b, d, f), a direct transmittance peak is only observed at low (5% w/w) concentrations. Above 5%, all of the incoming light is scattered. The anisotropy in light scattering, with excess scattering perpendicular to the direction of draw, vanishes and at high (20% w/w) concentrations an isotropic scattering pattern is obtained. At these high concentrations, the diffusive scattering limit for extremely multiple scattering phenomena does apply.^{3,16,17} In this limit it is assumed that light is scattered so many times that the shape of the scattering units becomes irrelevant resulting in an isotropic scattering distribution.

Integrated intensities of scattered radiation are quantified using the experimental integrating sphere set-up (Figure 5.3). The forward and backward intensities are plotted in Figure 5.15 as a function of the particle concentration in the transparent state (s-polarised light) of the polariser at a fixed wavelength (540 nm). In the transparent state, the amount of forward scattered light gradually decreases (curve a) whereas the backward scattered intensity increases (curve b). In a perfect polariser, the refractive indices between the matrix and the core-shell particles are exactly matched and there should be no influence of the particle concentration on the forward or backward scattered intensities. The increase in backward scattering at the cost of forward scattered light is again due to imperfect index matching resulting in undesired scattering losses, which are more pronounced at high (>10%) concentrations.

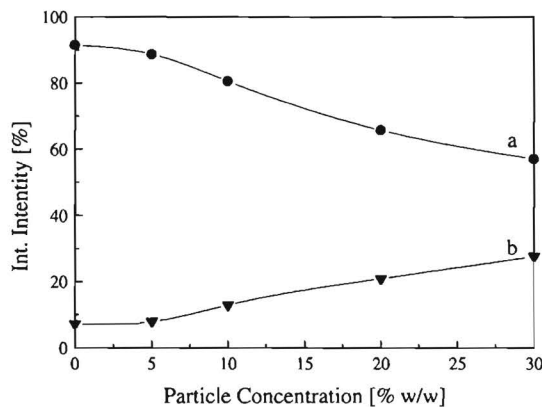


Figure 5.15: Integrated intensity of forward and backward scattering as a function of particle concentration in s-polarised light (540 nm) for PET/Core-Shell blends ($d=0.23$ mm): a) forward direction (●), b) backward direction (▼)

In the scattering state of the polariser (**p**-polarised light, Figure 5.16), there is first a sharp decay in forward scattered intensity (curve b) which levels off to a constant value ($\approx 30\%$) above a particle concentration of 10% w/w. Finally, it is observed that for **p**-polarised light there is an initial raise of backward scattering (curve a) which also levels off above a particle concentration of 10% w/w. The constant scattering levels at particle concentrations exceeding 10% w/w corresponds well with the constant level of polarising performance (PE/T_{sp}) as observed in the previous Chapter (Figure 4.11).

To summarise, it can be concluded that forward scattering is enhanced by a low concentration of scatterers in contrast to backward scattering which is more pronounced at high particle concentrations. This is interpreted in terms of the probability for light to pass the tape in the forward direction which decreases as the number density of scatterers increases.

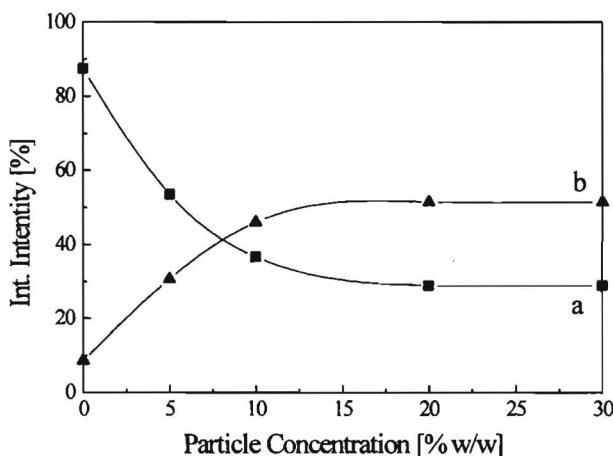


Figure 5.16: Integrated intensity of forward and backward scattering as a function of particle concentration in **p**-polarised light (540 nm) for PET/Core-Shell blends ($d=0.23$ mm): a) forward direction (■), b) backward direction (▲).

In general, scattering of light by particles depends on the wavelength of light.^{18,19} Light scattering is most efficient if the wavelength is in the range of, or smaller than the size of the particles. The wavelength dependence on the total amount of scattered radiation is studied here using the integrating sphere set-up in combination with three different lasers (section 5.2). The intensity of the backward scattered radiation in the opaque state of the polariser (**p**-polarised light) is plotted in Figure 5.17 as a function of wavelength. The wavelength dependence is, however, less than expected from theoretical considerations. Using the Rayleigh-Gans approximation, the scattered intensity should be inversely proportional to the wavelength in the power four ($I \sim 1/\lambda^4$)^{20,21} which is a much stronger wavelength dependence.

This implies that the Rayleigh-Gans approach is not directly applicable to the systems studied here. In the previous Chapter it was also reported that the transmitted light intensities were virtually independent on the wavelength of incident radiation (Figure 4.10).

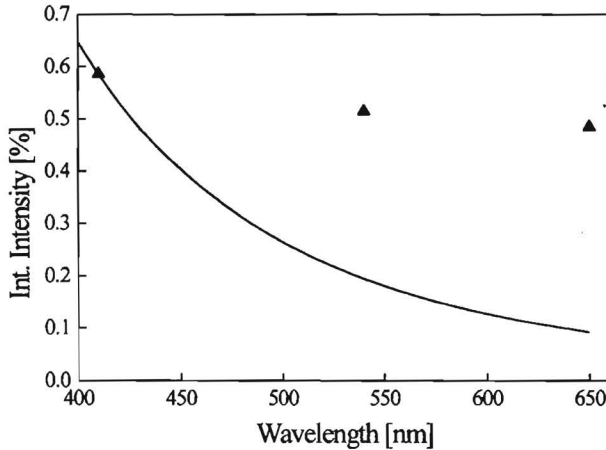


Figure 5.17: Integrated intensity of backward scattered, *p*-polarised light for a 30% (w/w) PET/Core-Shell tape ($d=0.38$ mm) as a function of wavelength: experimental data (\blacktriangle); theoretical curve according to Rayleigh-Gans approximation (—)

So far only results are evaluated concerning the oriented PET/S-Br core-shell tapes. At a particle concentration of 10% w/w, these blends transmit approximately 80% of light in the transparent state (Figure 5.15 curve a) and backscatter approximately 50% of the incoming light in the opaque state (Figure 5.16, curve a). In some of the practical applications, which will be discussed in the epilogue of this thesis, a more extreme forward to backward scattering ratio is necessary. For example, a polarising projection screen, ideally should transmit 100% of one (*s*-) polarisation direction and backscatter 100% of the other (*p*-) polarisation direction. With the specific PET/S-Br core-shell blends the amount of backscattering is insufficient, even at high (30% w/w) particle concentrations. In the previous Chapter, the properties of polarisers based on oriented PET/core-shell blends and on oriented PEN/NAS30 blends were investigated. There were no significant differences found in the polarising performance (PE and T_{sp}) between both polyester blends although the birefringence of oriented PEN ($\Delta n = 0.315$) was twice as high as the birefringence of oriented PET ($\Delta n = 0.135$). Therefore, the next section focuses on the influence of the matrix birefringence on both the scattering patterns and on the forward to backward scattering ratios.

The spatial distribution of light scattering for a PEN/NAS 30 tape (10% w/w, or 12 % v/v) is shown in Figures 5.18 for the forward direction and Figure 5.19 for the backward direction (different scale !).

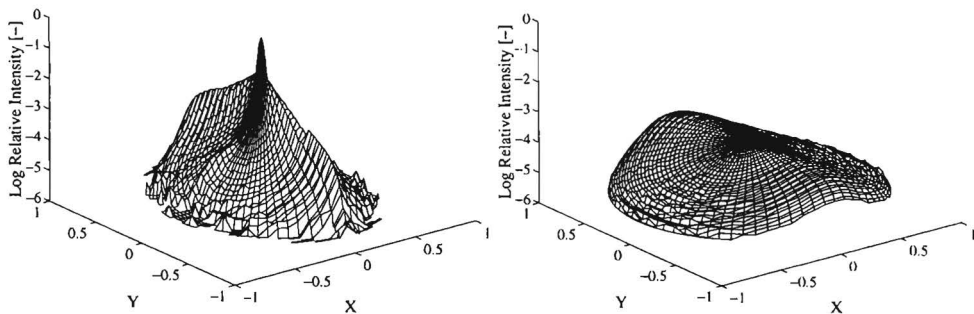


Figure 5.18: 3-D Forward scattering profiles for a drawn PEN/NAS 30 blend (10% w/w, $d=0.17$ mm, $T_{\text{draw}} = 130^{\circ}\text{C}$, $\lambda=4.6$) a) in **ss**-polarised light, and b) in **pp**-polarised light. $x = \sin\theta \cos\phi$; $y = \sin\theta \sin\phi$

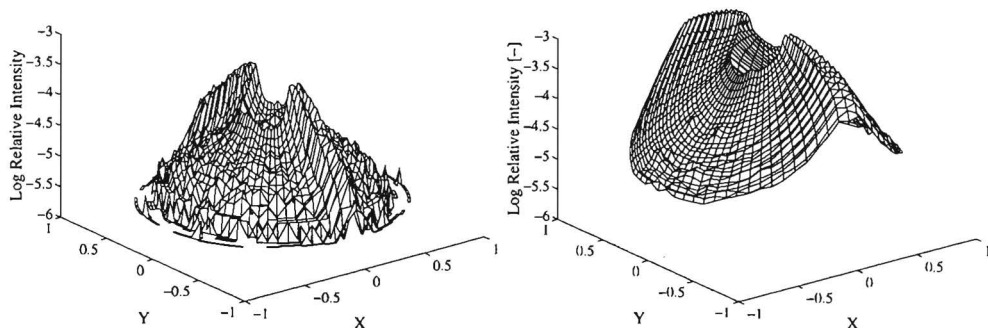


Figure 5.19: 3-D Backward scattering profiles for a drawn PEN/NAS 30 blend (10% w/w, $d=0.17$ mm, $T_{\text{draw}} = 130^{\circ}\text{C}$, $\lambda=4.6$) a) in **ss**-polarised light, and b) in **pp**-polarised light. $x = \sin\theta \cos\phi$; $y = \sin\theta \sin\phi$

The contrast ratio of the PEN polariser in the forward direction $(I_{\text{ss}}/I_{\text{pp}})_{\theta=0^{\circ}}$ is 1800, almost twice as high as the contrast ratio of the PET polarisers. The enhanced contrast is a result of the difference in birefringence between the two matrix polymers. At first sight, the shape of the scattering patterns of the PEN polarisers is identical to the PET polarisers, i.e., the scattered radiation is confined in a plane perpendicular to the orientation direction of the blends. Comparison of the PET and PEN scattering profiles (Figures 5.11/5.12 and 5.18/5.19, respectively), reveals that the anisotropy in the scattering profiles is more pronounced for the PEN blends. The anisotropy is also a result of the shape and alignment of the scattering units

which consists in both blends of cylindrical particles oriented towards the direction of draw. In the case of PEN, the aspect ratio of the dispersed NAS 30 particles is, however, much higher ($l/d_{\text{PEN}} = 70$, $l/d_{\text{PET}} = 20$) and enters the regime for a cylinder with infinite aspect ratio. From the Rayleigh-Gans theory (equation 2) it follows that the decay in intensity parallel to the long axis of the cylinder is much stronger as the length of the cylinder increases (for a cylinder with infinite length L , light is exclusively scattered perpendicular to the long axis¹⁹).

From the spatial scattering distributions it follows that in the opaque state of the polariser, more light is scattered into the backward direction than in the forward direction. Similar conclusions can be drawn from the integrating sphere measurements (Table 1) which show that in the opaque state 75 % of the incoming radiation is backscattered. The other component of light (s-polarised) is transmitted for almost 90%. The 10% of the incoming light which is backscattered includes reflection losses at the air/polymer interfaces (according to Fresnel's law these losses are approximately 8%).

Table 1: Integrating sphere results for a drawn PEN/NAS 30 system (10% w/w, $d=0.23$ mm) at 540 nm

Light polarisation	Forward scattered (%)	Backward scattered (%)	total (%)
p-polarised	24	75	99
s-polarised	88	10	98

For a good comparison of the two different polyester systems, the data of the PET/Core-Shell system with identical particle concentration and sample thickness are depicted in Table 2.

Table 2: Integrating sphere results for a drawn PET/Core-Shell system (10% w/w, $d=0.23$ mm) at 540 nm

Light polarisation	Forward scattered (%)	Backward scattered (%)	total (%)
p-polarised	44	41	85
s-polarised	89	8	97

The PET polarisers scatter p-polarised light to a lesser extent into the backward direction (41% instead of 75%). The fact that the PEN polarisers possess higher contrast ratios and more backscattering of light are a result of the higher mismatch in refractive indices parallel to the orientation direction of the tapes.

Just as in the previous Chapters, this discussion ends with a few critical remarks concerning the results presented in this Chapter. First, it is assumed that the scattering polarisers consist of an optically anisotropic matrix containing isotropic particles. For the PET/Core-Shell

system, this assumption is probably correct because the original spherical (and isotropic) particles are still present in the oriented matrix.²² The PEN/NAS 30 system is drawn at temperatures (130 °C) slightly above the glass transition temperature of the polyester matrix ($T_g^{\text{PEN}} = 125$ °C). Upon drawing, the dispersed NAS 30 phase is uniaxially aligned into long cylinders which may also become birefringent because the drawing temperature is not so far above the glass transition temperature of NAS 30 ($T_g^{\text{NAS30}} = 100$ °C). As a consequence, the assumption of an isotropic dispersed phase is questionable. Secondly, the theoretical Rayleigh-Gans approximations are restricted to single scattering and only used here to qualitatively describe the observed scattering phenomena. A model which quantitatively describes multiple scattering of light by ellipsoidal particles embedded in an anisotropic matrix is currently not available and needs to be developed.

5.4 Conclusions

The angular distribution of light scattering of oriented polyester blends has been investigated in this Chapter. It is shown that for both the PET/Core-Shell and PEN/NAS 30 polarisers, light scattering is anisotropic and more pronounced perpendicular to the orientation direction of the tapes. The anisotropic scattering is explained in terms of the morphology of the drawn blends, which consists of dispersed, uniaxially aligned strings of spherical particles (PET/Core-Shell) or long cylinders (PEN/NAS 30). The ratio forward to backward scattering can be changed by variation of the particle concentration and/or film thickness: An increase in concentration (thickness) increases the backward scattering and decreases the forward scattering. The probability for light to pass the tape in the forward direction after being (multiple) scattered decreases with an increase in concentration and/or tape thickness. The birefringence of PEN is twice as high as the birefringence of PET which results in polarisers possessing not only an improved contrast in the forward direction ($I_{ss}/I_{pp} = 1800$ for PEN versus 1000 for PET), but also improved backscattering properties (in the scattering state 75% of the incoming light is backscattered for PEN systems, whereas 41% is backscattered in the case of PET).

5.5 References

- 1 Driscoll W.G., Vaughan. W., *Handbook of Optics*, Mc Graw-Hill: New York, 1987
- 2 Bastiaansen C., Schmidt H.W., Nishino T., Smith P., *Polymer*, **1993**, 31, 579
- 3 Neijzen J.H.M., Boots H.M.J., Paulissen F.A.M.A., Van der Mark M.B., Cornelissen H.J., *Liq. Cryst.*, **1997**, 22, 255
- 4 Montgomery G.P., *J. Opt. Soc. Am. B*, **1988**, 5, 774
- 5 Whitehead J.B., Zümer S., Doane J.W., *J. Appl. Phys.*, **1993**, 73, 1057
- 6 Zümer S., Golemme A., Doane J.W., *J. Am. Opt. Soc.*, **1989**, 6, 403
- 7 Katime A.I., Quintana J.R., *Comprehensive Polymer Science*, Pergamon Press, Vol. 1, Chapter 5, 1989
- 8 Farwell H.W., *J. Opt. Soc. Am.*, **1938**, 28, 460
- 9 Stein R.S., Rhodes M.B., *J. Appl. Phys.*, **1960**, 31, 1873
- 10 Norris F.H., Stein R.S., *J. Polym. Sci.*, **1958**, 27, 87
- 11 Rhodes M.B., Stein R.S., *J. Polym. Sci. Part A*, **1969**, 7, 1539
- 12 Kotov Y.I., Novikov A.S., *Polym. Sci. USSR*, **1967**, A9, 1714
- 13 Matsuo M., Kakei K., Nagaoka Y., Ozaki F., Murai M., Ogita T., *J. Chem. Phys.*, **1981**, 75, 5911
- 14 Zümer S., Doane J.W., *Phys. Rev A.*, **1986**, 34, 3373
- 15 Dhont J.K.G., *An Introduction to Dynamics of Colloids*, Elsevier: Amsterdam, 1996
- 16 Durian D.J., *Phys. Rev. A*, **1994**, 50, 857
- 17 Zhu J.X., Pine D.J., Weitz D.A., *Phys. Rev. A*, **1991**, 44, 3948
- 18 Können G.P., *Polarized Light in Nature*, Cambridge University Press, 1984
- 19 Möller K.D., *Optics*, University Science Books: California, 1988
- 20 Mie G., *Ann. Phys.*, **1908**, 25, 377
- 21 Van de Hulst H.C., *Light Scattering by Small Particles*, Dover Publications: New York, 1981
- 22 The core-shell particles consist, in the systems studied here, of an isotropic core (styrene-butadiene) and an isotropic shell (crosslinked pmma). The refractive indices of core and shell are matched by varying the copolymer compositions. See for example: Haaf F., Breuer H., Stabenow J., *Angew. Makrom. Chem.*, **1977**, 58, 95

Technology Assessment

The aim of this thesis was to explore new concepts to produce linearly polarised light from thin film, flexible sheets which consist of thermoplastic polymers. This epilogue is dedicated to potential (display) applications of the new polarisation filters and to give recommendations for future research.

In the first part of this thesis, absorbance polarisers based on oriented polyolefins containing dichroic dyes were developed. From theoretical considerations it followed that ultra-drawable polyolefins are intrinsically better host-materials for the fabrication of polarisers in comparison with conventionally used, and less drawable poly(vinyl alcohol). Experimental results showed that the polyolefin polarisers possessed an optical performance at least equal to that of the poly(vinyl alcohol) polarisers. The main application area of the polyolefin polarisers is in displays which are exposed to rather extreme conditions (humidity and temperature). The polyolefin systems possess, due to their apolar character, enhanced stability under these conditions. For example in the automotive industry (dashboards), the new polarisation filters could extend the lifetime of the displays.

However, the polyolefin/dye polarisers described in this thesis were produced via uniaxial *unconstrained* drawing techniques (i.e. with lateral contraction) which resulted in relatively narrow dimensioned systems with an extremely fibrillar surface texture. For practical applications it is essential to produce broad and smooth polarisation filters, which is possible by drawing in the uniaxial *constrained* mode. The difference between these two drawing modes is that in the constrained mode, lateral contraction is prevented during uniaxial drawing. These constrained drawn systems do not possess fibre symmetry and the simple pseudo-affine deformation scheme (Chapter 2, equation 2) describing the orientation of the polymer, is not longer valid (for fibre symmetrical systems the orientation can be described by one angle (θ), whereas in constrained drawn systems two angles (θ and ϕ) are necessary). The theoretical model describing the polarising performance (Chapter 3) needs to be modified by using numerical solutions of the orientation distribution function for uniaxial constrained drawing in the affine mode.^{1,2} However, the main conclusion that enhanced drawability of the host-polymer results in an enhanced orientation of the guest-molecules and in an enhanced polarising performance, will remain valid.

Another problem of the polyolefin polarisers is that the dye molecules absorb light in a relatively small wavelength range (100 nm). Consequently, at least three different dye molecules are necessary for the production of polyolefin dye polarisers covering the entire visible wavelength range.^{3,4} Each of these dyes should operate in a specific part of the visual spectrum. Additionally, the molecular structure of the dye molecules needs to be highly

anisotropic (rod-like), to ensure a high polarising performance of the polariser. Finally, the dye molecules should be compatible with apolar polyolefins to prevent migration of the dyes from the bulk to the film surface. The above mentioned conditions demand for an extensive research on the synthesis of highly anisotropic (linear tri- or tetra- azo dyes), wavelength-tuned, polyolefin-compatible dyes.

In the second part of this thesis, light-scattering polarisers have been produced from oriented polyester blends. The polarisers operate on the principle of selectively matching and mismatching of refractive indices between an oriented polyester matrix and the dispersed phase. Polarisation of light is achieved without absorbing half (or more) of the incoming light, i.e., no heat is formed in the polariser. Application areas of the scattering polarisers are in projection displays, projection screens and in conventional backlit direct view displays (transmissive direct-view). Each of these applications will be shown below and discussed with respect to potential advantages of the scattering polarisers.

In Figure 1, a schematic representation is depicted of a projection system consisting of, respectively, a light source, a polariser, a Twisted Nematic (TN) Liquid Crystal cell, the second polariser, an aperture stop, projection lenses and finally a projection screen. In a conventional projection set-up, light absorbing polarisers are used (for example H-sheet polarisers). The image formed by the TN-cell in combination with the two polarisers is projected onto the screen. The first polariser absorbs at least half of the light coming from the light source and the absorbed light is transformed into heat. Consequently, in large area projection systems, requiring high-intensity light sources, excessive heating up is followed by thermal degradation of the polariser. In the new display configuration, the two absorbance polarisers are replaced by scattering polarisers. In the transparent state of the polarisers, a highly collimated beam passes the aperture stop and reaches the projection screen. In the scattering state, light is scattered in the forward and backward direction without heat formation. The (forward) scattered part is almost completely blocked by the aperture stop and can not reach the projection screen. By selectively addressing the liquid crystalline molecules (pixels), images are produced onto the screen. The main advantage of the scattering polariser is that light is linearly polarised without heat formation in the polarisers. Heat is now formed at the aperture stop which is less dramatic with respect to polar degradation and LC-heating. Consequently, thermal degradation effects are prevented and high-intensity light sources can be used.

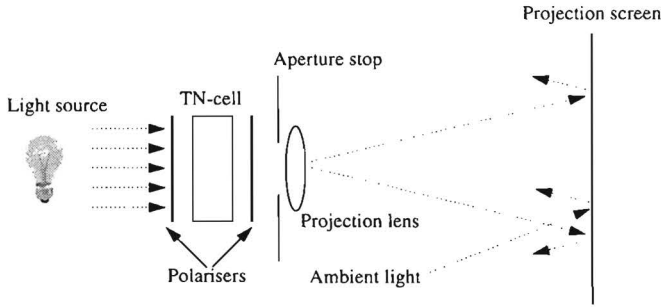


Figure1: Schematic representation of a projection display

Another disadvantage of conventional projection systems is that the contrast of the projected image is drastically reduced by ambient light (room illumination).⁵ This effect is demonstrated by means of a numerical example which is depicted in Table 1.

Table 1: Reduction of contrast by ambient radiation in projection systems with a standard and with a polarising projection screen. Intensities in arbitrary units (a.u.)

	No ambient light: 0			Ambient light: 20		
	Intensity bright state	Intensity dark state	Contrast ratio	Intensity bright state	Intensity dark state	Contrast ratio
Standard projection screen	200	2	100	220	22	10
Polarising projection screen	200	2	100	210	12	18

In a standard display configuration, the image is projected onto a screen which reflects all polarisation directions of the incoming light. The contrast is reduced (from 100 to 10) because all of the ambient radiation is also reflected by the screen which affects especially the dark state of the image. In a new display configuration, the projection system consists of a light source, polariser, TN-cell, projection lens and a polarising projection screen, i.e., the second polariser after the TN-cell has been removed and replaced by the polarising screen.⁶ The polarising screen ideally transmits one component of the incoming radiation whereas the orthogonal component is completely backscattered. Images are produced on the screen just as in a standard projection system, however the influence of the ambient radiation on the dark state of the image is reduced because only half of the ambient radiation is “reflected”. As a consequence, the contrast reduction is less (from 100 to 18) in comparison with a standard

projection screen. Especially the properties of the oriented PEN/NAS 30 polarisers are of interest with respect to the polarising projection screen because 90% of s-polarised light is transmitted in contrast to p-polarised light which is backscattered for 80% (Chapter 5). The backscattered part is confined in a plane perpendicular to the orientation direction of the film which implies that, for a polarising projection screen, the viewing angle is altered in only one direction. For example, if the projection screen is positioned with the drawing direction vertical, the viewing angle will be high in the horizontal plane which might be desirable in projection systems.

The last example of a practical application of light-scattering polarisers is in a backlit direct view display (notebook computers). In a standard backlit display the two conventional polarisers lead to undesired light losses which reduce the brightness of the display. The light-scattering polariser, mainly the PEN/NAS 30 systems, can enhance the light efficiency of such a system by recycling of light, as is explained in Figure 2. In a standard display configuration (a), light is directed through the waveguide and illuminates the LCD cell. The bottom polariser ideally transmits half of the incoming light, which is subsequently modulated by the liquid crystalline molecules to form an image together with the top polariser.

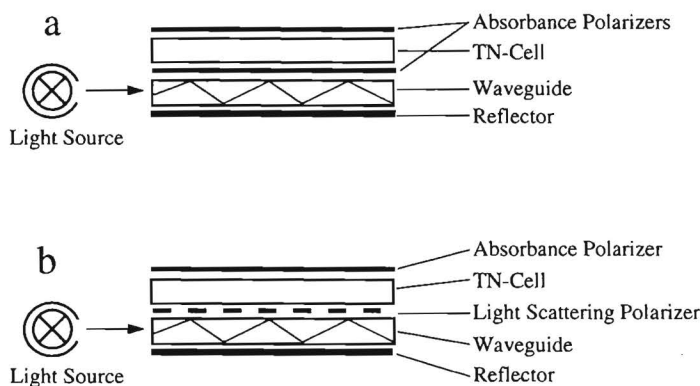


Figure 2: Schematic representation of a backlit direct view LCD a) without and b) with a light-scattering polariser

In the new display set up (b), the bottom absorbance polariser is replaced by a scattering polariser. The scattering polariser, ideally transmits one of the two principal polarisation directions, whereas the other polarisation direction is backscattered into the waveguide. The backscattered light is depolarised by multiple reflections in the waveguide and is finally redirected into the LCD cell. Whereas in the conventional display set-up half of the incoming

light is absorbed (and lost), the new set-up can recycle the backscattered light and, consequently, enhances the brightness and energy efficiency of the device.^{7,8}

The aforementioned applications demand for smooth, large-area light-scattering polarisers which cannot be produced with the uniaxial unconstrained drawing techniques used in this thesis. For the scattering polarisers it is, therefore, essential to draw the polymeric blends in the constrained mode. Initial experiments on constrained drawn PET blends showed that polarised light can be produced from constrained drawn systems indeed. For future research it is recommended to further optimise the PEN/NAS 30 system because in this thesis only one particle concentration was studied and no attention was paid to, for example, the influence of the particle size on the scattering properties.

References

- 1 Wu P.D., van der Giessen E., *Mech Res. Comm.*, **1992**, 19, 427
- 2 Wu P.D., van der Giessen E., *J. Mech. Phys. Solids*, **1993**, 41, 427
- 3 Land E.H., West C.D., *Colloid Chemistry*, ed. J. Alexander, Reinhold Publishing Corporation: New York, 1946
- 4 Scheffer T.J., *J. Appl. Phys.*, **1982**, 53, 257
- 5 Drzaic P.S., *Liquid Crystal Dispersions*, Vol. 1, World Scientific Publishing: Singapore, 1995
- 6 Uetsuki M., *Jpn. J. Appl. Phys.*, **1996**, 35, 772
- 7 Broer D.J., Lub J., Mol G.N., *Nature*, **1995**, 378, 467
- 8 Belayev S.V., Schadt M., Barnik M.I., Fünfschilling J., Malimoneko N.V., Schmitt K., *Jpn. J. Appl. Phys.*, **1990**, 29, L634

Appendix A: Characterisation of Polarisers

The performance of polarisers can be expressed in a variety of criteria which can be subdivided into two classes: i) parameters related to the orientation and optical characteristics of the dye molecules, and ii) parameters which are of practical importance. The dichroic ratio (R) and order parameter (S) belong to the first class, whereas the polarising efficiency (PE) and single-piece transmittance (T_{sp}) are typical examples of the second class. For all of these parameters, correct values for the principal absorbances (or transmittances), respectively parallel and perpendicular to the direction of draw need to be substituted into the relevant equations (Chapter 3, eqn. 10-13). The principal absorbances can be quantified using a double beam UV/VIS spectrometer which measures the absorbance as a function of wavelength. However, special care should be taken in these UV/VIS experiments to avoid influences of the source polarisation, the instrumental polarisation (due to, for instance, mirrors, prisms) or the sensitivity of the detector for the plane of polarisation.¹ Therefore, these polarisation phenomena need to be measured or eliminated, to avoid errors in the calculations of the polarising performance. This is easy if an auxiliary reference polariser is available that has a much higher optical quality than the one to be measured, but somewhat more complex if their performances are comparable. Both measuring procedures will be discussed in the next paragraphs in detail.

a) Measuring the performance of polarisers with moderate optical anisotropy

Two auxiliary reference polarisers (Nitto Denko NPF G1229 DU) need to be positioned horizontally in front of the measuring and reference beam of the spectrometer and a background correction (air versus air) is executed. The drawn, coated guest-host systems or light-scattering polarisers are subsequently put horizontally in the measuring beam and absorbance spectra are recorded in the visible wavelength range (400-800 nm). Special attention is paid to the correct positioning of the sample, so that the complete measuring spot illuminates the sample. The background correction procedure and sample measurements are repeated with the two reference polarisers in a vertical position. Finally the absorbance spectra are corrected for surface reflections to obtain the principal parallel ($A_{||}$) and perpendicular (A_{\perp}) absorbances from which the principal transmittances can be derived.

b) Characterisation of high-performance polarisers

The method described here to quantify the principal transmittances ($T_{||}$ and T_{\perp}) without the use of auxiliary polarisers was first used by Rupprecht et al.² Assume a source emitting light with intensity I_0 . The transmittance of the optical system without a polarising guest-host tape (i.e. only coated glass slides) in the measuring beam, T_0 can be defined as (equation A.1):

$$T_0 = \frac{1}{2} I_0 t_h + \frac{1}{2} I_0 t_v \quad (\text{A.1})$$

In this equation, t_h and t_v are the effective transmittances of the spectrometer with polarised light in the horizontal and vertical plane, respectively. In these two effective transmittances, all influences of instrument polarisation and air-glass reflections are lumped together as a product. If a polymer/dye polariser is placed in the measuring beam with the axis of draw fixed horizontally or vertically, the respective transmittances T_h and T_v are given by:

$$T_h = \frac{1}{2} I_0 t_h T_{\parallel} + \frac{1}{2} I_0 t_v T_{\perp} \quad (\text{A.2})$$

$$T_v = \frac{1}{2} I_0 t_h T_{\perp} + \frac{1}{2} I_0 t_v T_{\parallel} \quad (\text{A.3})$$

Combining equations A.1, A.2 and A.3 yields equation A.4:

$$\frac{T_h + T_v}{T_0} = T_{\parallel} + T_{\perp} \quad (\text{A.4})$$

Next, the transmittance T_{hv} , of two crossed polarisers is measured which is given by:

$$T_{hv} = \frac{1}{2} I_0 (t_h T_{\parallel} T_{\perp} + t_v T_{\perp} T_{\parallel}) \quad (\text{A.5})$$

From which it follows that:

$$\frac{T_{hv}}{T_0} = T_{\parallel} T_{\perp} \quad (\text{A.6})$$

The two principal transmittances (T_{\parallel} and T_{\perp}) are obtained by combining equations A.6 and A.4 using the solutions for a quadratic equation:

$$T_{\parallel} = \frac{T_h + T_v}{2T_0} \left[1 - \sqrt{1 - \frac{4T_0 T_{hv}}{(T_h + T_v)^2}} \right] \quad (\text{A.7})$$

$$T_{\perp} = \frac{T_h + T_v}{2T_{hv}} \left[1 + \sqrt{1 - \frac{4T_0 T_{hv}}{(T_h + T_v)^2}} \right] \quad (\text{A.8})$$

Substitution of equations A.7 and A.8 into the formulas for the polarising efficiency (PE) and single-piece transmittance (T_{sp}) results in relationships between the measured transmittances and the polarising performance:

$$PE = \sqrt{1 - \frac{4T_0 T_{hv}}{(T_h + T_v)^2}} \quad (\text{A.9})$$

$$T_{sp} = \frac{T_h + T_v}{2T_0} \quad (\text{A.10})$$

A typical example of a set of transmission measurements on a drawn ($\lambda=15$) i-PP/tri-azo dye tape is shown below (Figure A.1): Transmittance T_0 (curve a) with no sample in measuring beam, only two sandwiched glass slides containing mineral oil; transmittances T_h and T_v (curves b and c) with the tape positioned horizontally, respectively vertically; transmittance T_{hv} (curve d) with two crossed tapes in the measuring beam.

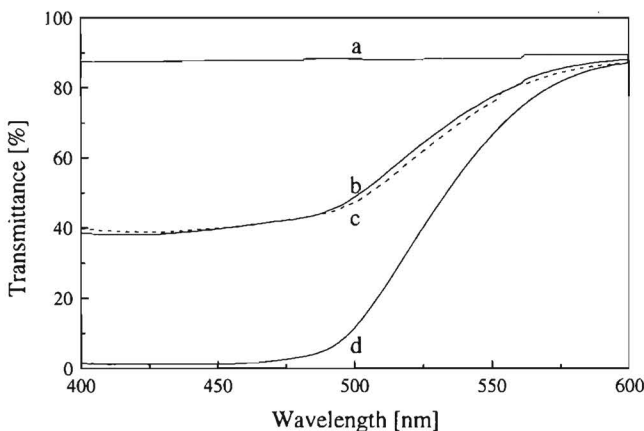


Figure A.1: Transmittance as a function of wavelength for a drawn i-PP/tri-azo dye tape: a) T_0 , b) T_v , c) T_h , d) T_{hv}

The corresponding polarising efficiencies and single-piece transmittances calculated using equations A.9 and A.10 are depicted in Figure A.2.

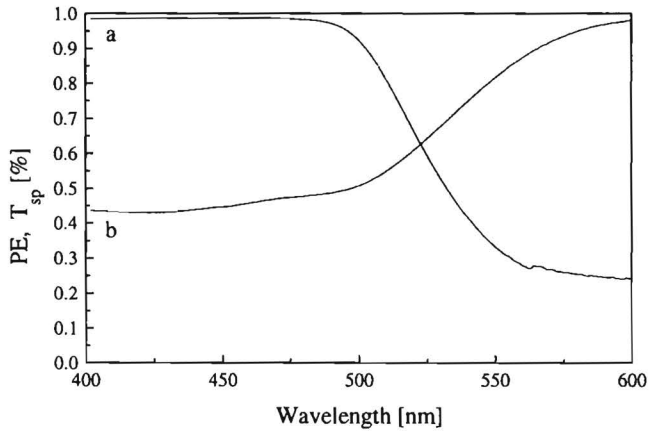


Figure A.2: a) Polarising Efficiency (PE) and, b) Single-piece Transmittance (T_{sp}) as a function of wavelength for a drawn i-PP/Tri-azo dye tape

References

- 1 Driscoll W.G., Vaughan W., *Handbook of Optics*, Mc Graw-Hill: New York, 1987
- 2 Rupprecht G., Ginsberg D.M., Leslie J.D., *J. Opt. Soc. Am.*, **1962**, 52, 665

Appendix B: The Lambert Beer's Law Approximation

In the theoretical model describing the optical properties of oriented polymer/dye polarisers, the parallel and perpendicular absorbances are calculated using Lambert-Beer's law (equations 6 and 7, § 3.2). In this law a linear correlation is assumed between the absorbance on one side and the dye concentration (or film thickness) on the other side. The theoretical model is validated using a model guest-host system consisting of oriented High-Density Polyethylene containing Sudan Red B as a dichroic guest. Therefore, we first want to verify if Lambert-Beer's law holds for this specific guest-host system. In Figure B.1, experimental values for the parallel and perpendicular absorbances (divided by the film thickness) of drawn HDPE/Sudan Red B tapes are depicted as a function of the dye concentration.

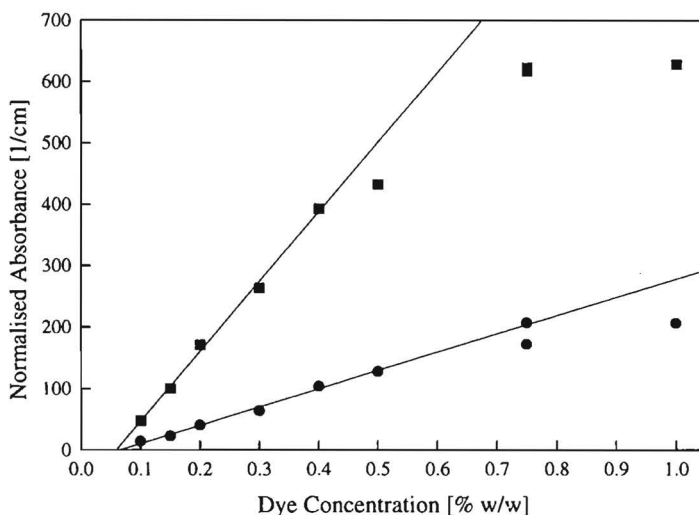


Figure B.1: Normalised Absorbance of drawn HDPE/Sudan Red B films ($\lambda=10$), corrected for variations in film thickness (d), as a function of the dye concentration: parallel absorbance, $A_{||}/d$ (■); perpendicular absorbance A_{\perp}/d (●)

The linear relationships which can be observed indicate that Lambert-Beer's law is valid for both absorbances. Deviations from Lambert-Beer for the parallel absorbance occur at higher ($c > 0.4$ % w/w) concentrations than the dye concentration (0.2%) used for the verification of the aggregate model (§ 3.5).

However, in the theoretical estimation of the ultimate optical properties (§ 3.6), substantially higher dye concentrations (>1% w/w) were used in the calculations. Consequently, the average distance between the dye molecules is reduced to the point where the electronic absorption transitions of a dye are influenced by its neighbours and Lambert-Beers law is no longer valid. At these high absorbances, in the order of $A=2$, application of Lambert-Beer's law will, of course, result in errors in the predictions of the polarising efficiency and single-piece transmittance. These errors will be mainly related to the parallel absorbance ($A_{||}$) which can attain high values at high draw ratios combined with high dichroic ratios. From the equations for the polarising efficiency and single-piece transmittance (§ 3.2, eqn. 12 and 13) it follows that:

$$\left| \frac{\delta PE}{PE} \right| = \frac{2 \cdot 10^{(A_{||} + A_{\perp})} \ln 10}{10^{2A_{||}} - 10^{2A_{\perp}}} \left| \delta A_{||} \right| \approx 2 \ln 10 \frac{A_{||}}{10^{A_{||}}} \left| \frac{\delta A_{||}}{A_{||}} \right| \quad (\text{B.1})$$

and

$$\left| \frac{\delta T_{sp}}{T_{sp}} \right| = \frac{\ln 10 A_{||} 10^{A_{\perp}}}{10^{A_{||}}} \left| \frac{\delta A_{||}}{A_{||}} \right| \approx \ln 10 \frac{A_{||}}{10^{0.9A_{||}}} \left| \frac{\delta A_{||}}{A_{||}} \right| \quad (\text{B.2})$$

assuming that $A_{\perp} \approx 0.1A_{||}$

So, for example, at an absorbance of $A_{||} = 2$, the relative error in the polarising efficiency is already ten times smaller than the relative error in the parallel absorbance. The same holds for the single-piece transmittance. In other words, at high absorbances, the PE and T_{sp} are mainly determined by the low perpendicular absorbance A_{\perp} for which Lambert-Beer's law does apply.

Appendix C: Depolarisation in light-scattering polarisers

Scattering by small dispersed particles can be interpreted as scattering by infinitesimally small volume elements. If such a volume element is identified with a point scatterer, this theory is called the Rayleigh-Gans approximation. The general Rayleigh-Gans expression describing the scattered field strength E_s is given by:

$$E_s = \epsilon_s \frac{1}{V} \int_V e^{-i\mathbf{q}\cdot\mathbf{r}} d\mathbf{r} \tag{C.1}$$

in which V represents the volume of the scattering particles, ϵ_s is a pre-factor, \mathbf{q} is the difference vector of the scattered and incoming wavevectors ($\mathbf{q} = \mathbf{k}_0 - \mathbf{k}_s$, see Figure 5.12) and \mathbf{r} the position co-ordinate of the scatterers.

Single scattering

The pre-factor ϵ_s contains a factor $\mathbf{u}_{out} \cdot \Delta\epsilon \cdot \mathbf{u}_{in}$. In this factor, \mathbf{u}_{out} and \mathbf{u}_{in} represent the unit vectors of polarisation of, respectively, the scattered light and the incoming light. The tensor $\Delta\epsilon$ represents the difference in dielectric constant between the scatterers and the surrounding medium (i.e., in this case the particles and the matrix). The dielectric constant is related to the refractive index as: $\Delta\epsilon = \Delta n^2$. For an isotropic medium (ϵ_m) containing isotropic particles (ϵ_p) the tensor $\Delta\epsilon$ is given by:

$$\Delta\epsilon = \begin{vmatrix} \epsilon_m - \epsilon_p & 0 & 0 \\ 0 & \epsilon_m - \epsilon_p & 0 \\ 0 & 0 & \epsilon_m - \epsilon_p \end{vmatrix} \tag{C.2}$$

Consequently, $\mathbf{u}_{out} \cdot \Delta\epsilon \cdot \mathbf{u}_{in}$ will equal $(\epsilon_m - \epsilon_p) \mathbf{u}_{out} \cdot \mathbf{u}_{in}$. In the situation of crossed polarisers (**sp** or **ps**), the inner products will be zero and therefore the scattered intensity, which is proportional to the square of the electric field strength, will be zero too. No depolarisation effects occur in the case of isotropic, single scattering.

In the case of an anisotropic medium containing isotropic scatterers, and there is only a mismatch in one direction, in this case the x direction. The corresponding dielectric tensor is given by:

$$\Delta\epsilon = \begin{vmatrix} \epsilon_m - \epsilon_p & 0 & 0 \\ 0 & 0 & 0 \\ 0 & 0 & 0 \end{vmatrix} \quad (\text{C.3})$$

The refractive indices are matched in the y and z directions and there is a mismatch in the x-direction. The mismatching direction (the drawing direction) can be represented by a unit vector $\mathbf{d} = (1 \ 0 \ 0)$, which is called the director. The dielectric tensor can be rewritten as the projection of $\Delta\epsilon$ on \mathbf{d} : $\Delta\epsilon = (\epsilon_m - \epsilon_p) \mathbf{d} \cdot \mathbf{d}$.

$\mathbf{u}_{\text{out}} \cdot \Delta\epsilon \cdot \mathbf{u}_{\text{in}}$ will therefore become: $(\epsilon_m - \epsilon_p) (\mathbf{u}_{\text{out}} \cdot \mathbf{d}) (\mathbf{u}_{\text{in}} \cdot \mathbf{d})$. If one of the two unit vectors of polarisation is perpendicular to the director \mathbf{d} (i.e. in the **ss**, **sp** and **ps** configurations), the electric field strength of the scattered radiation will be zero. Or, in other words, mismatching in only one direction will not result in depolarisation effects in the single scattering regime.

Double scattering

For an isotropic medium, the scattered intensity I in the case of double scattering is related to the state of polarisation by: $I \propto |\Delta\epsilon|^2 (1 + 2 (\mathbf{u}_{\text{out}} \cdot \mathbf{u}_{\text{in}})^2)$. Even when the unit vectors of polarisation are perpendicular ($\mathbf{u}_{\text{out}} \perp \mathbf{u}_{\text{in}}$), the scattered intensity will be non-zero. Consequently, upon multiple scattering in an isotropic medium, light will be depolarised.

If, however, the medium is anisotropic with mismatching in only one specific direction, the intensity I is proportional to: $I \propto |\Delta\epsilon|^2 (\mathbf{u}_{\text{out}} \cdot \mathbf{d})^2 (\mathbf{u}_{\text{in}} \cdot \mathbf{d})^2$. In this case the scattered intensity will be zero if one of the two polarisation vectors is perpendicular to the director \mathbf{d} (**ss**, **sp** and **ps** configurations). Therefore, upon multiple scattering in an anisotropic medium with one mismatching direction, no depolarisation of light occurs.

Samenvatting

Vlakfilm polarisatoren worden tegenwoordig veelvuldig toegepast in vloeibaar-kristallijne displays (LCDs). Deze polarisatiefilters zijn gemaakt van georiënteerde polymeren die dichroïtische gast-moleculen bevatten. De dichroïtische gast-moleculen absorberen licht met een polarisatierichting evenwijdig aan de optische as van het molecuul. Oriëntatie van alle gast-moleculen door het georiënteerde polymeer waarin ze gedispergeerd zijn, resulteert in macroscopisch dichroïtisch gedrag en de typische eigenschappen van een lineair polarisatiefilter: twee evenwijdige polarisatiefilters zijn transparant terwijl twee gekruiste filters nauwelijks licht zullen doorlaten.

Commerciële polarisatoren worden gemaakt van verstrekt, georiënteerd poly(vinyl alcohol) (PVAL) in combinatie met een dichroïtische kleurstof of Jood als gast-molecuul. Deze polarisatiefilters op basis van PVAL hebben als nadeel dat ze op de lange termijn niet stabiel zijn in een vochtige omgeving en/of bij een verhoogde temperatuur. Dit stabiliteitsprobleem beperkt de toepassing van vloeibaar-kristallijne displays in bijvoorbeeld automobiele applicaties (dashboards).

In de afgelopen jaren is aangetoond dat polarisatiefilters met een hoge dichroïtische verhouding en ordeparameter gemaakt kunnen worden door dichroïtische kleurstoffen te oriënteren in verstreckte polyolefinen. Bovendien hebben deze polarisatoren een verbeterde vocht- en temperatuurrezistentie.

In het eerste deel van dit proefschrift wordt een theoretisch model afgeleid om de optische eigenschappen te beschrijven van licht absorberende polarisatoren op basis van verstreckte polymeren die dichroïtische kleurstoffen bevatten. Een van de aannamen in het model is dat tijdens het verstrekken de oriëntatie van zowel het polymeer als de dichroïtische kleurstof beschreven kan worden met het pseudo-affiene deformatiemechanisme. Verder is er aangenomen dat de ontwikkeling van optische anisotropie met toenemende oriëntatiegraad beschreven wordt met behulp van een aggregaat van optische elementen. De macroscopische optische eigenschappen zoals contrast (polarising efficiency) en transpartheid (single piece transmittance) worden berekend op basis van een serieschakeling van de optische elementen van het aggregaat. Deze aannamen zijn geverifieerd aan de hand van diverse types smeltgekristalliseerde polyethylenen (lage dichtheid polyethyleen, lineair lage dichtheid polyethyleen, hoge dichtheid polyethyleen en ultra-hoog moleculair polyethyleen) in combinatie met dichroïtische di-azo kleurstoffen. De voorspellende eigenschappen van het model zijn getoetst aan de hand van experimentele resultaten van een model systeem (Hoge dichtheid polyethyleen/Sudan Red B), waarbij er een goede overeenkomst bestaat tussen

theorie en experiment. Het model is verder gebruikt om de parameters te bepalen die belangrijk zijn voor de (ultieme) optische prestaties van de polarisator. De voorwaarden voor de fabricage van een filter met een hoog contrast en transparantie zijn: (a) een hoge oriëntatiegraad van het polymeer en daarmee samenhangend polymeren en productieprocessen die resulteren in hoog-verstreekbare systemen ($\lambda > 15$), (b) kleurstof moleculen met een hoge optische anisotropie en een hoge aspect verhouding, (c) een geoptimaliseerde filmdikte en kleurstofconcentratie. Een direct gevolg van (a) is dat hoog-verstreekbare, lineaire polyolefinen intrinsiek beter zijn voor de productie van polarisatiefilters ten opzichte van het laag verstreekbaar poly(vinyl alcohol). Experimentele resultaten tonen inderdaad aan dat de optische eigenschappen van hoog-verstreekt polypropyleen in combinatie met een lineaire tri-azo kleurstof de theoretische limiet benaderen voor een perfecte polarisator.

Een onoverkomelijk probleem van zowel de conventionele PVAL als de nieuwe polyolefine polarisatoren is dat ze gebaseerd zijn op anisotrope absorptie van licht. Dit betekent dat zelfs in een perfecte polarisator de helft van het opvallende licht geabsorbeerd wordt door de gast-moleculen. Een gevolg hiervan is dat de licht en/of energie efficiëntie van LCD displays laag is omdat (minimaal) de helft van het licht verloren gaat. Bovendien veroorzaakt de geabsorbeerde energie een niet gewenste temperatuuroename van de polarisator die, in combinatie met hoge-intensiteits lichtbronnen (projectie systemen), de levensduur van het display verlaagt.

In het tweede deel van dit proefschrift is dientengevolge een ander concept beschreven voor de polarisatie van licht op basis van anisotrope verstrooiing in plaats van anisotrope absorptie. Deze licht verstrooiende polarisatiefilters zijn vervaardigd uit blends bestaande uit thermoplastische polyesters zoals poly(ethyleen tereftalaat) (PET) of poly(ethyleen 2,6-naftaleendicarboxylaat) (PEN) met daarin gedispergeerde deeltjes (rubberachtige core-shell deeltjes of thermoplastische styreen-methylmethacrylaat copolymeren). De blends zijn geëxtrudeerd tot tapes die vervolgens zijn verstrekt in de vaste toestand zodat er een hoog-dubbelbrekende matrix ontstaat die isotrope deeltjes bevat. De componenten van de blend zijn zodanig gekozen dat na de strekprocedure de brekingsindices van de matrix en de disperse fase loodrecht op de strekrichting gelijk zijn aan elkaar. In de strekrichting is er echter een groot verschil in brekingsindices tussen de matrix en disperse fase. Als gevolg hiervan zal licht met een polarisatie-richting loodrecht op de strekrichting doorgelaten worden vanwege de identieke brekingsindices, terwijl licht gepolariseerd in de strekrichting verstrooid wordt door het grote verschil in brekingsindices.

Deze georiënteerde polyester blends polariseren licht over het totale zichtbare golflengtegebied (400-700 nm) met een efficiëntie (polarising efficiency en single piece transmittance) die vergelijkbaar is met de licht absorberende PVAL filters. Net zoals bij de absorberende systemen kan de optische performance over een breed gebied gevarieerd worden

door de deeltjesconcentratie en/of filmdikte aan te passen. Een toename in de deeltjesconcentratie (filmdikte) resulteert in een hoger contrast en een lagere transparantie en vice versa. Uit de hoekafhankelijke lichtverstrooiing blijkt dat het licht hoofdzakelijk verstrooid wordt in een vlak loodrecht op de strekrichting van de blends. Deze anisotropie in verstrooide intensiteit is een gevolg van de cylinder vorm van de verstrooiende deeltjes die voor PET bestaat uit georiënteerde agglomeraten van meerdere core-shell deeltjes en in het geval van PEN bestaat uit lange cylinders. De hoeveelheid voorwaarts ten opzichte van terugwaarts verstrooid licht is een functie van de deeltjesdichtheid (concentratie), de filmdikte en de dubbele breking van de matrix. Voor de PET blends kan er maximaal 41% van het opvallende licht terugverstrooid worden terwijl 75% terugverstrooid wordt bij de PEN blends. De contrastverhouding in de voorwaartse richting is 1000 en 1800, respectievelijk voor de PET en PEN blends. Zowel de hogere contrastverhouding als de hogere terugverstrooiing van de PEN blends kunnen toegeschreven worden aan de hogere dubbele breking van de georiënteerde PEN blends ($\Delta n_{PEN} = 0.315$, en $\Delta n_{PET} = 0.135$).

Potentiële voordelen van het verstrooiings principe zijn dat, in een juiste display configuratie, al het opvallende licht omgezet kan worden in lineair gepolariseerd licht zonder dat er warmte wordt geproduceerd. Dit kan zowel de helderheid van conventionele displays verhogen maar daarnaast ook de levensduur van projectie systemen. Tenslotte zijn deze polarisatiefilters, in tegenstelling tot verstrooiende/reflecterende systemen op basis van vloeibaar-kristallijne materialen, gemaakt van thermoplastische polymeren en dientengevolge verwerkbaar op standaard film-verstrek apparatuur in combinatie met vlakfolie-extrusie hetgeen voordelig is voor de continue productie van deze polarisatoren.

Dankwoord

Op de eerste plaats wil ik Kees Bastiaansen en Theo Tervoort bedanken voor de prettige samenwerking, de inspirerende discussies en de theoretische ondersteuning van het onderzoek gedurende de afgelopen jaren. Verder gaat mijn dank uit naar alle mensen die als kamergenoot mee konden “genieten” van mijn onderzoek; met name Yvonne Engelen en Anne Spoelstra voor hun hulp bij het morfologisch onderzoek.

Waardering is er voor alle (ex) afstudeerders en researchstagiaires die een onmisbare bijdrage leverden aan het experimentele werk: Joost Broeders, Martine Dols, Henri Jagt, Henri van Lijssel, Chris Senden, Baljit Singh en Henk Thomassen. Een woord van dank aan Hennie Zirkzee die mij hielp bij de emulsiepolymerisaties.

Bij Philips Research Laboratories zou ik Rifat Hikmet en Henk Boots willen bedanken voor hun belangrijke bijdrage op het gebied van de hoekafhankelijke lichtverstrooiing. DSM Research ben ik erkentelijk voor het gebruik van strekapparatuur en met name Frans Gelissen voor zijn hulp bij de extrusie-experimenten.

Dank aan alle medewerkers en (ex) promovendi van de vakgroep; jullie collegialiteit heeft ertoe bij gedragen dat ik een zeer fijne en uitdagende tijd bij “TPK” gehad heb.

“Last but not least” een speciaal woord van dank aan mijn ouders voor hun steun en belangstelling gedurende de afgelopen jaren.

Curriculum Vitae

De schrijver van dit proefschrift werd geboren op 5 september 1969 te Stein, waar hij in 1987 aan de Scholengemeenschap Groenewald het Atheneum diploma behaalde. Aansluitend volgde hij de studie Scheikundige Technologie aan de Technische Universiteit Eindhoven die in 1992 voltooid werd binnen de vakgroep kunststoftechnologie van prof.dr. P.J. Lemstra. Van 1992 tot 1995 werd de tweejarige Onderzoekersopleiding Scheikundige Technologie gevolgd bij het Instituut Vervolgopleidingen Eindhoven. Het onderzoek behorende bij de tweejarige opleiding werd voortgezet binnen de vakgroep kunststoftechnologie en de resultaten zijn in dit proefschrift weergegeven. Vanaf oktober 1997 zal de schrijver van dit proefschrift een post-doctoraal onderzoek verrichten in de groep van prof.dr. P. Smith aan de ETH Zürich.

Stellingen

behorende bij het proefschrift

Polarisers Based on Anisotropic Absorbance or Scattering of Light

van

Yvo Dirix

- 1) Het pseudo-affiene deformatiemodel waarbij de oriëntatie uitsluitend door de verstrekgraad bepaald wordt, kan uitstekend gebruikt worden om zowel de oriëntatie van smeltgekristalliseerde polyethenen als van dichroïtische gastmoleculen te beschrijven.

Dit proefschrift hoofdstukken 2 en 3

Dirix Y., Tervoort T.A., Bastiaansen C.W.M., Lemstra P.J. *J. Text. Inst.*, **1995**, 86, 314

- 2) Lineaire, hoog-verstreekbare polyolefinen zijn intrinsiek betere gastheren voor de oriëntatie van dichroïtische gastmoleculen dan het gebruikelijke poly(vinylalcohol).

Dit proefschrift hoofdstuk 3

- 3) Nieuwe technologie kan gedateerd wetenschappelijk onderzoek, waarvoor ogenschijnlijk geen toepassingen bestonden, zeer actueel en relevant maken.

Land E.H. *J. Opt. Soc. Am.*, **1951**, 41, 957

- 4) De door T. Kaino beschreven bulkpolymerisatie van methylmethacrylaat bij een temperatuur van 135°C onder vacuum is niet uitvoerbaar omdat het kookpunt van methylmethacrylaat onder atmosferische omstandigheden 100°C bedraagt.

Kaino T., *J. Polym. Sci. Part A*, **1987**, 25, 37

Kaino T., Fujiki M., Jinguji K., *Review ECL.*, **1984**, 32, 478

Brandrup J., Immergut E.H., *Polymer Handbook*, 3th ed., John Wiley&Sons, **1989**

- 5) Het feit dat de eigenschappen van botcement in heupprothesen niet optimaal zijn door ondermeer de onvolledige uitharding, betekent dat er nog voldoende werk is voor polymeertechnologen op dit gebied.

Kruft M.A.B., *New Radio-opaque Polymeric Biomaterials*, Proefschrift Technische Universiteit Eindhoven, 1997

- 6) Niet de absolute leeftijd is bepalend of men zich te oud voelt om te werken, doch de leeftijd waarop men verwacht te kunnen stoppen.
- 7) Het personeel aannamebeleid van grote ondernemingen lijkt vaak meer op differentiërend dan op proportioneel regelen.
- 8) Het feit dat werkzoekenden een computer met internetaansluiting aangeboden krijgen zodat men thuis kan solliciteren, betekent dat er in de toekomst naast thuiswerkers ook thuiswerklozen zullen ontstaan.
- 9) Een automobiel heeft in tegenstelling tot een motor twee wielen te veel om echt rijgenot te verschaffen.
- 10) Technologische Top-instituten en Top-onderzoekscholen hebben alle kans om in de toekomst uit te groeien tot echte Tob-instellingen.